Physically and Chemically Induced Band Bending Changes at the Surfaces of TiO_2 Nanoparticles Studied by Photoluminescence Spectroscopy

Shiliang Ma
Linyi, Shandong, China

Master of Engineering, Zhejiang University, 2013

A Dissertation presented to the Graduate Faculty
of the University of Virginia in Candidacy for the Degree of
Doctor of Philosophy

Department of Chemistry

University of Virginia
May, 2018

Abstract

TiO_2-based photocatalytic/photovoltaic applications have received enormous research interest. However, one key problem inhibiting practical application is the fast photoexcited electron/hole pair recombination rate, thus understanding photoexcited electron hole behavior is of critical importance. Band bending, which has been seldom studied but widely exist in semiconductor photochemistry, may play important roles in dictating electron and hole behavior. In this thesis, photoluminescence (PL) spectroscopy was employed to study the band bending changes in TiO_2 nanoparticle powders caused by physical or chemical means.

We studied the effect of mixing singled-walled carbon nanotubes (SWNT) into TiO_2 nanoparticle powders on charge transport improvement. It was found that SWNTs accept electrons from photoexcited TiO_2 and quench the PL intensity from TiO_2. However, charge transport through TiO_2 nanoparticles is not improved by mixing SWNTs, which is inferred from similar time constant of the PL increase under continuous UV irradiation. This is due to the effect of charge immobilization caused by positively charged TiO_2 particles which inhibit electrons transferred to SWNTs from being transported away through SWNT channels.

We also found that small coverages of 3 nm-Au nanoparticles deposited on TiO_2 significantly diminish the 540 nm (2.3 eV) PL emission from TiO_2 due to injection of photoexcited electrons into the Au nanoparticles. The lack of PL increase from Au/TiO_2 during continuous UV irradiation is due to a short circuit established through Au nanoparticles where transferred electrons in Au recombine non-radiatively with holes in

TiO_2. The photoexcited electron transfer from TiO_2 to the Au nanoparticles can occur from the Au particle perimeter over a distance of at least 4 nm.

Oxygen adsorption was found to change the band bending of the anatase phase TiO_2 in P25 nanopowder in different ways. First, oxygen can adsorb through irreversible reaction with defects, reducing the intrinsic upward band bending at the TiO_2 surface and resulting in increased PL emission. Second, oxygen exposure also leads to molecular chemisorption that yields an outermost negative charge at the surface which increases the upward band bending of TiO_2 and decreases the PL emission. Since band bending plays an active role in directing charge carrier to the surfaces, the finding that oxygen adsorption can have two different, and quite opposite, effects on the band bending of TiO_2 provides a new perspective on how oxygen may influence photocatalytic reaction efficiencies.

We also found that the band bending of TiO_2 may change during the course of photoelectrochemical reactions. The PL intensity of TiO_2 increases when exposed to hydrogen cations under continuous UV irradiation, signaling a decrease in the upward band bending and increased electron-hole radiative recombination rate, is caused by charge transfer during photoreduction of hydrogen cations. Residual photoexcited holes left in TiO_2 due to the transfer of photoexcited electrons to hydrogen cations lowers the original upward band bending and increases the radiative charge recombination rate. This unusual observation that charge transfer during a photoelectrochemical reaction at a semiconductor interface alters the surface band bending and photoexcited electron/hole recombination rate suggests that photocatalytic activity may change during reactions.

ACKNOWLEDGEMENTS

I would particularly thank Professor John T. Yates, Jr. for accepting me into his group and giving me the opportunity to study in this interesting field. His patience and enthusiasm toward science and research taught me how to enjoy my study here despite that there were many hardships.

I also would particularly thank Professor Ian Harrison for taking over my research projects after Professor Yates' retirement due to health issues. He kept me on the right track of my study and helped me solve most of the problems I encountered in my research. I also really appreciate the freedom he gave me to explore subjects I am interested in which made my study experience joyful.

I also want to thank Dr. Ana Stevanovic for building the instrument and teaching me how to use the instrument. I am very grateful for the help from Dr. Zhen Zhang and Dr. Matt Reish, Dr. Monica McEntee, and Ilsa Cooke. They helped me out of a lot of problems with interpretations of data, experimental designs and instrument troubleshooting. I also want to thank all the professors, staff members, and my fellows for their help in my study and research at University of Virginia.

Last but not least I would greatly thank the support I received from my wife Yujie Zhao. She made a big sacrifice of her own career to accompany me and made Charlottesville my home during my study at UVa. I am very grateful for all she has done for me and mere words are inadequate to express my sincere gratitude to her.

Table of Contents

1 Introduction

Research interests in TiO_2-based photocatalysis sprung from 1972 since the pioneering work by Fujishima and Honda[1] in which H_2 and O_2 were produced by UV irradiation of a TiO_2 anode to split water. Photocatalytic remediation of hazardous wastes in both water and air using TiO_2 emerged as a practical research interest.[2] TiO_2 was also found to be a promising material for the manufacture of low-cost, non-toxic photovoltaic cells after the fabrication of dye sensitized TiO_2 solar cells by Oregan and Gratzel.[3] Although these TiO_2-based photo-technologies target different applications, the common driving force is photoexcitation and photoexcited electron/hole pair recombination is one of the main factors that reduces device efficiency. Therefore, understanding the behavior of photoexcited electrons and holes is central to improving photocatalytic efficiencies.

The main focus of this thesis is the photoluminescence (PL) study of surface band bending of TiO_2 nanoparticles, which has been reported to have significant impacts on tuning the electron and (or) hole availability at the TiO_2 surface.[4] Studies in this thesis include: (1) the effect of Single-Walled Carbon Nanotubes (SWNT) on charge transport; (2) the effect of Au nanoparticle deposition on quenching PL; (3) the different effects of oxygen reaction with TiO_2 on band bending of TiO_2; and (4) the change of surface band bending of TiO_2 due to charge transfer during photoreactions.

1.1 Mechanism of Photocatalysis

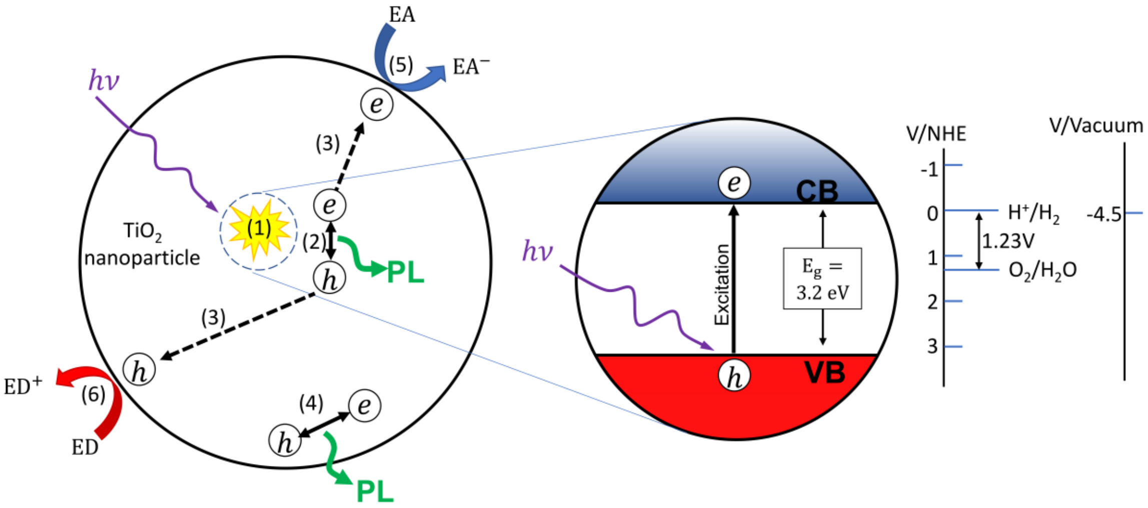

Figure 1.1. Mechanism of TiO_2 based photocatalysis. Band gap of TiO_2 is 3.0 – 3.2 eV. (1) photoexcitation, (2) bulk recombination, (3) charge separation, (4) surface recombination, (5) surface reduction reaction, (6) surface oxidation reaction.[5]

Figure 1.1 shows the basic mechanism of photocatalysis. The electronic structure of TiO_2 consists of a valence band (VB) which is fully-filled at ground state and a conduction band (CB) which is completely empty at ground state. There exists a band gap of ~ 3.0 – 3.2 eV between the VB and CB in which there exist no electron orbitals (ideal case). When irradiated with photons with energy larger than the band gap energy ($h\nu \geq E_g$, incident photon wavelength shorter than 387 nm for TiO_2), electrons residing in the VB can be excited into the CB with positively charged holes left in the VB (process 1), resulting in photoexcited electron/hole pairs. Both the electrons in CB and holes in VB are able to move within the TiO_2 nanoparticles. The photoexcited electron/hole pairs can separate and migrate to the surfaces to participate in reactions (process 3). The photoexcited electrons are strong reducing agents and are able to reduce electron acceptors (process 5) while the photoexcited holes are strong oxidizing agents and are able to oxidize electron donors (process 6). If both the electron donor and electron acceptor are water molecules, the net reaction can be H_2 and O_2 production by water splitting.[6] If the electron acceptor molecules are O_2 while the electron donor molecules are organic pollutants, the reaction can be used for the remediation of environmental pollutants.[2] If the electrons and holes are collected by two separate electrodes and recombine through an external circuit, the process works as a photovoltaic cell which converts solar energy into electrical energy. For chemical reactions to occur on the surface of TiO_2, the energy levels of electrons and holes have to satisfy the thermodynamic laws, i.e., the electrochemical potential of photoexcited electrons need to be more negative than the potential of the reduction reaction and the potential of photoexcited holes need to be more positive than the potential of the oxidization reaction.[6-7] The potential relationship between TiO_2 and the water splitting reaction is shown in Figure 1.1.

In addition to the charge separation processes and chemical reactions on TiO_2 surfaces, the photoexcited electron/hole pairs can also recombine either in the bulk of TiO_2 (process 2) and (or) at the surface of TiO_2 (process 4). If the energy is released as photon emission, photoluminescence (PL) can be measured from TiO_2. The energy can also be released as heat. The fast recombination rate of electrons and holes is considered as one of the main reasons that limit the efficiency of TiO_2-based photo-applications.[7-8] Therefore, it is of great importance to study factors that affect the electron-hole separation and recombination rate.

1.2 Methods to improve photocatalytic efficiency

The photocatalytic efficiency of pure TiO_2, especially for hydrogen production reaction, is actually very low. In pure water-splitting without hole scavengers, the photocatalytic hydrogen yield can be zero.[9] Therefore, researchers have studied various methods to improve the efficiency of TiO_2-based photo-technologies. Here, several important concepts that relate to the results in this thesis are briefly introduced. More information can be found from the literature.[5-8, 10-12]

1.2.1 Noble metal loading

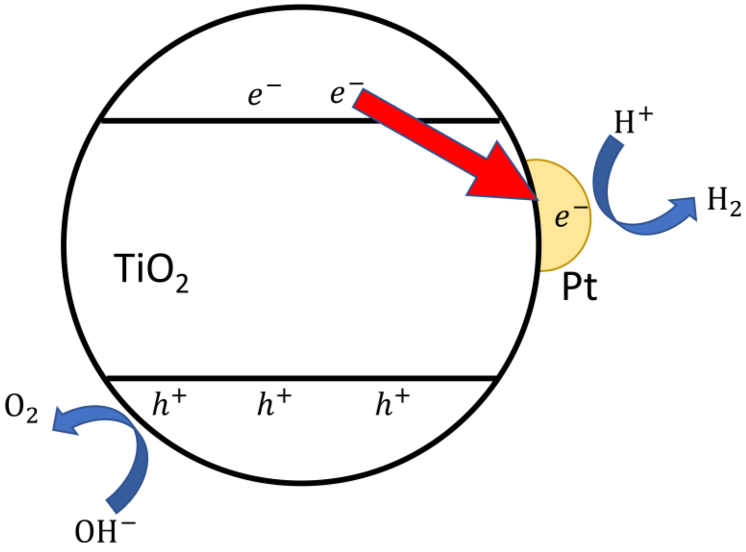

Figure 1.2. Mechanism of noble metal loading in increasing photocatalytic activity

Because the work functions of noble metals, such as Pt, Au, Ag, are higher than the work function of TiO_2,[13] the Fermi energies (chemical potential) of noble metals are lower than that of TiO_2, as shown in Figure 1.2 (the top of Pt conduction band is lower than CB of TiO_2). Hence, photoexcited electrons tends to be captured by the noble metal islands deposited on TiO_2, with holes left in the VB of TiO_2, enhancing charge carrier separation and suppressing charge carrier recombination.[7-8, 14] (A more detailed analysis on this subject can be found at Appendix A). Moreover, because noble metals are also good catalysts, the photocatalytic efficiency improvement, especially for hydrogen production occurring on metal islands, is considered also originating from the catalytic property of noble metals.[7-8]

1.2.2 Adding hole or electron scavenger

Adding hole scavengers which react rapidly with photoexcited holes can suppress the electron/hole pair recombination by competitive hole consumption, thereby increasing the number of electrons available for desired reactions at surfaces. Electron scavengers work similarly to increase the number of available holes.[8] Another important reason for adding hole or electron scavengers is to suppress back reactions. For example, in hydrogen production through water splitting, the back reaction between H_2 and O_2 to form H_2O, which is thermodynamically favorable, especially on the surface of noble metals, greatly inhibits the net rate of hydrogen production.[8] Adding methanol to react with holes can suppress the production of O_2 and therefore greatly improve the hydrogen production rate. Sreethawong et al. showed that H_2 production on Pt/TiO_2 can be improved from 0 μmol/h to ~ 1400 μmol/h with the addition of methanol as a hole scavenger.[9]

1.2.3 Composite semiconductor

Figure 1.3 shows the mechanism by which composite semiconductors can enhance charge separation. Upon photon illumination, photoexcited electrons in CdS tend to inject into the CB of TiO_2 which has a lower energy while holes remain in CdS because of its higher VB potential which is lower energy for positively charged holes(i.e. holes “float”).

Moreover, if excitation also occurs in TiO_2, electrons will remain in CB of TiO_2 while holes will inject into the VB of CdS. This composite scheme separates electrons and holes into different materials and thus improves charge separation and reduces charge recombination.[5] For composite semiconductors to work, both the VB and CB of one semiconductor need to be higher than those of the other semiconductor.

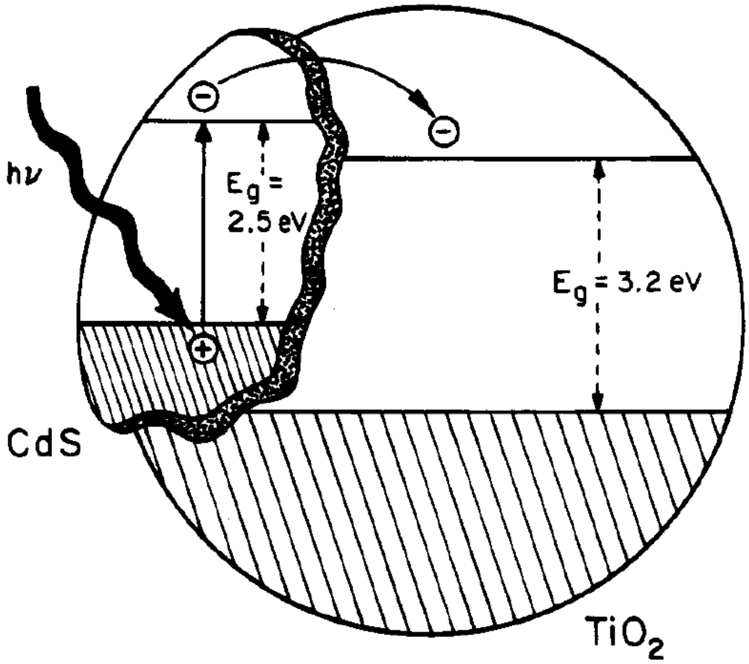

Figure 1.3. Mechanism of composite semiconductors[5]

1.3 Phases of TiO_2

In nature, TiO_2 is found to exist in three different phases: anatase, rutile, and brookite.[15] Both anatase and rutile phase TiO_2 are semiconductors with bandgap energies between 3.0 - 3.2 eV and are well studied. However, the brookite structure is not often used for photocatalytic studies due to its low photocatalytic activity. The lattice structures of both rutile and anatase belong to the distorted octahedron class and their structures are illustrated in Figure 1.4. [5, 15]

Although anatase and rutile phase TiO_2 are both photoactive and they possess similar band gap energies, some of their properties are quite different. First, it is commonly considered that anatase TiO_2 is more active than rutile phase TiO_2. Karakitsou & Verykios showed that the rate of H_2 production decreases linearly with the increase of rutile phase fraction in anatase-rutile composite.[16] Second, the rutile phase is usually considered more stable than the anatase phase, especially for large particles. It has been widely reported that anatase will transform into the rutile phase when the temperature is higher than 600 – 900 °C. [16] For the last several decades, surface studies mainly focused on the rutile (110) surface due to the lack of anatase single crystals.[17] Only recently have several surface science studies on anatase (101) surfaces been reported.[18-19]. Hence, there still exist gaps in correlating the measured photocatalytic activity on anatase nanoparticles with the surface processes studied by surface science techniques on rutile(110) surfaces.

P25 TiO_2 nanopowder is a commercial product from the Degussa company that is widely used in research to benchmark activities of synthesized TiO_2 photocatalysts. The P25 TiO_2 consists of 75% of anatase with an average diameter of 85 nm and 25% of rutile with an average diameter of 25 nm.[20]

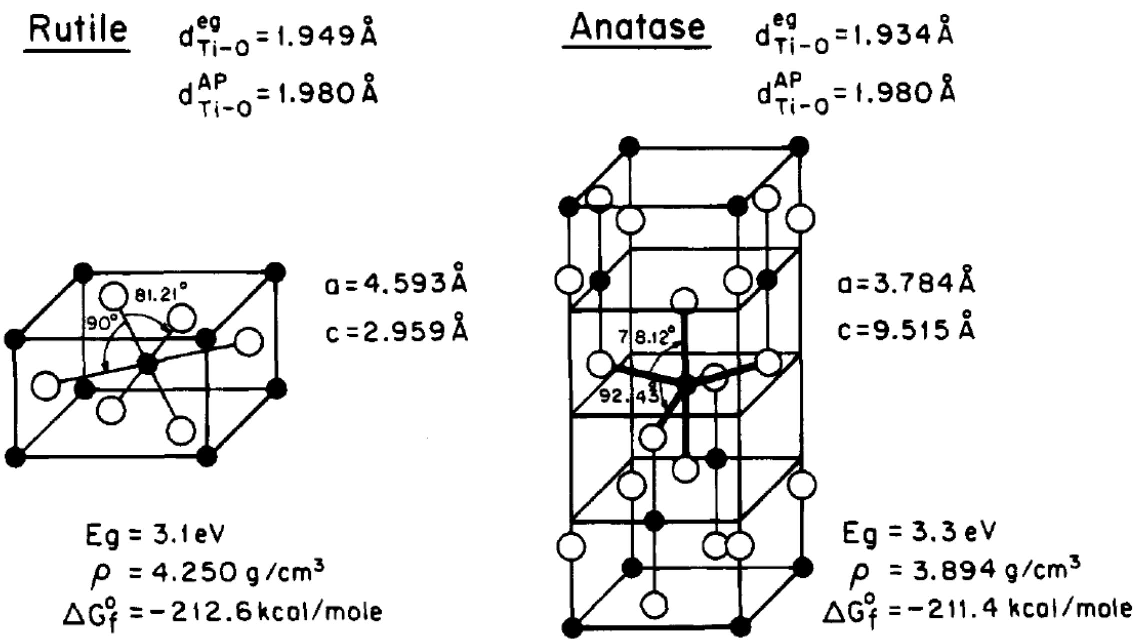

Figure 1.4. Lattice structure of rutile and anatase TiO_2 [5]

1.4 Band bending

The band structure of TiO_2 is characterized by its CB and VB. The CB and VB should be flat if the TiO_2 lattice is infinitely large with no defects, i.e. the CB potential energy is evenly distributed spatially across the TiO_2 lattice and so is the VB. However, due to multiple reasons, the CB and VB of TiO_2 are usually not flat and bend near surfaces or interfaces. The phenomenon that the CB and VB bend from the flat band situation is called band bending, which was first developed by Schottky and Mott to explain the rectifying effect at a metal/semiconductor interface.[12]

The main driving force of band bending is that when materials with different Fermi energy (a different term of chemical potential widely used in solid state physics[21]) are in contact, electrons flow from the material with higher Fermi energy to the material with lower Fermi energy until the Fermi energies equilibrate. For example, in Figure 1.5, because the Fermi energy of Au is lower than that of TiO_2, electrons in TiO_2 are injected into Au nanoparticles until their Fermi energies equilibrate. The excess electrons injected into Au and leftover holes in TiO_2 form a dipole spanning across the Au/TiO_2 interface, creating an S-shaped potential curve which elevates the CB energy of TiO_2 near the interface, thus resulting in band bending. The region where band bending exists is called depletion layer if the band bending is upward, or accumulation layer if the band bending is downward. It is worth noting that because the dielectric constants of metals are usually considered infinity, there exists no band bending at the metal side. A more detailed analysis using TiO_2 and semiconducting single-walled carbon nanotube (SWNT) as an example is provided in Appendix B.

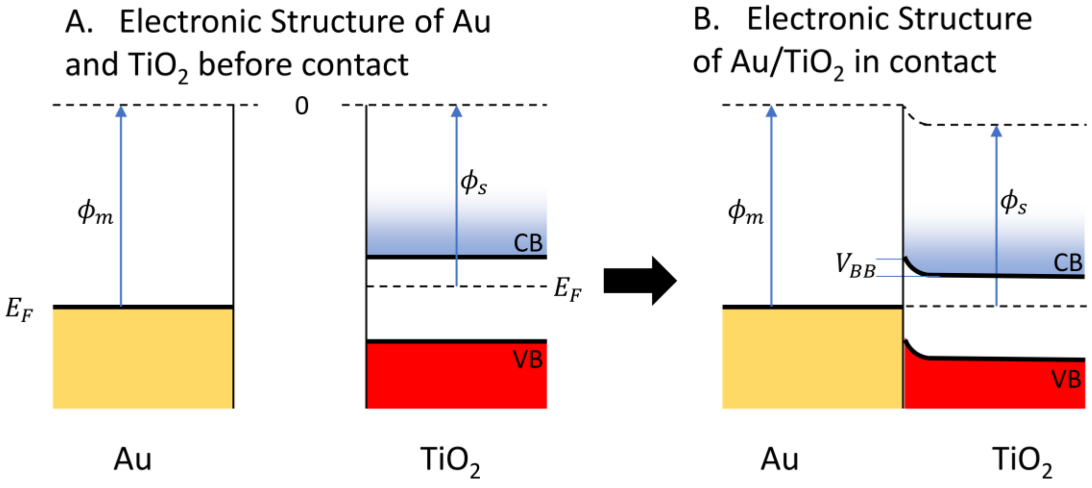

Figure 1.5. Band bending formed at Au/TiO_2 interface. ϕ_m – work function of Au, ϕ_s – work function of TiO_2, V_{BB} – band bending potential. The difference between the vacuum energy and the Fermi energy is the work function.[14]

1.4.1 Origins of band bending or band bending change

Metal/semiconductor contact. As discussed in Figure 1.5, the injection of electrons into metals from semiconductors usually results in upward band bending in the semiconductors.

Applied electric field. As shown in Figure 1.6, when a voltage is applied between a semiconductor and a metal plate to form a capacitor, charges accumulate at the surfaces of both the metal and semiconductor. Unlike metals which can completely shield the electric field by rearranging the charge distribution on their surfaces, the electric field can penetrate into the semiconductor and cause the bands to bend. When the plate is positively charged, the band bending is downward (which can be treated as electron energy decrease due to electrostatic attraction between CB electrons and the positive charges from the metal, for simplicity), and when the plate is negatively charged, the band bending is upward.[12]

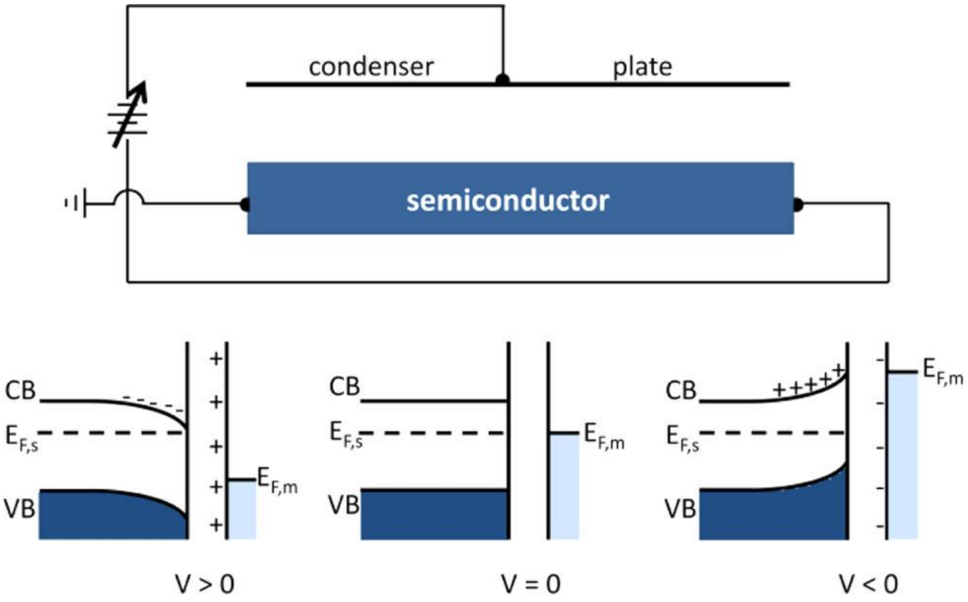

Figure 1.6. The induction or change of band bending in semiconductor due to applied electric field.[12]

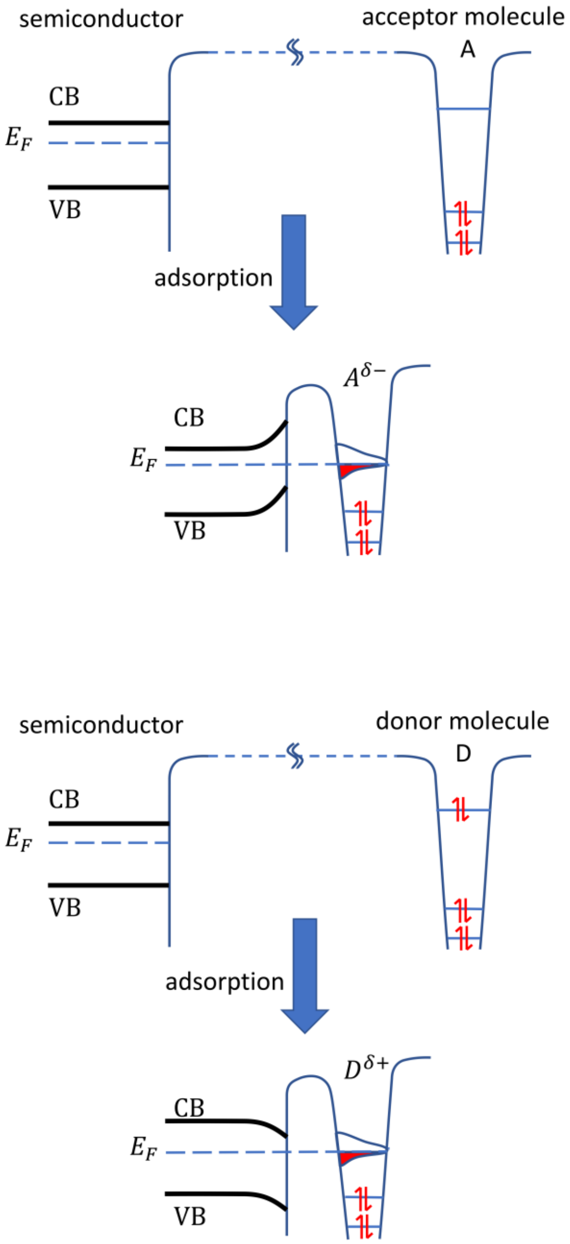

Figure 1.7. Band bending caused by acceptor molecule and donor molecule[4, 12]

Adsorption of donor and acceptor molecules. Because of the different chemical potentials of electrons in semiconductor and gas molecules, electron transfer usually occurs when molecules adsorb on semiconductor surfaces, especially for chemisorption.[22] When adsorbed on semiconductor surfaces, the electron potential in neutral acceptor molecules is lower than the Fermi energy of semiconductor, thus electrons tend to flow from semiconductor to acceptor molecules and resulting in negatively charged acceptor molecules on semiconductor, causing upward band bending in the semiconductor due to electrostatic repulsion, as shown in Figure 1.7.[4] Similarly, if donor molecules adsorb on semiconductor, the donor molecules possessing positive charge after donating electrons into semiconductor cause downward band bending. The band bending caused by gas molecule adsorption is similar to the applied electric field situation since both are caused by local charge accumulation at semiconductor surface.

Surface state. Even on a clean semiconductor surface, surface states may still exist due to the termination of the bulk lattice periodicity. Unpaired electrons in surface dangling bonds usually result in an electronic state with a narrow energy band lying in the band gap of the semiconductor, as shown in Figure 1.8. Similar to the situation of metal/semiconductor interface, the equilibration of Fermi energies results in upward band bending for n-type semiconductor due to the electron migration from the bulk to the surface. The introduction of band bending shown in Figure 1.8 is also applicable to band bending induced in composite semiconductors which consists of at least two semiconductors with different CB, VB and Fermi energies.

1.4.2 Band bending of TiO_2

It is broadly accepted that TiO_2 is an n-type semiconductor due to the formation of oxygen vacancies (V_O) and interstitial Ti^{3+} sites which donate electrons into the TiO_2 lattice.[23-27] And thus, TiO_2 naturally possesses an upward band bending according to Figure 1.8.[28-29]

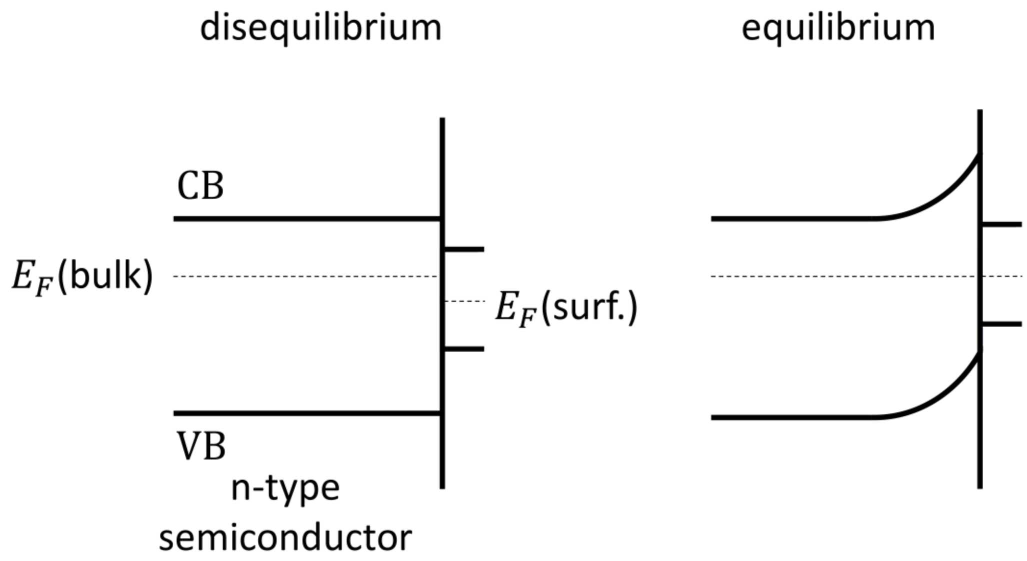

Figure 1.8. Band bending caused by surface state.[12]

1.4.3 Effects of band bending

Influences on charge recombination rate. Charge recombination rate in the band bending region is suppressed compared to the flat band region for several reasons. As shown in Figure 1.9, both photoexcited electrons and holes tends to migrate to locations with lower potential energy. The opposite charges possessed by electrons and holes cause the photoexcited electrons and holes to migrate in different directions, i.e. electrons migrate to the bulk while holes migrate to the surface, resulting in charge separation. Thus, radiative charge recombination (resulting in PL) in the band bending region is suppressed and the lifetime of photoexcited charge carriers are elongated, which enhances the probability of nonradiative relaxation.[30-31] In addition, the minority carriers (which are holes in Figure 1.9) generated in the band bending region are accumulated at the surface where nonradiative recombination dominates, also resulting in decreased radiative charge recombination.[31] A downward band bending also decreases radiative charge recombination compared to the flat band situation except that the roles of electrons and holes are switched. Therefore, if the band structure gradually changes from upward band bending, to flat band, and to downward band bending, an increase of PL intensity followed by a decrease of PL should be expected.

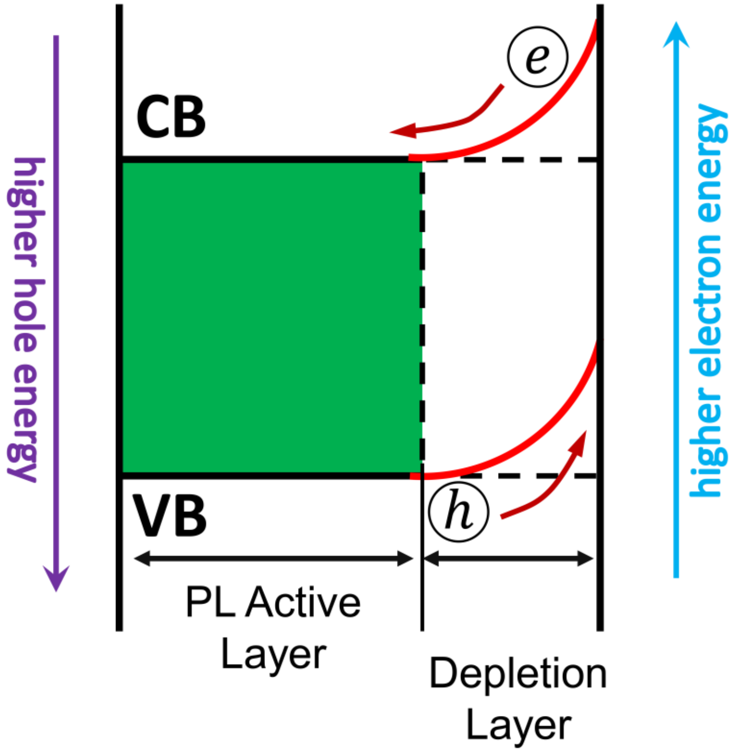

Figure 1.9. Photoexcited charge separation due to band bending.

Influences on surface reactions. As discussed above, photoexcited charge carriers are separated in the band bending region and their lifetimes are elongated. Moreover, because upward band bending tends to accumulate holes at the TiO_2 surface while downward band bending tends to accumulate electrons at the TiO_2 surface, tuning band bending of TiO_2 provides a way to modulate the availabilities of photoexcited charge carriers at the TiO_2 surfaces.

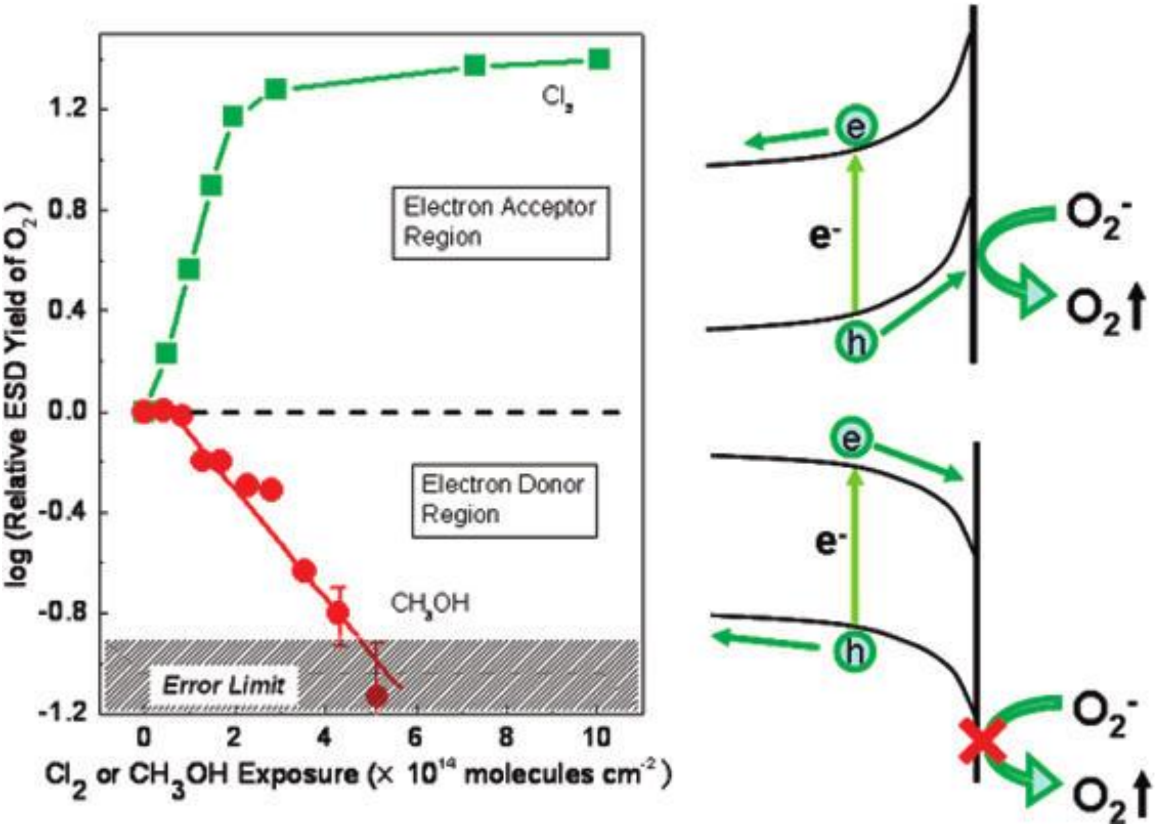

Figure 1.10. Effect of band bending on oxygen desorption from TiO_2 surface.[4]

Zhang and Yates[4] studied the effect of band bending on hole-mediated oxygen desorption from TiO_2 surface. As shown in Figure 1.10, adsorbing methanol on TiO_2 which induces downward band bending decreases oxygen desorption rate by driving photoexcited holes away from TiO_2 surface. On the other hand, adsorbing Cl_2 on TiO_2 surfaces induces upward band bending and increases oxygen yield due to the increased hole availability at the TiO_2 surface. By tuning the band bending of TiO_2, a 100-fold difference in oxygen desorption rate was achieved, demonstrating that tuning band bending is an effective way to modulate surface reactions.

Some may argue that the competitive reaction idea from section 1.2.2 can also explain the behavior in Figure 1.10. For example, the decrease of oxygen yield due to CH_3OH adsorption can be explained by that CH_3OH can also be oxidized by holes and thus the number of holes available at TiO_2 surface is reduced due to the competitive reaction with CH_3OH. However, this possibility was ruled out by Zhang and Yates by an $^{16}O_2$ and $^{18}O_2$ co-adsorption experiment. It was found that the co-adsorption of $^{16}O_2$ increases the yield of $^{18}O_2$. Thus, the mechanism must not be the competitive reaction path because the competitive reaction between holes and $^{16}O_2$ should decrease the yield of $^{18}O_2$. This study suggests that band bending may play an important role in photocatalytic processes which have not been carefully studied.

1.5 Band bending studied by PL

The band bending in semiconductors can be measured by different techniques, such as surface photovoltage spectroscopy,[32-33] photoelectron spectroscopy[34], and PL.[12, 14, 24, 30-31, 35-38] In this thesis, I will mainly focus on the study of band bending by PL.

1.5.1 Dead layer model

As discussed in section 1.4.3, the potential energy curve in the band bending region separates photoexcited electrons and holes and suppresses the radiative recombination. Thus, there is little PL emission from the band bending region, which is considered a dead layer for PL emission (theoretically the dead layer and the band bending region are not exactly the same, but they are quite close).[31] The observed PL mainly comes from the bulk of TiO_2 where the band is flat, as shown in Figure 1.9. Because of the exponential decay of light intensity inside the semiconductor, the PL intensity from a 1D semiconductor sample can be described as[31]

$$\mathrm{I_{PL}} = \mathrm{I}_{PL}^{FB}\exp(-\alpha D) \tag{1.1}$$

in which *FB* stands for the flat band situation, α is the light absorption coefficient and *D* is the depletion layer depth. Also, for 1D semiconductor surfaces, the depletion layer depth and the band bending voltage $\mathrm{V_{BB}}$ can be correlated by[12]

$$\mathrm{D} = \sqrt{\frac{2\varepsilon_r\varepsilon_0 V_{BB}}{eN_d}} \tag{1.2}$$

in which ε_r and ε_0 are the relative dielectric constant and the vacuum permittivity and $\mathrm{N_d}$ is the donor density. Combining the above two equations, PL intensity provides a measure of the band bending voltage.

It is worth noting that the usual depletion layer depth is ~ 10 nm and thus for nanoparticles, the above equations cannot be directly applied because the nanoparticle has to be treated as a sphere instead of a 1D plane. Thus, PL intensity is usually used as a method to qualitatively detect band bending change, instead of estimating the band bending voltage.

1.5.2 Band bending change due to gas molecule adsorption

The band bending changes of TiO_2 due to the adsorption of various gas molecules have been studied, such as NH_3, CO,[30, 39] CH_3OH, Cl_2,[4] H_2, O_2,[24, 30] and many hydrocarbons.[36] The study of the various gas molecules suggests that the formation of negatively charged adsorbates (acceptor molecules) causes PL intensity to decrease, while the formation of positive adsorbates (donor molecules) results in PL intensity increase,[36] which agrees well with the aforementioned band bending change due to gas molecule adsorption on initially clean TiO_2 with upward band bending. Further, Anpo et al[36] also found that the fraction of PL quenching correlates with the ionization potential of adsorbates, suggesting that the band bending change is a general physical process instead of a site-specific chemical process.

1.5.3 UV induced band flattening

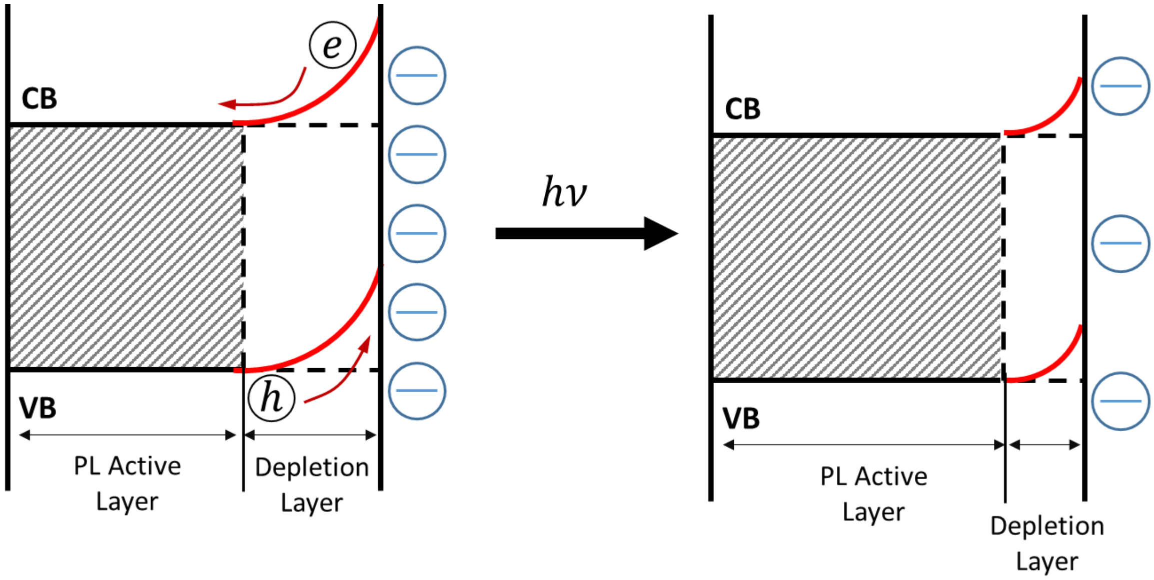

Figure 1.11. Mechanism of UV induced band flattening [30]

Stevanovic et al.[30] studied the effect of UV irradiation induced surface band bending flattening effect using PL spectroscopy. It was found that the PL emission intensity from TiO_2 gradually increases during continuous UV irradiation. The mechanism of the increase was explained by the UV induced band flattening effect shown in Figure 1.11. Before UV irradiation, the as-prepared TiO_2 sample possesses an upward bending as discussed before, which can be treated due to negative charges trapped on TiO_2 surface which shift the bands upward. Under continuous UV irradiation, photoexcited electrons and holes generated in the depletion layer will separate under the potential energy difference caused by the band bending, driving holes to the surface of TiO_2 while electrons to the bulk. The photoexcited holes arriving at the TiO_2 surface are able to neutralize the original negative charges trapped on the surface and thus decrease the upward band bending, which reduces the depth of depletion layer and increases PL intensity.

1.5.4 Electron hopping through TiO_2 particles

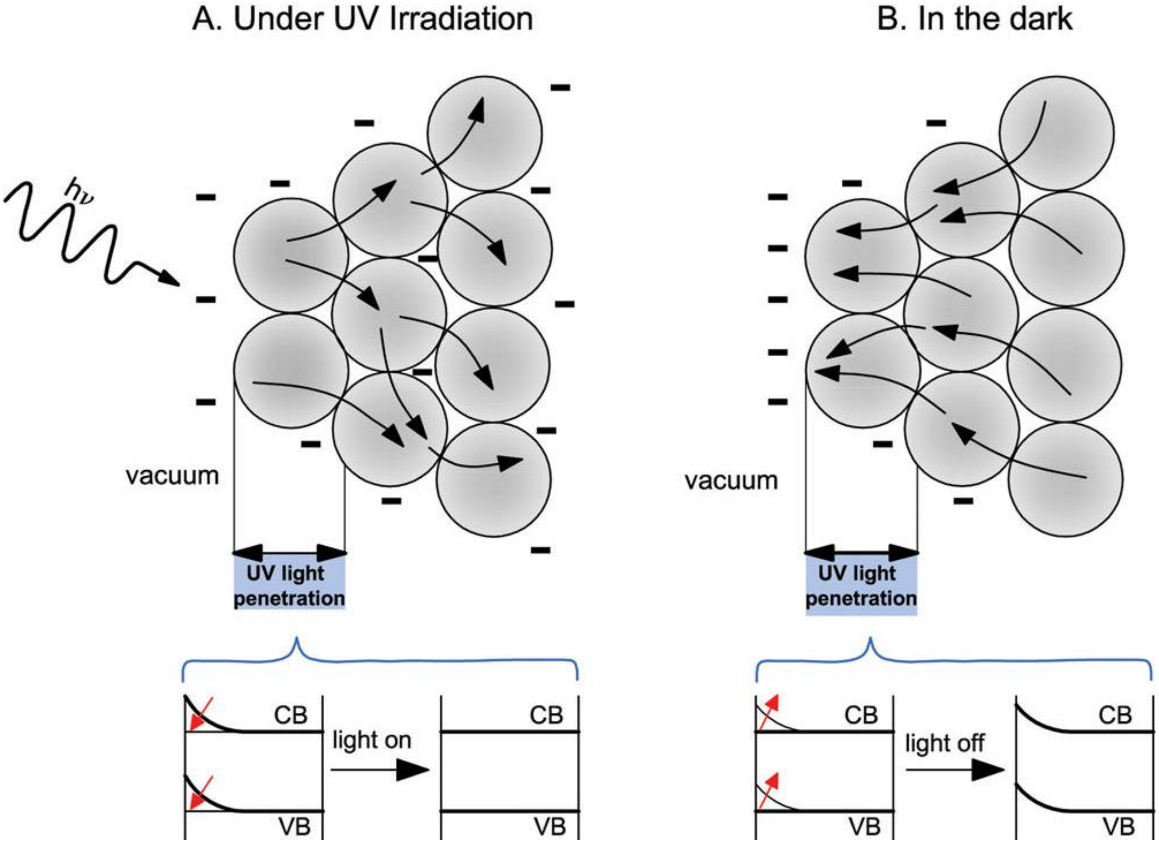

Figure 1.12. Electron hopping studied by PL spectroscopy[37]

In addition to the above mentioned PL flattening effect, Stevanovic et al[37] also found that the increased PL intensity during UV irradiation decreases in the dark and the

PL decrease rate in the dark increases with the increase of temperature. Moreover, it was also found that the time constant for the PL decrease is many orders of magnitude larger than that of electron transport inside a particle but is close to the time constant of electron hopping through particles. Thus, the authors refined their band bending flattening model from the above section with a new feature as shown in Figure 1.12. Because the UV irradiation can only penetrate one layer of the TiO_2 particles, the PL collected are only from the first layer of TiO_2. During UV irradiation, when holes are driven to the surface of the photoexcited TiO_2 in the first layer, the photoexcited electrons can hop through TiO_2 particles into the non-photoexcited TiO_2 particles, leaving holes in the first layer of TiO_2, which causes PL intensity to increase. When UV irradiation is turned off, electrons that hopped into non-photoexcited TiO_2 particles gradually hop back to the first layer of TiO_2 and recombine with the holes, thus restoring the initial upward band bending and reducing PL intensity.

References

1. Fujishima, A.; Honda, K., Electrochemical Photolysis of Water at a Semiconductor Electrode. *Nature* **1972**, *238*, 37-38.
2. Hoffmann, M. R.; Martin, S. T.; Choi, W. Y.; Bahnemann, D. W., Environmental Applications of Semiconductor Photocatalysis. *Chemical Reviews* **1995**, *95*, 69-96.
3. Oregan, B.; Gratzel, M., A Low-Cost, High-Efficiency Solar-Cell Based on Dye-Sensitized Colloidal TiO_2 Films. *Nature* **1991**, *353*, 737-740.
4. Zhang, Z.; Yates, J. T., Effect of Adsorbed Donor and Acceptor Molecules on Electron Stimulated Desorption: $O_2/TiO_2(110)$. *Journal of Physical Chemistry Letters* **2010**, *1*, 2185-2188.
5. Linsebigler, A. L.; Lu, G. Q.; Yates, J. T., Photocatalysis on TiO_2 Surfaces - Principles, Mechanisms, and Selected Results. *Chemical Reviews* **1995**, *95*, 735-758.
6. Chen, X. B.; Shen, S. H.; Guo, L. J.; Mao, S. S., Semiconductor-Based Photocatalytic Hydrogen Generation. *Chemical Reviews* **2010**, *110*, 6503-6570.
7. Zhu, J. F.; Zach, M., Nanostructured Materials for Photocatalytic Hydrogen Production. *Current Opinion in Colloid & Interface Science* **2009**, *14*, 260-269.
8. Ni, M.; Leung, M. K. H.; Leung, D. Y. C.; Sumathy, K., A Review and Recent Developments in Photocatalytic Water-Splitting Using TiO_2 for Hydrogen Production. *Renewable & Sustainable Energy Reviews* **2007**, *11*, 401-425.
9. Sreethawong, T.; Puangpetch, T.; Chavadej, S.; Yoshikawa, S., Quantifying Influence of Operational Parameters on Photocatalytic H_2 Evolution over Pt-Loaded Nanocrystalline Mesoporous TiO_2 Prepared by Single-Step Sol-Gel Process with Surfactant Template. *Journal of Power Sources* **2007**, *165*, 861-869.
10. Chiarello, G. L.; Dozzi, M. V.; Selli, E., TiO_2-Based Materials for Photocatalytic Hydrogen Production. *Journal of Energy Chemistry* **2017**, *26*, 250-258.
11. Nakata, K.; Fujishima, A., TiO_2 Photocatalysis: Design and Applications. *Journal of Photochemistry and Photobiology C-Photochemistry Reviews* **2012**, *13*, 169-189.
12. Zhang, Z.; Yates, J. T., Band Bending in Semiconductors: Chemical and Physical Consequences at Surfaces and Interfaces. *Chemical Reviews* **2012**, *112*, 5520-5551.
13. Sangpour, P.; Hashemi, F.; Moshfegh, A. Z., Photoenhanced Degradation of Methylene Blue on Cosputtered $M:TiO_2$ (M = Au, Ag, Cu) Nanocomposite Systems: A Comparative Study. *Journal of Physical Chemistry C* **2010**, *114*, 13955-13961.
14. Stevanovic, A.; Ma, S. L.; Yates, J. T., Effect of Gold Nanoparticles on Photoexcited Charge Carriers in Powdered TiO_2-Long Range Quenching of Photoluminescence. *Journal of Physical Chemistry C* **2014**, *118*, 21275-21280.
15. Thompson, T. L.; Yates, J. T., Surface Science Studies of the Photoactivation of TiO_2-New Photochemical Processes. *Chemical Reviews* **2006**, *106*, 4428-4453.
16. Karakitsou, K. E.; Verykios, X. E., Effects of Altervalent Cation Doping of TiO_2 on Its Performance as a Photocatalyst for Water Cleavage. *Journal of Physical Chemistry* **1993**, *97*, 1184-1189.
17. Fujishima, A.; Zhang, X. T.; Tryk, D. A., TiO_2 Photocatalysis and Related Surface Phenomena. *Surface Science Reports* **2008**, *63*, 515-582.

18. Setvin, M.; Aschauer, U.; Scheiber, P.; Li, Y. F.; Hou, W. Y.; Schmid, M.; Selloni, A.; Diebold, U., Reaction of O_2 with Subsurface Oxygen Vacancies on TiO_2 Anatase (101). *Science* **2013**, *341*, 988-991.
19. Jackman, M. J.; Thomas, A. G.; Muryn, C., Photoelectron Spectroscopy Study of Stoichiometric and Reduced Anatase TiO_2(101) Surfaces: The Effect of Subsurface Defects on Water Adsorption at near-Ambient Pressures. *Journal of Physical Chemistry C* **2015**, *119*, 13682-13690.
20. Ohno, T.; Sarukawa, K.; Tokieda, K.; Matsumura, M., Morphology of a TiO_2 Photocatalyst (Degussa, P-25) Consisting of Anatase and Rutile Crystalline Phases. *Journal of Catalysis* **2001**, *203*, 82-86.
21. Ashcroft, N. W.; Mermin, N. D., *Solid State Physics*; Holt, Rinehart and Winston: New York, 1976.
22. Henderson, M. A., A Surface Science Perspective on TiO_2 Photocatalysis. *Surface Science Reports* **2011**, *66*, 185-297.
23. Henderson, M. A.; Epling, W. S.; Perkins, C. L.; Peden, C. H. F.; Diebold, U., Interaction of Molecular Oxygen with the Vacuum-Annealed TiO_2(110) Surface: Molecular and Dissociative Channels. *Journal of Physical Chemistry B* **1999**, *103*, 5328-5337.
24. Ma, S. L.; Reish, M. E.; Zhang, Z.; Harrison, I.; Yates, J. T., Anatase-Selective Photoluminescence Spectroscopy of P25 TiO_2 Nanoparticles: Different Effects of Oxygen Adsorption on the Band Bending of Anatase. *Journal of Physical Chemistry C* **2017**, *121*, 1263-1271.
25. Lu, G. Q.; Linsebigler, A.; Yates, J. T., Ti^{3+} Defect Sites on TiO_2(110) - Production and Chemical-Detection of Active-Sites. *Journal of Physical Chemistry* **1994**, *98*, 11733-11738.
26. Lira, E.; Wendt, S.; Huo, P. P.; Hansen, J. O.; Streber, R.; Porsgaard, S.; Wei, Y. Y.; Bechstein, R.; Laegsgaard, E.; Besenbacher, F., The Importance of Bulk Ti^{3+} Defects in the Oxygen Chemistry on Titania Surfaces. *Journal of the American Chemical Society* **2011**, *133*, 6529-6532.
27. Wendt, S.; Schaub, R.; Matthiesen, J.; Vestergaard, E. K.; Wahlstrom, E.; Rasmussen, M. D.; Thostrup, P.; Molina, L. M.; Laegsgaard, E.; Stensgaard, I., et al., Oxygen Vacancies on TiO_2(110) and Their Interaction with H_2O and O_2: A Combined High-Resolution STM and DFT Study. *Surface Science* **2005**, *598*, 226-245.
28. Stevanovic, A. Electron and Hole Behavior in Powered TiO_2 - Photoluminescence and Infrared Studies. University of Virginia, Charlottesville, 2014.
29. McEntee, M.; Stevanovic, A.; Tang, W. J.; Neurock, M.; Yates, J. T., Electric Field Changes on Au Nanoparticles on Semiconductor Supports - the Molecular Voltmeter and Other Methods to Observe Adsorbate-Induced Charge-Transfer Effects in Au/TiO_2 Nanocatalysts. *Journal of the American Chemical Society* **2015**, *137*, 1972-1982.
30. Stevanovic, A.; Buttner, M.; Zhang, Z.; Yates, J. T., Photoluminescence of TiO_2: Effect of UV Light and Adsorbed Molecules on Surface Band Structure. *Journal of the American Chemical Society* **2012**, *134*, 324-332.
31. Hollingsworth, R. E.; Sites, J. R., Photo-Luminescence Dead Layer in P-Type InP. *Journal of Applied Physics* **1982**, *53*, 5357-5358.

32. Kronik, L.; Shapira, Y., Surface Photovoltage Phenomena: Theory, Experiment, and Applications. *Surface Science Reports* **1999**, *37*, 1-206.
33. Jing, L. Q.; Sun, X. J.; Shang, J.; Cai, W. M.; Xu, Z. L.; Du, Y. G.; Fu, H. G., Review of Surface Photovoltage Spectra of Nano-Sized Semiconductor and Its Applications in Heterogeneous Photocatalysis. *Solar Energy Materials and Solar Cells* **2003**, *79*, 133-151.
34. Horn, K., Semiconductor Interface Studies Using Core and Valence Level Photoemission. *Applied Physics a-Materials Science & Processing* **1990**, *51*, 289-304.
35. Meyer, G. J.; Lisensky, G. C.; Ellis, A. B., Evidence for Adduct Formation at the Semiconductor Gas Interface - Photoluminescent Properties of Cadmium Selenide in the Presence of Amines. *Journal of the American Chemical Society* **1988**, *110*, 4914-4918.
36. Anpo, M.; Tomonari, M.; Fox, M. A., *in situ* Photoluminescence of TiO_2 as a Probe of Photocatalytic Reactions. *Journal of Physical Chemistry* **1989**, *93*, 7300-7302.
37. Stevanovic, A.; Yates, J. T., Electron Hopping through TiO_2 Powder: A Study by Photoluminescence Spectroscopy. *Journal of Physical Chemistry C* **2013**, *117*, 24189-24195.
38. Stevanovic, A.; Ma, S. L.; Yates, J. T., Photoexcited Electron Hopping between TiO_2 Particles: Effect of Single-Walled Carbon Nanotubes. *Journal of Physical Chemistry C* **2014**, *118*, 23614-23620.
39. Stevanovic, A.; Yates, J. T., Probe of NH_3 and CO Adsorption on the Very Outermost Surface of a Porous TiO_2 Adsorbent Using Photoluminescence Spectroscopy. *Langmuir* **2012**, *28*, 5652-5659.

2 Experimental

2.1 High vacuum system

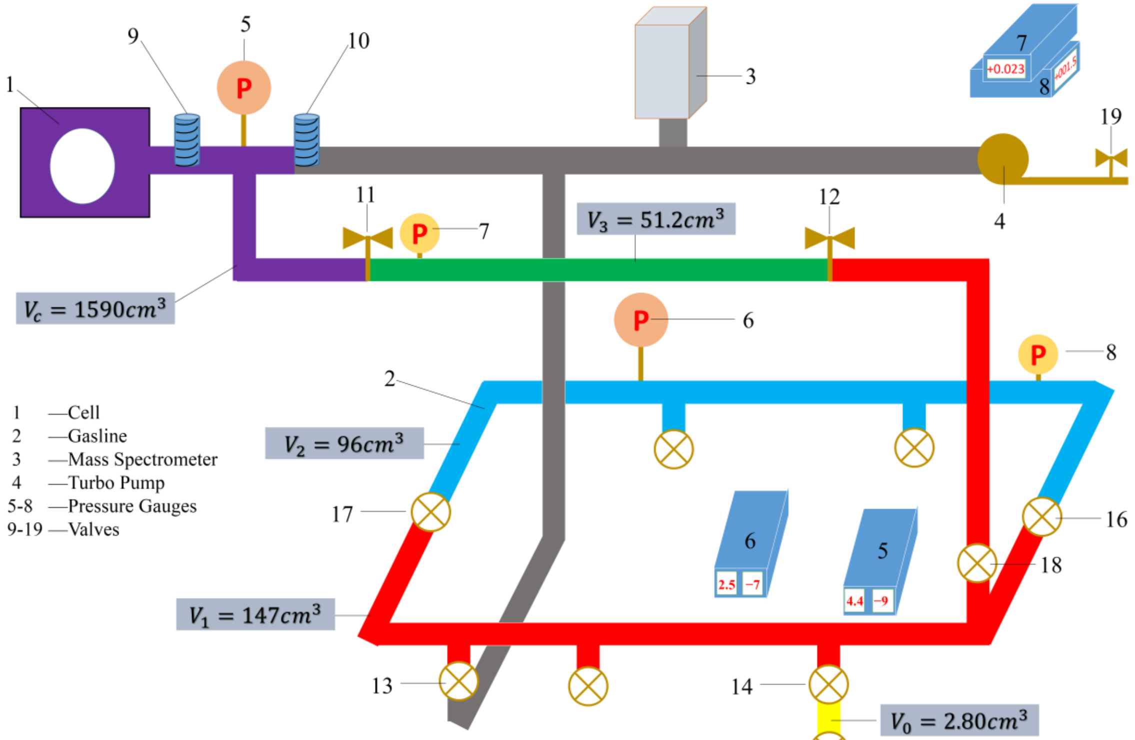

Figure 2.1. Schematic diagram of the high vacuum system.

The stainless-steel high vacuum system employed in this research is illustrated as Figure 2.1. The system was continuously pumped by a turbo pump followed by a mechanical pump. A base pressure of ~ 2.0×10^{-9} Torr can be achieved by baking out at 100 – 120 °C for ~ 30 hours. The pressure of the vacuum system was monitored by two cold cathode gauges (MKS series 423 I-MAG) and two Baratron gauges. The pressure of the chamber was measured by cold cathode gauge 5 whose output was continuously recorded by a LabVIEW program with an NI-DAQ (National Instruments Data Acquisition) device and the pressure of the gas line was measured by cold cathode gauge 6. Gas bulbs with research grade (≥ 99.99%) gas such as O_2, H_2, CO, He etc. were connected to the gas line through valve 14. Gases were introduced into the gas line by operating valves 14 and 15, and the gas pressure in the gas line were monitored by Baratron gauge 8 (scale of 1000.0 Torr). A gas control module which has a volume $V_3 = 51.2\ \text{cm}^3$ with its pressure measured by Baratron gauge 7 (scale of 1.000 Torr) was used to control the amount of gas molecules dosed or the target cell pressure. The calibration of the volumes was described before.[1] A quadrupole mass spectrometer (SRS RGA 200) was installed between the chamber and the turbo pump to analyze the purity of gases and detect molecules desorbed from the TiO_2 sample.

2.2 High Vacuum Chamber

Figure 2.2 shows the structure of the high vacuum chamber. The cell of the high vacuum chamber is a stainless-steel cube with six 4.5-inch ports. Two CaF_2 transparent windows were installed to two opposite horizontal ports of the cell allowing both UV and visible light to transmit. As shown in Figure 2.3, the CaF_2 windows allow more than 90% of light from 300 nm to 900 nm to pass through. An XYZ three-dimensional manipulator was connected to the top of the cell which allows precise adjustment of the sample position with an accuracy of 0.001 inches horizontally and 0.04 inches vertically. A reentrant Dewar was attached to the manipulator to provide liquid nitrogen cooling for the sample. A feedthrough with two copper leads conducting electricity and two K-type thermocouple wires was attached to the bottom of the reentrant Dewar. An L-shape sample holder made of oxygen-free high-conductivity (OFHC) copper was attached to the two copper leads of the feedthrough. The L shape was designed to bring the sample close to the CaF_2 window because the PL intensity imaging into the detector is very sensitive to the sample position.[1]

The TiO_2 powdered sample was pressed at 6000 psi onto a tungsten grid containing ~ 0.022 cm × 0.022 cm square openings as a circular disk with a diameter of ~ 7 mm and a thickness of ~ 0.0095 cm. The tungsten grid with the TiO_2 sample was clamped to the OFHC copper sample holder. A K-type thermocouple was spot-welded onto the tungsten grid at the periphery of the sample to measure the sample temperature. The sample temperature could be precisely controlled within 0.1 K in the range of 81 – 1000 K by adjusting the amount of electrical heating across the tungsten grid using a LabVIEW program which implements a proportional-integral-derivative (PID) control algorithm.

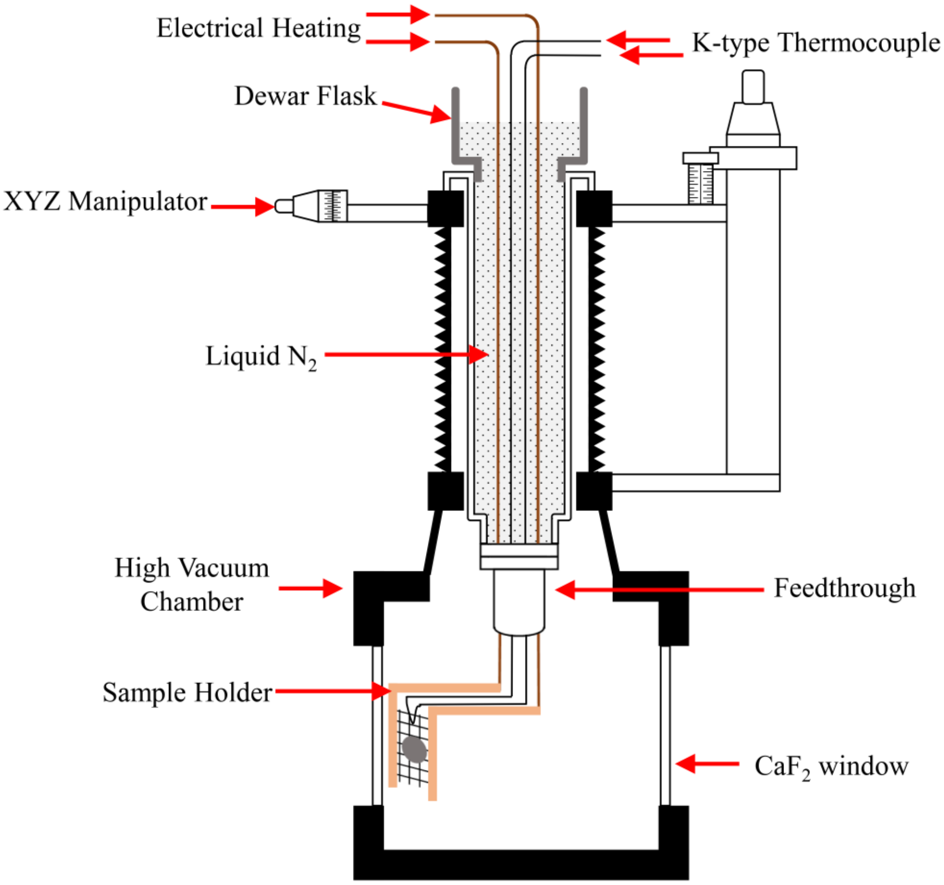

Figure 2.2. Schematic diagram of the high vacuum chamber

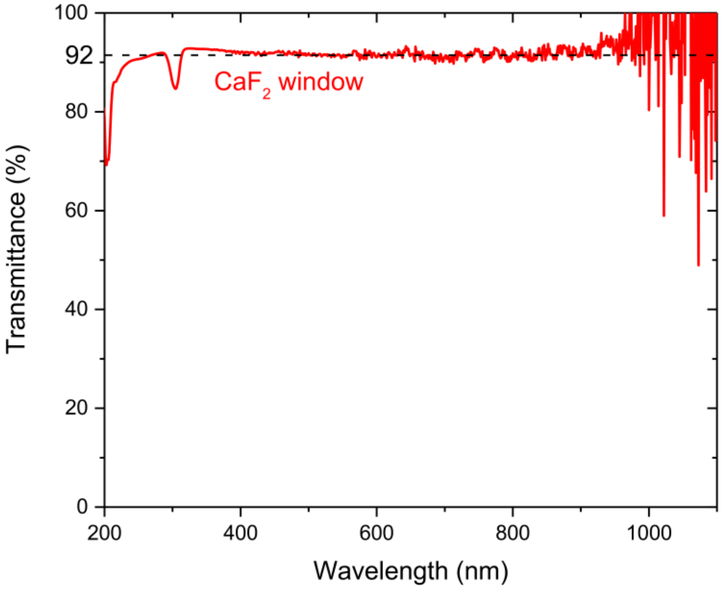

Figure 2.3. Transparency of CaF_2 window

2.3 PL spectrometer

PL of TiO_2 was collected by a Perkin Elmer FL 55S florescence spectrometer placed close to the high vacuum chamber. The spectrometer was equipped with a Xe light source and a photomultiplier tube with a detecting range from 200 to 900 nm. The excitation of TiO_2 (bandgap energy of ~ 3.2 eV, corresponding to 388 nm) was by 320 nm UV irradiation selected by gratings installed inside the spectrometer and an additional 320 nm bandpass filter. A 390 nm cutoff filter was used to reduce the interreference of PL intensity due to irradiation light reflected by the CaF_2 window.

2.4 PL of TiO_2

The TiO_2 sample examined in this study was mainly the widely used P25 powder (Evonik Industries, formerly Degussa) if not otherwise specified. The P25 TiO_2 nanoparticle is a mixture of ~ 75 % of the anatase phase with a mean size of 85 nm and ~

25 % of the rutile phase with a mean size of 25 nm.[2] Pure anatase TiO_2 (30 nm diameter, > 99.98 % purity, US Research Nanomaterials Inc.) and pure rutile TiO_2 (30 nm diameter, > 99.9 % purity, US Research Nanomaterials Inc.) were also studied in order to understand the origin of PL from P25. X-ray diffraction (XRD) patterns of TiO_2 samples were collected using a Panalytical X'Pert Pro MPD diffractormeter to confirm the lattice structure and phase fraction. The TiO_2 samples were usually pretreated first by heating to 680 K in ~ 0.7 Torr O_2 for 40 min in order to oxidize the organic ligands on TiO_2 nanoparticle surfaces. Then the cell was pumped out for 10 min at 680 K and then cooled down to ~ 84 K to collected PL spectrum. The parameters including time, temperature, and pressure may change according to experiment conducted and are specified in each experiment.

Figure 2.4 (A) shows the PL emission spectra of P25, pure anatase, and pure rutile samples at 84 K in vacuum. The 390 nm peak is due to a reflection of the 320 nm exciting light off the CaF_2 window which enters the PL spectrometer at an oblique angle. The 390-nm peak is invariant among different measurements taken on the same sample and therefore can be neglected (refer to figures in following chapters). The 390 nm peaks seen in Figure 2.4 (A) vary because the samples were put into the chamber separately such that the geometries between the chamber and the PL spectrometer varied slightly. The 780 nm peak is a second order feature of the 390 nm reflection because the PL spectrometer uses gratings to filter light beams with different wavelengths. The PL emission from P25 samples is centered at ~525 nm, which is the same as the emission from the pure anatase samples. There is no observable PL emission from the pure rutile sample under our experimental conditions, although some researchers reported a PL emission from rutile at ~ 835 nm.[3]

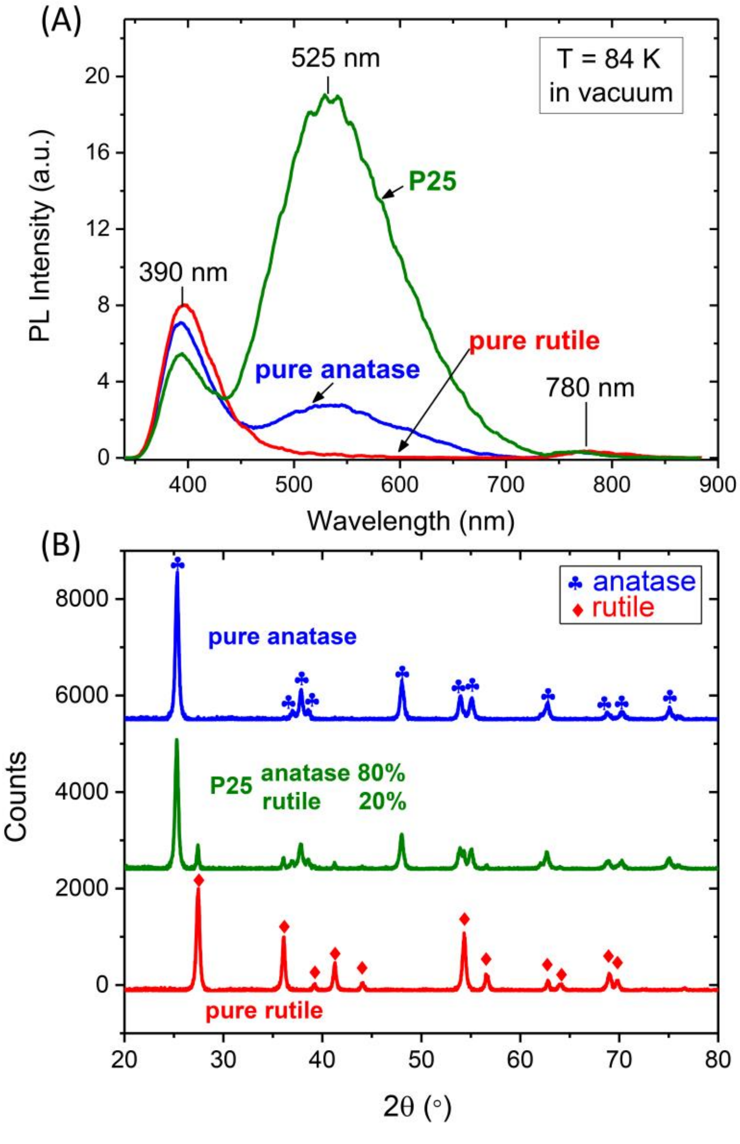

Figure 2.4. (A) PL emission spectra from P25, pure anatase, and pure rutile samples; (B) XRD patterns of P25, pure anatase, and pure rutile samples.[4]

Figure 2.4 (B), which shows the XRD patterns of P25, pure anatase, and pure rutile samples, confirms that the anatase and rutile samples are pure with no phase contamination and that P25 is a mixture of anatase and rutile (80% and 20% respectively based on calculations using measured XRD peak intensities, which is close to the nominal 75% and 25% ratio reported). These findings indicate that the observed PL emission at ~ 525 nm from P25 samples is from the anatase phase of TiO_2 in P25. Thus, the PL of P25 serves as a method to study oxygen adsorption on the band bending change of anatase TiO_2, which is considered more active as a photocatalyst.

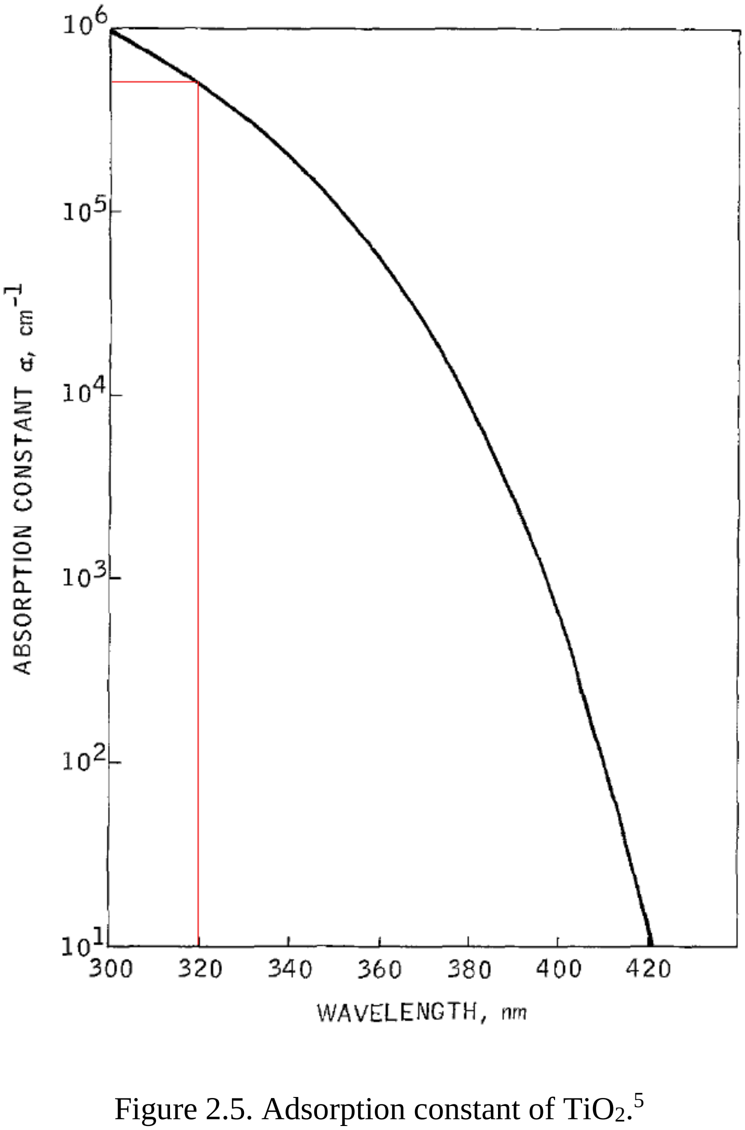

Figure 2.5. Adsorption constant of TiO_2.[5]

Figure 2.5 shows the adsorption constant of TiO_2 reported by Ghosh and Maruska[5]. The adsorption constant at 320 nm is ~ 7×10^5 cm^{-1}, thus the penetration depth which is the inverse of the adsorption constant is ~ 14 nm. Although the penetration depth varies from different reports, it is within the range of 15 – 25 nm. Considering that the anatase TiO_2 particle size in P25 is 85 nm, it is reasonable to assume that the PL emission comes from the first layer of TiO_2, although there are ~ 1000 layers of TiO_2 in the pressed TiO_2 sample.

References

1. Stevanovic, A. Electron and Hole Behavior in Powered TiO_2 - Photoluminescence and Infrared Studies. University of Virginia, Charlottesville, 2014.
2. Ohno, T.; Sarukawa, K.; Tokieda, K.; Matsumura, M., Morphology of a TiO_2 Photocatalyst (Degussa, P-25) Consisting of Anatase and Rutile Crystalline Phases. *Journal of Catalysis* **2001**, *203*, 82-86.
3. Shi, J. Y.; Chen, J.; Feng, Z. C.; Chen, T.; Lian, Y. X.; Wang, X. L.; Li, C., Photoluminescence Characteristics of TiO_2 and Their Relationship to the Photoassisted Reaction of Water/Methanol Mixture. *Journal of Physical Chemistry C* **2007**, *111*, 693-699.
4. Ma, S. L.; Reish, M. E.; Zhang, Z.; Harrison, I.; Yates, J. T., Anatase-Selective Photoluminescence Spectroscopy of P25 TiO_2 Nanoparticles: Different Effects of Oxygen Adsorption on the Band Bending of Anatase. *Journal of Physical Chemistry C* **2017**, *121*, 1263-1271.
5. Ghosh, A. K.; Maruska, H. P., Photoelectrolysis of Water in Sunlight with Sensitized Semiconductor Electrodes. *Journal of the Electrochemical Society* **1977**, *124*, 1516-1522.

3 Effect of Single–Walled Carbon Nanotubes on Photoexcited Electron Hopping between TiO_2 Particles

(modified from *J. Phys. Chem. C*, **2014**, 118(41): 23614-23620)

Abstract

Photoluminescence (PL) spectroscopy was employed to study the effect of embedded single-walled carbon nanotubes (SWNTs) on charge transport in powdered TiO_2. It was found that 1-5wt% SWNTs mixed with TiO_2 accept electrons from photoexcited TiO_2 and quench the PL intensity from TiO_2. The PL quenching efficiency by SWNTs is proportional to the fraction of TiO_2 particles which experience electrical contact with SWNTs. Ultraviolet light was used to cause surface charging of the SWNT/TiO_2 sample and the charging/discharging rate was measured using PL. The PL charging/discharging rate of all SWNT/TiO_2 mixtures is identical to that of pure TiO_2, indicating that SWNTs only accept photoexcited electron from TiO_2 but do not transport electrons under conditions of the experiment. This is due to the effect of positively charged TiO_2 particles which immobilize the photoexcited electrons transferred to SWNTs at the interface between first-layer TiO_2 and SWNTs, inhibiting charge transport through SWNT channels. The inhibition of charge transport through SWNTs may be removed by applying an external voltage to overcome the built-in electric field which prevents current flow in the SWNTs.

3.1 Introduction

In the optimization of inorganic photovoltaic devices, a major challenge is to enhance the rate of charge transport between semiconductor particles to improve the efficiency of collecting photogenerated electrons by the back electrode.[1] The charge transport phenomenon in metal-oxide semiconductor particles (TiO_2, ZnO and others) has been extensively studied due to the capability of these materials to be photo-activated by sunlight.[2-6] Upon absorption of the light from the solar spectrum with energy higher than the band gap energy ($E_{bg} \sim 3$ eV), these metal-oxide semiconductors can be electronically excited. The charge transport induced by ultraviolet irradiation has been studied by surface photovoltage spectroscopy[7-9], photoluminescence spectroscopy[10-12] and modeling[13-15]. It was found that photoexcited electrons in the semiconductor particle can move freely in the conduction band or become trapped at a defect site. For such trapped electrons, hopping from a site to a neighbor site or from a particle to a neighbor particle takes place. We previously demonstrated that continuous UV irradiation on n-type TiO_2 electrically charges the TiO_2 powder by distributing photoexcited electrons deep into the TiO_2 powder bed causing the surface photovoltage on the exterior geometric surface of the compressed disk to become more positive; upward bent bands therefore flatten as holes migrate to the TiO_2 surface. However, in the dark, the powder discharges as negative charge relaxes back to the TiO_2 surface; the charged capacitor discharges by the slow electron hopping process partially restoring negative surface charge.[16] These measurements made by studies of the time dependence of photoluminescence from TiO_2 provide a useful method for measuring charge transport between TiO_2 particles in a powdered configuration. The relaxation of negative charge back to the surface is found to be a very slow process on a time scale of hundreds of seconds at 110 K in contrast to *in situ* transport processes within a single TiO_2 particle which occur on a picosecond time scale in crystalline TiO_2.[17]

One way proposed to amplify the rate of charge transport between TiO_2 particles is to link the semiconductor particles together with highly conjugated molecules. The addition of these molecules is expected to enhance electrical conductance between TiO_2 particles. The unique electronic properties of single-walled carbon nanotubes, a highly conjugated molecule with enormous specific surface area, suggest that SWNTs are good candidates for enhancement of the electrical conductance between TiO_2 particles. The conductivity of a SWNT is related to electron delocalization through its conjugated sp^2 orbitals and thus, this molecule should be capable of withdrawing photoexcited charges from TiO_2 particles and then possibly assisting in charge conduction between particles.[18-19]

Studies have shown that SWNT molecules are expected to behave as acceptor molecules for TiO_2 electrons which have been excited by UV light into the TiO_2 conduction band (CB) due to the lower energy of the SWNT-CB compared to TiO_2.[20-21] The experimentally measured charge carrier mobility in SWNTs is ~ 10^8 m^2 V^{-1} s^{-1} at room temperature[22] and is strongly governed by the density of defects and by electron scattering by phonons in the material[23]. The carrier mobility controlled by electron hopping between TiO_2 particles[16] is ~ 10^{-10} m^2 V^{-1} s^{-1}, ~18 orders of magnitude below SWNT mobility, suggesting that vastly improved conduction should be achieved by mixing SWNTs into TiO_2. It was reported that SWNTs and other fullerenes enhance interparticle conduction between TiO_2 particles. Kamat et al.[24-26] studied several nanostructures where molecules such as SWNT, C_{60} and graphene oxide were employed to link TiO_2 semiconductor particles together. Their findings, measuring the photocurrent of the TiO_2 that contained SWNTs, show that carbon nanotube molecules act as electron acceptors and also as conductors as they are capable of withdrawing charge and transporting it away from TiO_2 particles. It should be pointed out that Kamat's studies are carried out in solutions (ethanol or toluene) with an applied electric field while our studies involve SWNT/TiO_2 mixtures which have been mechanically prepared and then processed at elevated temperatures in high vacuum, under conditions where no external electric field has been applied.

We present experiments like that shown in Figure 3.1 that involve a new photoluminescence (PL) decay method developed in our laboratory to measure the enhancement of particle-particle conductivity in vacuum, under well-controlled surface conditions, employing different fractions of SWNTs to explore their electron accepting and conducting abilities when mixed with TiO_2 particles.[16] This method involves charging of the TiO_2 powder and SWNT/TiO_2 mixture by continuous UV irradiation at 3.88 eV which causes a redistribution of electrons within the TiO_2 powder bed. Changes in surface photovoltage are observed due to electron transfer away from the TiO_2 sample, bending the bands downward and decreasing the depletion layer thickness. An increase of the PL intensity of TiO_2 is shown in Figure 3.1 where a decrease in the depletion layer thickness causes an increase in the active depth for PL emission. It is noted here that due to the limited depth of UV penetration (~ 20 nm), photoexcitation occurs only in TiO_2 particles on the very outmost surface of the powder which consists of TiO_2 particles of 50 nm nominal size. In contrast to charging by UV light, upon discontinuation of irradiation, the distributed electrons tend to return back to the surface, partially reducing the surface photovoltage as observed by a decrease in the PL intensity as shown in Figure 3.1. By employing this method, we are able to distinguish between electron acceptor and electron conducting properties of a linker molecule. We find that photoluminescence due to electron-hole recombination in TiO_2 is suppressed as the concentration of SWNTs increases, showing that SWNTs possess electron acceptor capabilities in agreement with the literature. We postulate that the suppression of PL by SWNTs is simply related to the fraction of TiO_2 particles in the first layer which contact a SWNT and which donate charge to the contacting nanotube. In contrast to the electron acceptor property of SWNTs, it was also found that incorporation of 1-5 wt% of SWNTs produced no change in the PL development rate upon continuous UV irradiation and that the discharge rate is also not influenced by SWNTs, showing that electron conductance in SWNT/TiO_2 mixtures is the same as in pure TiO_2.

The effect of adsorbed oxygen and other species such as organic solvent molecules and water solvent can be neglected in our experiments as all work is done under high vacuum conditions.

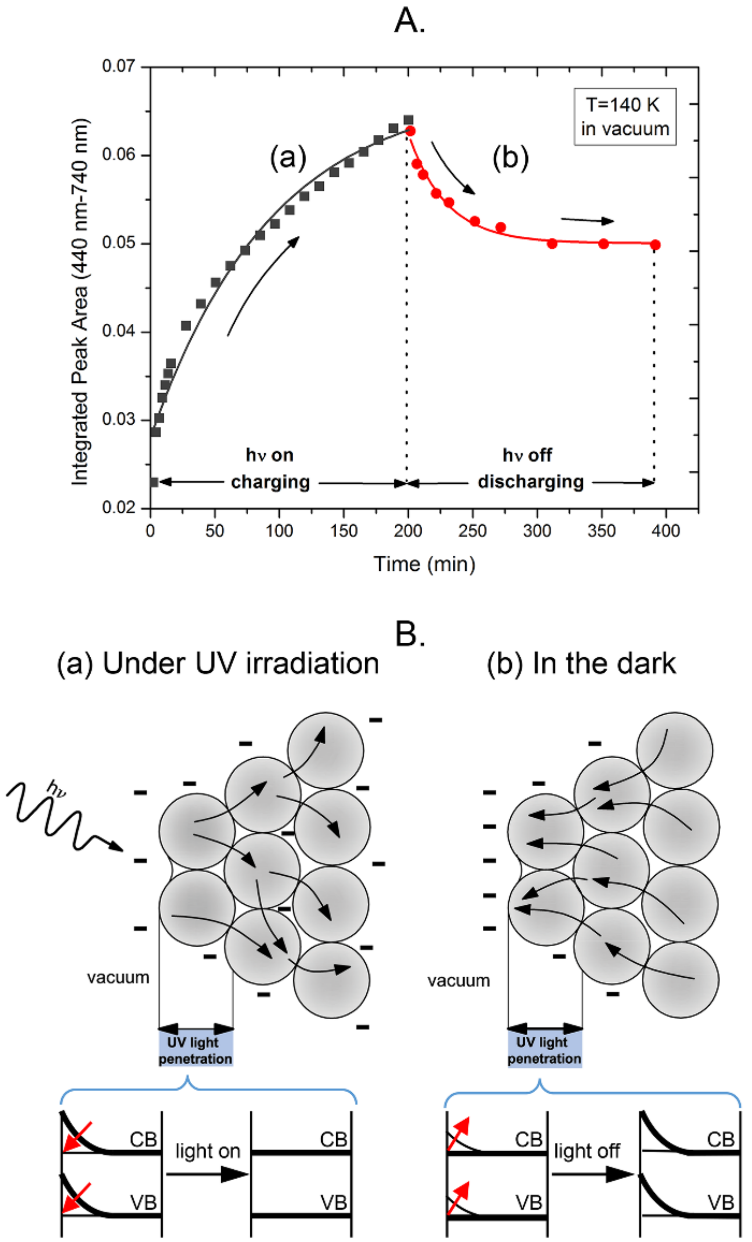

Figure 3.1. A. Photoluminescence development (a) during continuous irradiation and (b) in the dark; B. Schematic of charging the pure TiO_2 powder particles on the surface by continuous irradiation which induces charge redistribution toward a flat-band condition; discharging in the dark restores upward band bending. Discharging by electron hopping between TiO_2 particles is temperature dependent with an activation energy of 15 meV.

Band bending effects are confined in the TiO_2 particles at the surface of the powder deposit. Taken from ref. 16.

3.2 Experimental methods

The instrument used in this study was described in chapter 2. The SWNT/TiO_2 composites were synthesized by mixing a mixture of metallic (60 %) and semiconducting (40%) SWNTs (South West Nanotechnology) and TiO_2 powder (Evonik Industries, formerly Degussa P-25). Typically, 0.1 g of SWNTs was dispersed into deionized water and sonicated for 10 minutes. To obtain composites with different mass ratios of SWNTs to TiO_2, various amounts of TiO_2 were added into the SWNT-water slurry and then sonicated for another 10 minutes to better disperse the nanotubes in the TiO_2 slurry. The slurry was dried under vigorous stirring at 353 K and dried SWNT/TiO_2 mixtures with 1:100, 3:100, and 5:100 weight ratios were produced. Also, the reference sample, pure TiO_2, was suspended in deionized water, sonicated, and dried at 353 K. The pure TiO_2 sample was pressed into the upper section of the grid while the SWNT/TiO_2 samples were pressed into the lower section. The two samples were studied on the same grid under identical conditions, by adjusting the vertical position of the grid, and the pure TiO_2 samples serve as an internal standard in each experiment.

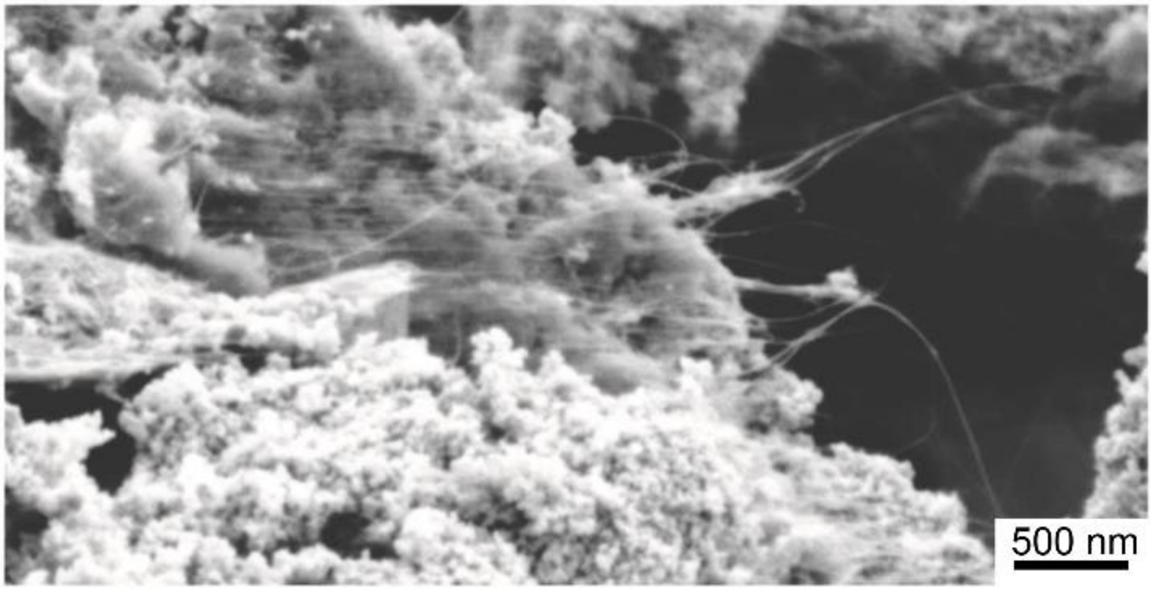

Figure 3.2. SEM micrograph of 5 wt% SWNT/TiO_2 composite.

Before PL and IR measurements, the samples were heated in vacuum to 680 K in 1.0 Torr of research-grade O_2 (99.99%) for 40 min to remove surface impurities and to partially oxidize the sample. The sample was then evacuated at 680 K for 10 min to reach high vacuum, and then cooled down to 84 K for PL and IR measurements.

An electron micrograph of the SWNT/TiO_2 composite is shown in Figure 3.2 for the 5% mixture. It may be seen that the SWNTs exist primarily in bundles, bonded together by van der Waals forces, as they interact with multiple TiO_2 particles.

3.3 Experimental results

Figure 3.3 shows the PL intensity of TiO_2 when different concentrations of SWNTs are mixed together with TiO_2. The PL peak intensity of the clean TiO_2 powder reference (red spectrum) is compared with PL emission of TiO_2 powders that contain (A) 1 %; (B) 3 % and (C) 5 % of SWNTs by weight (gray spectra). All spectra show the same PL emission peak at ~ 525 nm (2.36 eV) at 84 K. The small feature at 390 nm is an artifact that originates from the constant reflection of a component of the incident UV beam off the CaF_2 window and tungsten grid and this is constant throughout all experiments including those made with the clean grid and therefore can be disregarded. The mixed SWNT/TiO_2 composites (1 - 5 % SWNTs) show a decrease in PL intensity to 82 %, 55 % and 40 % respectively (as shown in Figure 3.3 A – C), compared to the PL intensity of the pure TiO_2 sample. The decrease in PL intensity of TiO_2 indicates that a fraction of TiO_2 particles are affected by contact with SWNTs as SWNTs efficiently accept electrons from photoexcited TiO_2 particles. The fractional decrease in PL is a measure of the fraction of TiO_2 particles in the first layer which experience an electrical contact with a SWNT and scales roughly with fraction of SWNTs in the mixture. The withdrawal of photogenerated electrons by SWNTs reduces the magnitude of the electron-hole recombination rate in TiO_2 and hence the photoluminescence intensity. Because of the relatively large quenching effect on PL intensity by a small fraction of SWNT and the small penetration depth of UV irradiation (~ 25 nm), an alternate model involving light absorption by the SWNTs to reduce the PL yield is not validated.

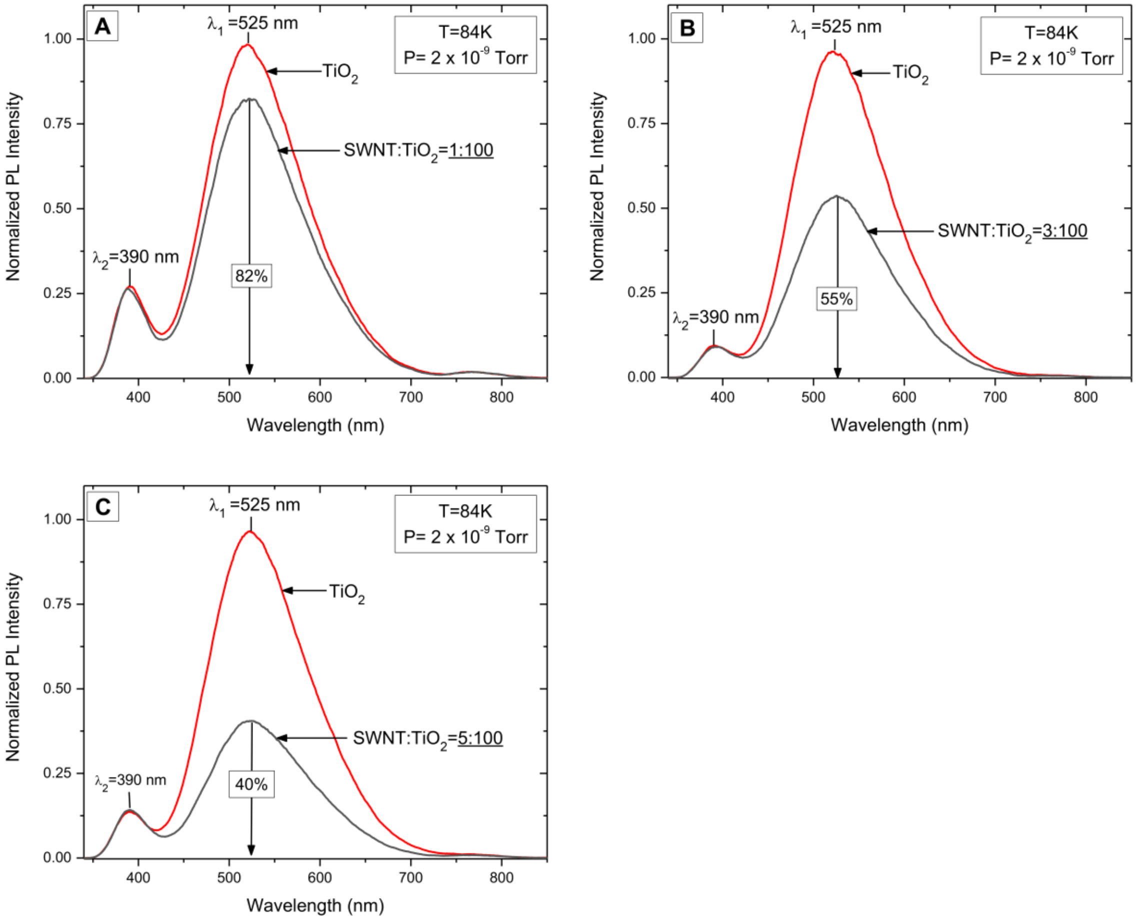

Figure 3.3. Photoluminescence spectra of pure TiO_2 (red curves) and SWNT/TiO_2 composites (gray curves). The mixed SWNT/TiO_2 composites contain: (A) 1 %; (B) 3 % and (C) 5 % of SWNTs in TiO_2 powder. All samples show an emission maximum at ~ 525 nm upon excitation by 3.88 eV (320 nm) irradiation in vacuum at 84 K. Spectra from TiO_2 that contain SWNTs are normalized to the spectrum of the clean TiO_2 reference sample present in each experiment; the two measurements are carried out by moving the grid vertically in the cell.

Figure 3.4 shows the charging and discharging rates for several TiO_2 samples that contain 0 %, 1 %, 3 %, and 5 % of SWNTs at 110 K under vacuum. Our previous finding[16] indicated that electrons show hopping mobility through TiO_2 at this temperature where electron hopping occurs with an activation energy of 0.015 eV over the temperature range from 84 to 140 K. During continuous UV irradiation with 3.88 eV photons for 185 min in vacuum, the PL intensity of pure TiO_2 and all SWNT/TiO_2 composites increases with very similar PL development rates (charging rates) related to the increase of surface photovoltage on first-layer TiO_2 particles in the powdered samples. When the UV irradiation is discontinued, the PL intensity immediately begins to decrease as the electron hopping direction is reversed. These measurements show that, in SWNT/TiO_2 samples, the SWNTs act as electron acceptors by reducing the PL intensity; in comparison, the SWNT/TiO_2 samples exhibit the same charging/discharging rates as pure TiO_2 powder at a constant temperature. The inset in Figure 3.4 shows the charging/discharging rates as the concentration of SWNTs increases. The average charging rate at 110 K is $k_c \sim 1.4 \times 10^{-4}\ s^{-1}$, while the average discharging rate at 110 K is $k_d \sim 3.4 \times 10^{-4}\ s^{-1}$. This result implies that SWNTs which connect TiO_2 particles accept electrons and therefore interfere with electron-hole recombination in the outermost particles of TiO_2, but do not have any measurable effect on the rate of electrical conduction between TiO_2 particles either during charging or discharging. Since the time constants for charging are very similar for all samples, we show only one charging curve (gray squares) in Figure 3.4 which is an average of all charging curves.

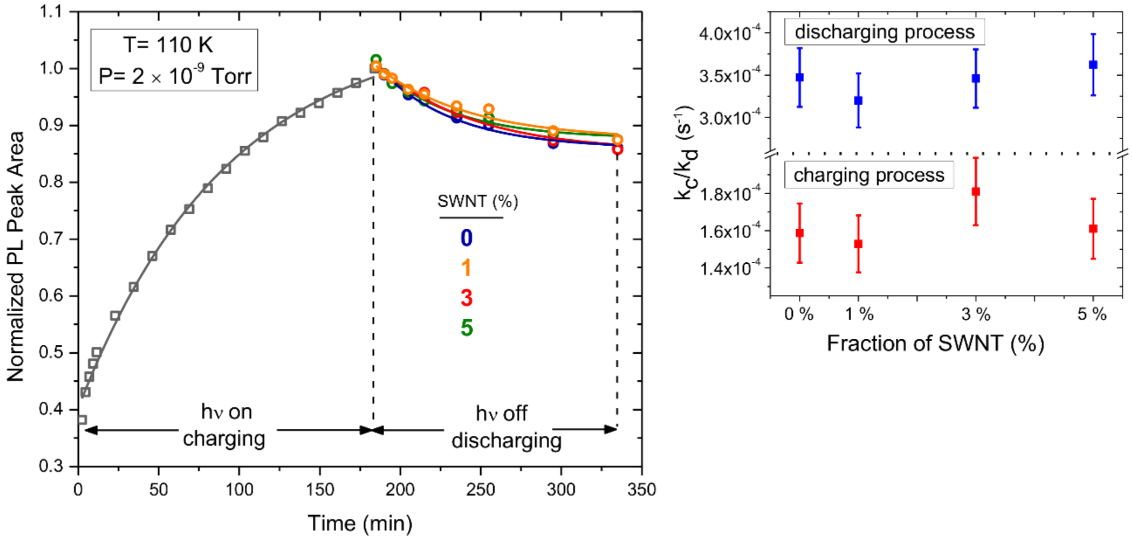

Figure 3.4. Charging curve (gray squares) is obtained upon continuous UV irradiation for 185 min in vacuum. Discharging curves for clean TiO_2 (blue), 1 wt% SWNT (orange), 3 wt% SWNT (red), and 5 wt% SWNT (green) upon discontinuation of UV light for 150 min. Inset shows the rates for both charging (red squares) and discharging (blue squares) processes. All data were collected at 110 K in vacuum. The measurements of the discharging rates are not influenced significantly by the periodic application of UV light for a short time to measure the PL intensity.

3.4 Discussion

3.4.1 Photoexcited electron transfer from TiO_2 to SWNT: PL quenching

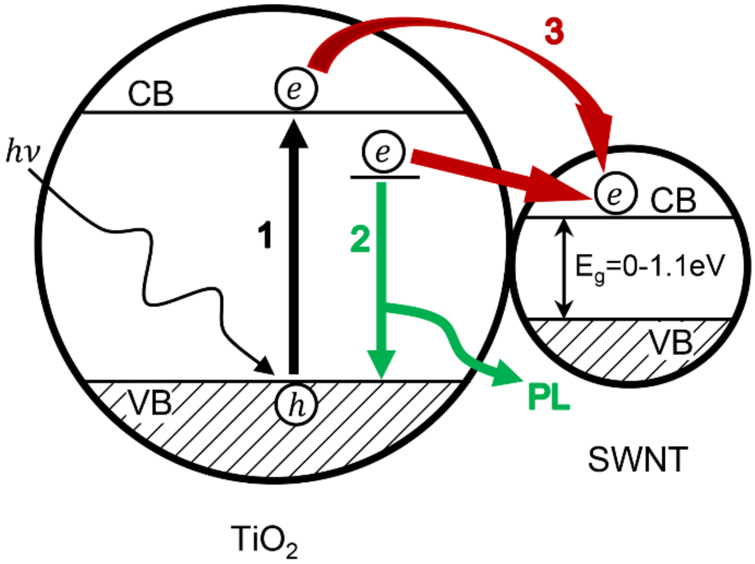

Figure 3.5. Schematic diagram of the proposed mechanism for electron transfer from TiO_2 to a SWNT. The electrons from the valence band in TiO_2 are promoted to the conduction band by absorption of photon energy of $h\nu \geq 3.2$ eV (process 1); then, they either relax to a TiO_2 defect site recombining with a hole and emitting PL light (process 2) or they transfer to an adjacent SWNT (process 3), where PL at 525 nm does not occur. The SWNT band gap ranging from 0 to 1.1 eV represents both metallic and semiconducting SWNTs.

As shown in Figure 3.5, the energy of the conduction band of TiO_2 when compared to metallic or semiconducting SWNTs (with band gap ranging from 0 to 1.1 eV) is always higher than the energy of the SWNT conduction band which results in energetically favorable transfer of photoexcited electrons from TiO_2 to the conduction band of SWNTs[20-21]. Upon excitation of TiO_2 by UV irradiation, photogenerated electrons in the TiO_2 conduction band of TiO_2 can evolve in one of the following ways: (1) de-excite to the bottom of the TiO_2 conduction band and then quickly find a defect site within TiO_2 where they can recombine with a hole, emitting PL light or heat;[27-28] or (2) de-excite by transferring to the lower-energy conduction band of a carbon nanotube resulting in suppressed PL emission from TiO_2 particles. We observe that SWNTs behave as electron acceptor molecules. All samples which contained different fractions of SWNT in TiO_2 powder show approximately proportional suppression of PL intensity relative to the pure TiO_2 powder.

In this study, the UV penetration depth is only ~ 20 nm[10, 29-31], which is smaller than the average TiO_2 particle size, ~ 50 nm. Therefore, the PL signal only comes from the first layer of TiO_2 particles. A fractional reduction of PL intensity observed is interpreted to be the fraction of first-layer TiO_2 particles which make effective electrical contact with an electron-acceptor SWNT molecule.

3.4.2 Electron behavior in SWNTs and TiO_2

During continuous UV irradiation (Figure 3.4) of both pure TiO_2 and SWNT/TiO_2 samples at 110 K, we observed that charging rates for samples that contained SWNTs do not differ from the charging rate of a pure TiO_2 sample. Here, the average charging rate is $k_c = 1.4 \times 10^{-4}\ s^{-1}$. This indicates that the SWNTs have no influence on the charge hopping between TiO_2 particles during irradiation. In addition, upon discontinuation of UV irradiation, the discharging rates for all SWNT/TiO_2 samples and pure TiO_2 are also similar to an average rate constant $k_d = 3.4 \times 10^{-4}\ s^{-1}$. The increase in the SWNT fraction (from 1% to 5%) in powdered samples has no influence on the charging/discharging rate of the TiO_2 powder. This result implies that SWNTs in the experimental configuration employed here show only electron accepting properties but do not influence the charge conductance between TiO_2 particles.

We propose a schematic electron immobilization model shown in Figure 3.6 to explain the physics causing SWNTs to produce no effect on the charging/discharging rate of TiO_2. As shown in Figure 3.6 (A), there are no photoexcited electrons in either TiO_2 or SWNTs in the dark. Photoexcited electrons are generated in the first-layer of TiO_2 particles when exposed to UV irradiation. A fraction of the photoexcited electrons are injected from the first-layer of TiO_2 to electron acceptor SWNTs, causing charge separation at the SWNT/TiO_2 interface as the SWNTs become negatively charged leaving positive holes behind in TiO_2 particles. A fraction of the photoexcited electrons in the first-layer of TiO_2 hop to the non-photoexcited TiO_2 particles in the interior of the sample due to the electron diffusion caused by the photoexcited electron density gradient.[16] Similar ideas have been proposed in which a gradient of Fermi level between interconnecting TiO_2 particles is postulated to drive electrons from one TiO_2 particle to another.[15, 32] This electron hopping process into the interior of the TiO_2 powder bed also contributes to charge separation. The tungsten grid sample holder can be treated as an insulator isolated from the TiO_2 because of its thick oxide coating.[33] The separated positive charges in the first-layer of photoexcited TiO_2 and negative charges in SWNTs cannot be neutralized by an external connection to ground. In addition, there is no effect by chemical species since all work was done in high vacuum. As a result, the positive and negative charges in TiO_2 and SWNTs remain separate and a large electric field builds up at the interface between SWNTs and first-layer of photoexcited TiO_2. A smaller electric field is produced in the TiO_2 particles, which tends to pull the separated electrons back to the first-layer of TiO_2 particles.

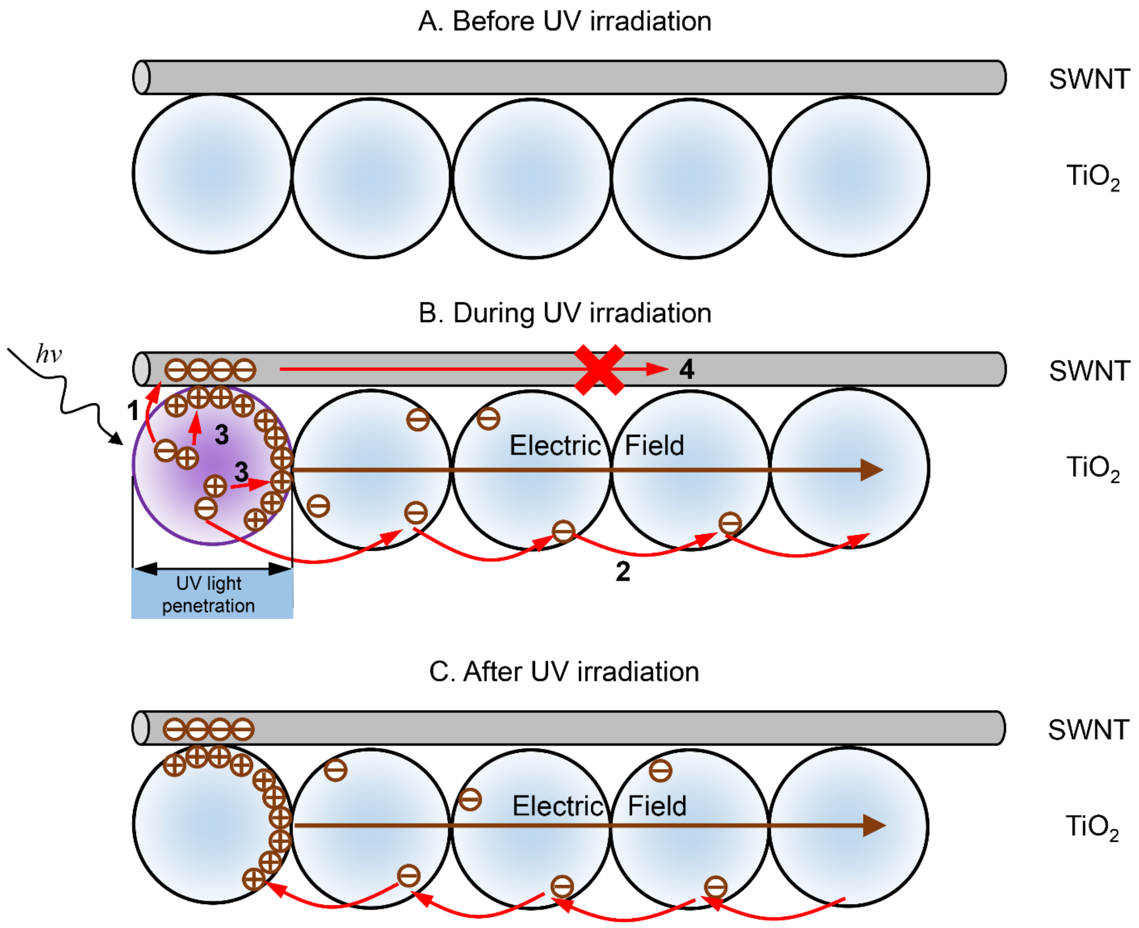

Figure 3.6. Schematic diagram for charge transport in SWNT/TiO_2 composite. (A) Before UV irradiation, there are no photoexcited electrons in either SWNTs or TiO_2. (B) During UV irradiation. (1) Photoexcited electron injection occurs into SWNTs; (2) Electron hopping occurs through TiO_2 particles; (3) Hole migration occurs to TiO_2 surfaces due to band bending in the outermost TiO_2 particles (see Figure 3.1). A positive outward electric field builds up as the positive charges accumulate at the first-layer TiO_2 surface; (4) Electron transport in SWNTs does not occur as electrons injected into SWNTs are immobilized by the built-in electric field at the interface between the first-layer TiO_2 particles and SWNTs. (C) When UV irradiation is off, electrons are attracted by the positive charged first-layer TiO_2 particles and they hop back through TiO_2. The main

point is that the electric field induced at the interface between first-layer TiO_2 and SWNTs prevents electron transport through the SWNTs both during irradiation and after. The charging and discharging of the TiO_2 capacitor occurs in the absence of electron transport in the embedded SWNT molecules.

During UV irradiation, the electron transport behavior in both SWNTs and TiO_2 is determined by two main factors: (1) forward electron diffusion due to the electron density gradient caused by photoexcitation in the first-layer of TiO_2 particles; and (2) backward electron drift due to the built-in electric field caused by separated positive and negative charges. Combining the diffusion and drift effects, the excess negative electrons in SWNTs finally establish an equilibrium distribution along the depth through the sample disk, controlled by efficient screening of the electric field along the SWNTs. The screening of the electric field along the SWNTs, causing a short range for the equilibrium distribution of the excess negative electrons in SWNTs, is very similar in principle to the shielded Coulomb potential caused by an ionic atmosphere in ionic solution (the Debye-Hückel theory). The excess negative electron distribution along SWNTs is described by an exponential decay as (more details in Appendix C)[34]

$$n = Ae^{-z/\lambda} \tag{3.1}$$

where n is the excess electron density, A is the pre-exponential factor to be determined by the total number of excess electrons in SWNTs, z is the depth across the sample disk, and λ is the Debye screening length which can be described as

$$\lambda = \sqrt{\frac{\varepsilon_0 \varepsilon_r k_B T}{Ne^2}} \tag{3.2}$$

in which ε_0 is the vacuum permittivity, ε_r is the relative permittivity, k_B is the Boltzmann constant, T is the temperature, N is the intrinsic charge carrier density in SWNTs and e is the electron charge. The above analysis also applies to excess negative electrons in the non-photoexcited TiO_2 particles if we neglect the complex electron diffusion mechanism for a trap-filling model[13-14] and treat it just as simple diffusion which can be described by Fick's laws.

Equation (3.2) shows that the screening length is inversely proportional to the square root of the intrinsic charge carrier density N of the materials. The intrinsic free electron density of SWNTs [21, 35], ~ 10^{21} cm^{-3}, is much higher than that of TiO_2 [36], which is ~ 10^{17} cm^{-3}. Therefore, the screening length in SWNTs is much shorter than in TiO_2 and the excess electron distribution in SWNTs is highly converged at the contact between the first-layer TiO_2 and SWNTs, as shown in Figure 3.7. As a result, the photoexcited excess electrons injected into SWNTs are immobilized at the interface between the first-layer TiO_2 and SWNTs by the built-in electric field, inhibiting electron transport through SWNT channels, as shown in Figure 3.6 (B) (as process 4). However, due to the extended screening length in TiO_2 particles, electron hopping through TiO_2 particles still occurs. The different screening length in SWNTs and TiO_2 caused by the highly different intrinsic charge carrier density causes SWNT/TiO_2 mixtures to have identical charging/discharging rates compared to pure TiO_2 as electrons in SWNTs remain immobilized and to therefore exhibit similar kinetics for PL development and PL decay.

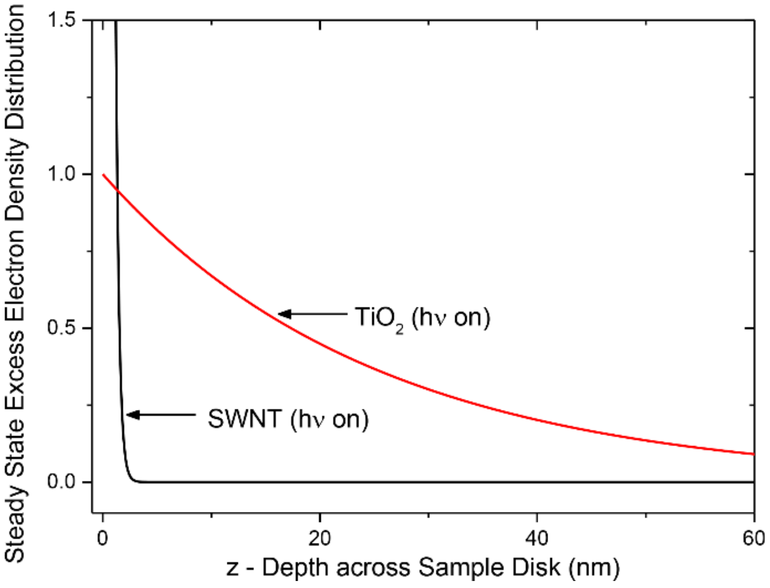

Figure 3.7. Steady state excess electron density distribution along the depth across the sample disk during photoexcitation using equations (1) and (2) with a relative permittivity of 100. The excess electrons in SWNTs are highly converged in a region less than 1 nm in length, while excess electrons in TiO_2 can spread over a range of more than 50 nm.

When UV irradiation is off, photoexcited electrons are no longer generated in the first-layer of TiO_2, diminishing the driving force for forward hopping. Therefore, under the attraction from the positive charged first-layer TiO_2, the electrons slowly hop back through TiO_2 and neutralize the surface positive charges, as shown in Figure 3.1 (B) and Figure 3.6 (C).[34]

3.5 Conclusion

By employing photoluminescence spectroscopy which observes charging/discharging processes in photoexcited SWNT/TiO_2 mixtures we found the following results:

(1). SWNTs exhibit electron accepting behavior as the PL intensity of SWNT/TiO_2 composites systematically decreases with the increase of the fraction of SWNTs mixed into TiO_2 powder. The fractional decrease in PL intensity is proportional to the average number of SWNT/TiO_2 contact points in the first layer of TiO_2.

(2). SWNTs do not affect the rate of electron hopping between TiO_2 particles. Measured charging/discharging rates are similar to those for pure TiO_2, for a 5-fold ratio change for SWNTs in TiO_2.

(3). Because of the high intrinsic charge carrier density and short screening length in SWNTs, the built-in electric field immobilizes excess electrons in SWNTs at the interface between SWNTs and first-layer TiO_2 particles. The electrostatic attraction between localized electrons in embedded SWNTs and holes in TiO_2 strongly inhibits electron transport through SWNT channels.

(4). The basic finding of this work is that the addition of efficient conducting units to a powdered semiconductor undergoing photoexcitation under field-free conditions will not be useful in increasing electron mobility in the composite structure. We postulate that this deficiency can be overcome by the application of an external electric field, to overcome the Coulomb interaction between photo-produced holes in the semiconductor and electrons in the conductor, as is done in photovoltaic devices.

References

1. Gratzel, M., Dye-Sensitized Solid-State Heterojunction Solar Cells. *Mrs Bulletin* **2005**, *30*, 23-27.
2. Thompson, T. L.; Yates, J. T., Surface Science Studies of the Photoactivation of TiO_2-New Photochemical Processes. *Chemical Reviews* **2006**, *106*, 4428-4453.
3. Linsebigler, A. L.; Lu, G. Q.; Yates, J. T., Photocatalysis on TiO_2 Surfaces - Principles, Mechanisms, and Selected Results. *Chemical Reviews* **1995**, *95*, 735-758.
4. Diebold, U., The Surface Science of Titanium Dioxide. *Surface Science Reports* **2003**, *48*, 53-229.
5. Fujishima, A.; Zhang, X. T.; Tryk, D. A., TiO_2 Photocatalysis and Related Surface Phenomena. *Surface Science Reports* **2008**, *63*, 515-582.
6. Yates, J. T., Photochemistry on TiO_2: Mechanisms Behind the Surface Chemistry. *Surface Science* **2009**, *603*, 1605-1612.
7. Kronik, L.; Shapira, Y., Surface Photovoltage Spectroscopy of Semiconductor Structures: At the Crossroads of Physics, Chemistry and Electrical Engineering. *Surface and Interface Analysis* **2001**, *31*, 954-965.
8. Duzhko, V.; Timoshenko, V. Y.; Koch, F.; Dittrich, T., Photovoltage in Nanocrystalline Porous TiO_2. *Physical Review B* **2001**, *64*.
9. Jing, L. Q.; Sun, X. J.; Shang, J.; Cai, W. M.; Xu, Z. L.; Du, Y. G.; Fu, H. G., Review of Surface Photovoltage Spectra of Nano-Sized Semiconductor and Its Applications in Heterogeneous Photocatalysis. *Solar Energy Materials and Solar Cells* **2003**, *79*, 133-151.
10. Stevanovic, A.; Buttner, M.; Zhang, Z.; Yates, J. T., Photoluminescence of TiO_2: Effect of UV Light and Adsorbed Molecules on Surface Band Structure. *Journal of the American Chemical Society* **2012**, *134*, 324-332.
11. Anpo, M.; Chiba, K.; Tomonari, M.; Coluccia, S.; Che, M.; Fox, M. A., Photocatalysis on Native and Platinum-Loaded TiO_2 and ZnO Catalysts-Origin of Different Reactivities on Wet and Dry Metal-Oxides. *Bulletin of the Chemical Society of Japan* **1991**, *64*, 543-551.
12. Idriss, H.; Andrews, R. M.; Barteau, M. A., Application of Luminescence Techniques to Probe Surface-Adsorbate Interactions on Oxide Single-Crystals. *Journal of Vacuum Science & Technology A-Vacuum Surfaces and Films* **1993**, *11*, 209-218.
13. Nelson, J.; Chandler, R. E., Random Walk Models of Charge Transfer and Transport in Dye Sensitized Systems. *Coordination Chemistry Reviews* **2004**, *248*, 1181-1194.
14. Anta, J. A.; Nelson, J.; Quirke, N., Charge Transport Model for Disordered Materials: Application to Sensitized TiO_2. *Physical Review B* **2002**, *65*.
15. Vanmaekelbergh, D.; de Jongh, P. E., Driving Force for Electron Transport in Porous Nanostructured Photoelectrodes. *Journal of Physical Chemistry B* **1999**, *103*, 747-750.
16. Stevanovic, A.; Yates, J. T., Electron Hopping through TiO_2 Powder: A Study by Photoluminescence Spectroscopy. *Journal of Physical Chemistry C* **2013**, *117*, 24189-24195.
17. Hendry, E.; Wang, F.; Shan, J.; Heinz, T. F.; Bonn, M., Electron Transport in TiO_2 Probed by THz Time-Domain Spectroscopy. *Physical Review B* **2004**, *69*.

18. Biercuk, M. J.; Ilani, S.; Marcus, C. M.; McEuen, P. L., Electrical Transport in Single-Wall Carbon Nanotubes. *Carbon Nanotubes* **2008**, *111*, 455-493.
19. Ilani, S.; McEuen, P. L., Electron Transport in Carbon Nanotubes. *Annual Review of Condensed Matter Physics, Vol 1* **2010**, *1*, 1-25.
20. Yao, Y.; Li, G.; Ciston, S.; Lueptow, R. M.; Gray, K. A., Photoreactive TiO_2/Carbon Nanotube Composites: Synthesis and Reactivity. *Environmental Science & Technology* **2008**, *42*, 4952-4957.
21. Kongkanand, A.; Kamat, P. V., Electron Storage in Single Wall Carbon Nanotubes. Fermi Level Equilibration in Semiconductor-Swcnt Suspensions. *ACS Nano* **2007**, *1*, 13-21.
22. Dresselhaus, M. S.; Dresselhaus, G.; Saito, R., Physics of Carbon Nanotubes. *Carbon* **1995**, *33*, 883-891.
23. Park, J. Y.; Rosenblatt, S.; Yaish, Y.; Sazonova, V.; Ustunel, H.; Braig, S.; Arias, T. A.; Brouwer, P. W.; McEuen, P. L., Electron-Phonon Scattering in Metallic Single-Walled Carbon Nanotubes. *Nano Letters* **2004**, *4*, 517-520.
24. Kamat, P. V., TiO_2 Nanostructures: Recent Physical Chemistry Advances. *Journal of Physical Chemistry C* **2012**, *116*, 11849-11851.
25. Kongkanand, A.; Dominguez, R. M.; Kamat, P. V., Single Wall Carbon Nanotube Scaffolds for Photoelectrochemical Solar Cells. Capture and Transport of Photogenerated Electrons. *Nano Letters* **2007**, *7*, 676-680.
26. Williams, G.; Kamat, P. V., Graphene-Semiconductor Nanocomposites: Excited-State Interactions between ZnO Nanoparticles and Graphene Oxide. *Langmuir* **2009**, *25*, 13869-13873.
27. Jing, L. Q.; Qu, Y. C.; Wang, B. Q.; Li, S. D.; Jiang, B. J.; Yang, L. B.; Fu, W.; Fu, H. G.; Sun, J. Z., Review of Photoluminescence Performance of Nano-Sized Semiconductor Materials and Its Relationships with Photocatalytic Activity. *Solar Energy Materials and Solar Cells* **2006**, *90*, 1773-1787.
28. Abazovic, N. D.; Comor, M. I.; Dramicanin, M. D.; Jovanovic, D. J.; Ahrenkiel, S. P.; Nedeljkovic, J. M., Photoluminescence of Anatase and Rutile TiO_2 Particles. *Journal of Physical Chemistry B* **2006**, *110*, 25366-25370.
29. Palik, E. D., *Handbook of Optical Constants of Solids*; Academic Press: Orlando, 1985, p xviii, 804 p.
30. Mo, S. D.; Ching, W. Y., Electronic and Optical-Properties of 3 Phases of Titanium-Dioxide - Rutile, Anatase, and Brookite. *Physical Review B* **1995**, *51*, 13023-13032.
31. Eagles, D. M., Polar Modes of Lattice Vibration and Polaron Coupling Constants in Rutile (TiO_2). *Journal of Physics and Chemistry of Solids* **1964**, *25*, 1243-1251.
32. Park, Y.; Kim, W.; Monllor-Satoca, D.; Tachikawa, T.; Majima, T.; Choi, W., Role of Interparticle Charge Transfers in Agglomerated Photocatalyst Nanoparticles: Demonstration in Aqueous Suspension of Dye-Sensitized TiO_2. *Journal of Physical Chemistry Letters* **2013**, *4*, 189-194.
33. King, D. A.; Madey, T. E.; Yates, J. T., Interaction Oxygen with Polycrystalline Tungsten. II. Corrosive Oxidation. *Journal of Chemical Physics* **1971**, *55*, 3247-&.
34. Koryta, J.; Dvořák, J.; Kavan, L., *Principles of Electrochemistry - Second Edition*; John Wiley & Sons Ltd.: England, 1993.
35. Zhao, Y.; Liao, A.; Pop, E., Multiband Mobility in Semiconducting Carbon Nanotubes. *IEEE Electron Device Letters* **2009**, *30*, 1078-1080.

36. Docampo, P.; Guldin, S.; Steiner, U.; Snaith, H. J., Charge Transport Limitations in Self-Assembled TiO_2 Photoanodes for Dye-Sensitized Solar Cells. *Journal of Physical Chemistry Letters* **2013**, *4*, 698-703.

4 Effect of Gold Nanoparticles on Photoexcited Charge Carriers in Powdered TiO_2 – Long Range Quenching of Photoluminescence

(modified from *J. Phys. Chem. C*, **2014**, 118(36): 21275-21280)

Abstract

Photoluminescence spectroscopy was employed to study the photoinduced charge transfer between TiO_2 nanoparticles and Au nanoparticles under vacuum conditions. We found that small coverages of 3 nm-Au nanoparticles deposited on TiO_2 significantly diminish the 540 nm (2.3 eV) photoluminescence emission from TiO_2 due to the redistribution of the photoexcited charge to Au nanoparticles which are capable of accepting negative charges behind the Schottky barrier. The lack of development of the photoluminescence emission of Au/TiO_2 during continuous UV irradiation occurs due to a short circuit established through Au nanoparticles where transferred electrons in Au recombine non-radiatively with holes in TiO_2. The photoexcited electron transfer from TiO_2 to the Au nanoparticles occurs beyond the Au particle perimeter over a distance of at least 4 nm. The quenching of photoluminescence by resonance energy transfer from TiO_2 to Au nanoparticles is unimportant as Au plasmonic absorption is not observed.

4.1 Introduction

The interaction of metals with semiconductor surfaces has become a topic of major contemporary interest as a result of recent advances in the field of photonics.[1-4] Here, metal deposits on semiconductor surfaces may cause enhanced interaction of the semiconductor with an incident electromagnetic field as a result of radiation coupling to metal particles via plasmon excitation in the metal[3, 5-7] or conversely to couple electronically excited TiO_2 to plasmonic excitation in the metal[8-9], a process producing a resonance between a photoluminescence feature and the metal plasmon. This investigation deals with a non-plasmonic situation where the metal particles are too small to interact plasmonically with the electronically excited TiO_2.

The contact interface between the metal and the semiconductor initially becomes charged as a result of the equilibration of the Fermi level in the metal and semiconductor, resulting in band bending in the semiconductor and the production of a Schottky barrier at the contact point between the metal and semiconductor[10-12]. The degree of band bending governs the transfer rate of photoexcited charge carriers at the semiconductor-to-metal contact. Such charge transfer effects are of importance in photovoltaic devices and photocatalysis.[13-18] Most studies of the metal-semiconductor interface have been conducted at macroscopic interfaces such as for thin metal films on semiconductor single crystal surfaces. It was found by comparing the photoconductance of both pure TiO_2 and Pt/TiO_2 powders, that small coverages of Pt on TiO_2 cause suppressed photoconductance due to the charge transfer from TiO_2 to Pt nanoparticles[19-20]. In addition, Anpo et al.[21] observed no change in the Ti^{3+} signal in Pt/TiO_2 samples while the Ti^{3+} signal in pure TiO_2 powder increased during continuous UV irradiation as detected by electron paramagnetic resonance (EPR). This decrease and invariance of the Ti^{3+} signal in Pt/TiO_2 was attributed to the transfer of photoexcited electrons from TiO_2 to Pt particles. It was found by Kamat et al.[7, 22] that in an ethanol suspension of Au/TiO_2 or Ag/TiO_2, photoexcited electrons from TiO_2 transfer to Au (or Ag) nanoparticles achieving a charge equilibrium. However, the possible recombination of electrons in Au (or Ag) and holes in TiO_2 could not be studied as holes are scavenged by ethanol. There are several studies[23-26] on quenching of the photoluminescence (electron-hole recombination) effect due to the charge transfer from semiconductors to Au nanoparticles. However, none of these papers deal with the spatial range of photoluminescence quenching by metal nanoparticles.

In this work, we use photoluminescence (PL) spectroscopy to probe a TiO_2 semiconductor surface in contact with 3 nm non-plasmonic Au particles. Photoluminescence originates from the electron-hole recombination in semiconductors, which is the limiting process in increasing the efficiency of both photocatalysts and photovoltaic devices. Therefore, it is important to detect the ways to suppress the electron-hole recombination. We find that small coverages of Au particles strongly diminish the PL effect from the **entire** TiO_2 particle surface as well as the associated surface photovoltage charging effect caused by UV irradiation. The surface photovoltage effect results from light-induced hole production and hole transport to the n-type TiO_2 surface.

Upon photoexcitation of Au/TiO_2 powder, we find that photoexcited electrons transfer to Au nanoparticles while photoexcited holes diffuse efficiently toward the Au/TiO_2 interface. Here, the Au nanoparticles cover about only 0.15 fraction of the TiO_2 particle surface. A long-range quenching effect on photoluminescence is observed to occur. In the extended region charge carriers are found to utilize long pathways to achieve non-radiative recombination in the widely-separated metal particles. This effect causes a short circuit between the TiO_2 and the Au which allows charge carriers to bypass the normal radiative recombination processes at defect sites in the TiO_2 and instead to undergo non-radiative recombination in the widely-spaced metal nanoparticles. Such metal nanoparticle induced recombination processes therefore bypass normal electron-hole recombination processes at defect sites in TiO$_2$, eliminating photoluminescence from the TiO$_2$. The evidence for non-radiative recombination on Au/TiO$_2$ comes from the observation that irradiation is ineffective in producing surface charging or surface photovoltage on TiO$_2$ causing the suppression of PL intensity growth, in contrast to the behavior of pure TiO$_2$.

4.2 Experimental methods

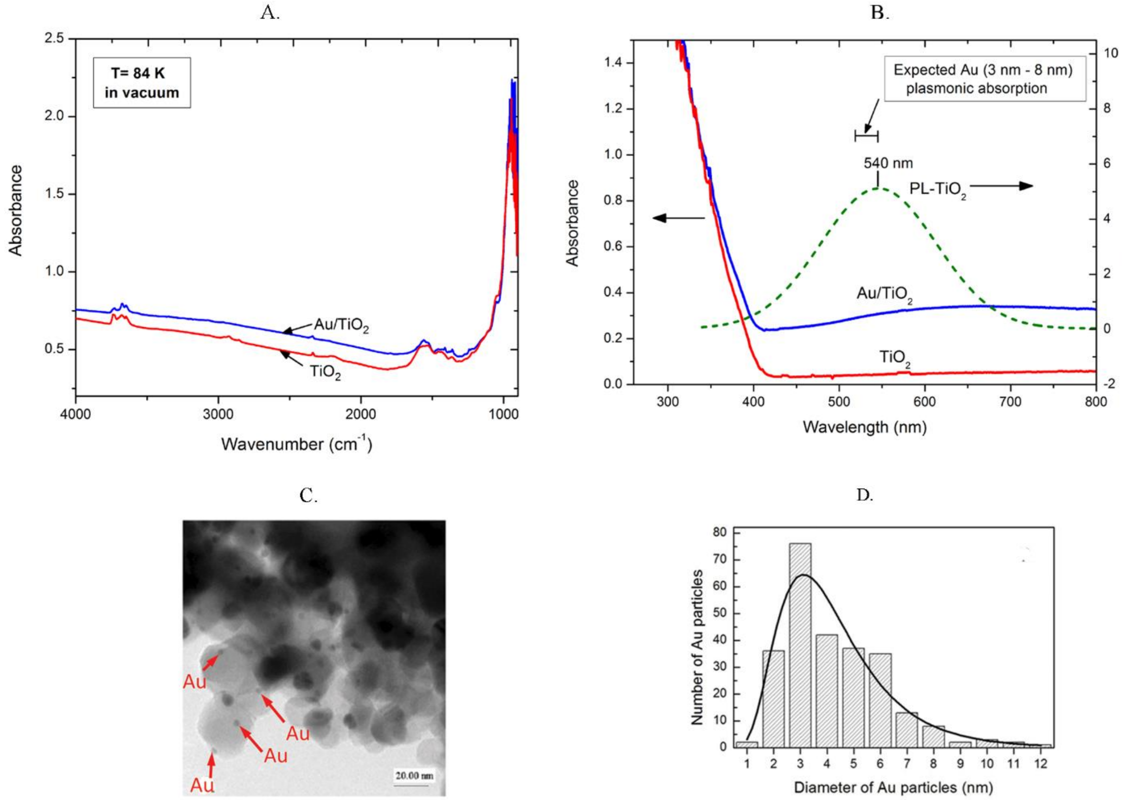

Figure 4.1. Characterization of TiO$_2$ and Au/TiO$_2$ samples. A. Infrared spectra of a clean TiO$_2$ (red) and Au/TiO$_2$ (blue) surface at 84 K in vacuum. B. UV-Vis diffuse reflectance spectrum of TiO$_2$ and Au/TiO$_2$ compared to the PL spectrum of pure TiO$_2$. A plasmonic absorption peak for 3-8 nm Au nanoparticles[7, 27] is absent. The dashed green line shows the PL spectrum of TiO$_2$ at 110K. C. Electron micrograph. D. Particle size histogram of

8 % Au by weight particles on TiO_2. The most probable diameter of the Au particles is ~3 nm[28].

The instrument was described in chapter 2. Gold particles were chemically deposited onto the surfaces of TiO_2 using the slow hydrolysis of $HAuCl_4$ in a water solution of urea containing suspended P-25 TiO_2 powder and following the procedure of Zanella[29]. The TiO_2 particles consisted of a mixture of anatase crystals and rutile crystals (25 % and 75 %, respectively) with a surface area of 60 m^2/g. The interparticle pore size distribution was mainly in the range of 5 – 25 nm as measured by N_2 adsorption isotherm behavior. The measured average TiO_2 particle size was 50 nm. The Au/TiO_2 composite contained 8% Au by weight.

Before PL and IR measurements, the samples were heated in vacuum to 680 K in 0.8 Torr of research-grade O_2 (99.99%) for 40 min to remove surface impurities and to partially oxidize the samples. The samples were then evacuated at 680 K for 10 min, and then cooled to 110 K for PL and IR measurements. A transmission infrared spectrum of the Au/TiO_2 composite is shown in Figure 4.1 (A). Here IR bands corresponding to a tiny coverage of OH species on TiO_2 are seen (~3734 cm^{-1}; 3675 cm^{-1}; 3648 cm^{-1}) along with traces of CO_3^{2-} functionalities on TiO_2 in the range ~ 1684-1297 cm^{-1}. A low coverage of impurity hydrocarbon species is hardly visible with absorption bands near 2958 cm^{-1}, 2925 cm^{-1}, and 2856 cm^{-1}. This type of Au/TiO_2 composite material has been widely studied as an active catalyst for mild oxidation reactions involving various molecules such as CO, H_2 and hydrocarbons and other organic molecules[28, 30-32] and the adsorption and catalytic behavior of the material indicates that it contains a mixture of clean Au and almost clean TiO_2 surfaces. Figure 4.1 (B) shows the diffuse reflectance spectra of both TiO_2 and

Au/TiO_2 samples. The figure shows that a plasmonic absorption peak expected for 3-8 nm Au particles is absent. Figure 4.1 (C) and (D) show an electron micrograph of Au/TiO_2 and a histogram with a Au particle size distribution that indicates a most probable Au particle diameter of 3 nm, respectively. Assuming that our sample consists of hemispherical 3 nm diameter particles distributed on 50 nm diameter TiO_2 spheres, it may be shown that the Au/TiO_2 contact area is ~ 0.15 of the geometrical area of the TiO_2 support.

4.3 Experimental results

Figure 4.2 shows the PL spectra of pure TiO_2 and Au/TiO_2 in vacuum measured at 110 K. Figure 4.2 (A) shows the initial PL emission when the samples have not been previously irradiated with UV radiation while Figure 4.2 (B) shows the PL emission of both samples after continuous UV irradiation for 45 min at 110 K that is known to enhance the PL intensity of TiO_2 due to the surface charging and associated upward band bending decrease caused by the surface photovoltage effect[33]. The pure TiO_2 sample shows a PL peak maximum at about 540 nm (red curve). The intensity of the PL emission of the Au/TiO_2 sample is significantly suppressed compared to the pure TiO_2; the PL peak is only a few percent of its intensity as measured on the pure TiO_2 standard (gray curve). This result is evidence of Au nanoparticles capturing photoexcited electrons from TiO_2 [18] and supplying a recombination route which does not generate PL. As a result, the probability for excited electrons to radiatively recombine with holes in TiO_2 is strongly suppressed. There are also two peaks observed at 390 and 780 nm in Figure 4.2. The peak at 390 nm is due to a small amount of reflected incident radiation off the CaF_2 window and the tungsten grid while the peak at 780 nm is a second-order feature of the 390 nm reflected light. Both peaks remained invariant during the experiment and are neglected. In addition, the two reflected light peaks were observed when the PL spectrum of an empty portion of the W-grid was recorded.

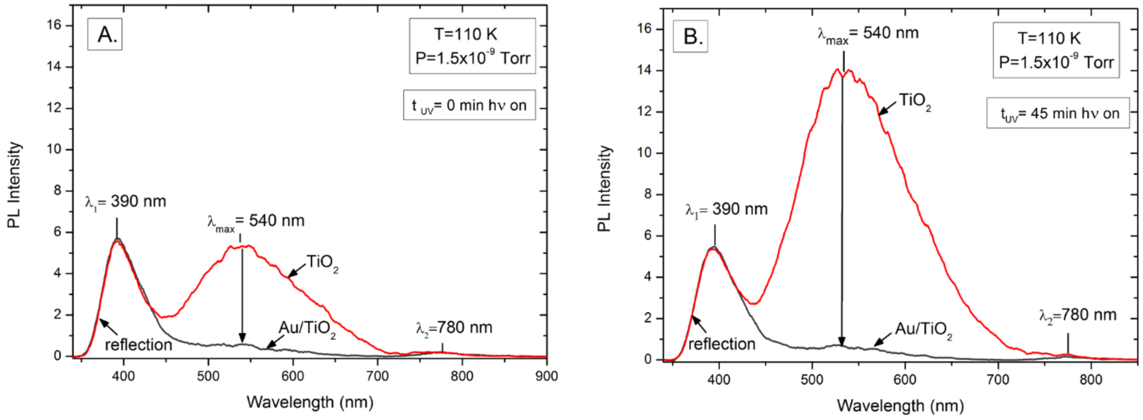

Figure 4.2. Photoluminescence spectra of pure TiO_2 (red spectrum) and Au/TiO_2 (gray spectrum) in vacuum at 110 K before and after surface charging by UV illumination. The PL intensities are shown without any normalization. The PL emission exhibits a maximum at ~ 540 nm upon excitation by 320 nm (3.88 eV) light. A. PL spectra before UV irradiation; B. PL spectra after 45 min of continuous UV irradiation at a UV flux of ~1.4 × 10^{14} photons cm^{-2} s^{-1}. The PL intensity of TiO_2 is significantly suppressed in the Au/TiO_2 sample. The peak at 390 nm and a second-order feature at 780 nm are due to reflection of a portion of the incident light from both the CaF_2 window and the tungsten grid and are neglected.

Figure 4.3 shows the PL development during continuous 320 nm irradiation in vacuum at 110 K for both pure TiO_2 (red squares) and Au/TiO_2 (gray squares) samples. For TiO_2, the PL signal increases inverse-exponentially with time during continuous exposure to UV radiation. This PL intensity development in pure TiO_2 is associated with a decrease in the degree of upward band bending in n-type TiO_2 [33] as photogenerated holes in the valence band diffuse to the TiO_2 surface, causing an increase in positive surface photovoltage. As a result, the depletion layer, corresponding to the surface region experiencing band bending, contracts, providing more underlying PL-active sites and the enhancement of PL emission. Unlike pure TiO_2, the Au/TiO_2 sample shows very low PL emission. Furthermore, the very low intensity of PL emission is invariant during continuous UV irradiation for 95 min at 110 K in vacuum, indicating that electrons transferred to Au recombine non-radiatively with photogenerated holes from TiO_2, preventing positive charge buildup on the TiO_2 regions surrounding the Au nanoparticles upon exposure to 3.88 eV photons.

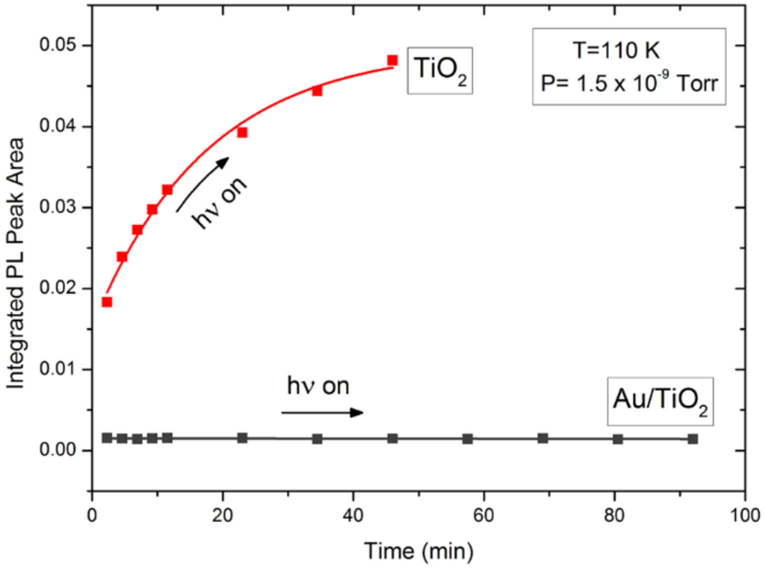

Figure 4.3. Photoluminescence development of TiO_2 (red curve) and Au/TiO_2 (gray curve) upon continuous UV irradiation of 3.88 eV ($\lambda_{exc.}$= 320 nm) in vacuum at 110 K. Upon continuous UV irradiation, the PL development for TiO_2 shows an exponential increase in the PL signal. The PL emission of the Au/TiO_2 sample is initially very small, and the PL development during illumination is completely suppressed.

4.4 Discussion

4.4.1 Suppression of electron-hole recombination and photoluminescence by Au particles

The contact between Au nanoparticles and TiO_2 particles induces a Schottky barrier between the metal and the semiconductor as shown in Figure 4.4 (A) and (B). The maximal allowed potential energy of electrons in the Au particles (the Au Fermi energy) is lower than the potential energy of defect-bound electrons in TiO_2 below E_F, which results in electron flow from TiO_2 to Au particles upon contact. This electron transfer causes Fermi level shifting in the Au until the equilibrium is reached and the Schottky barrier is established upon Fermi energy alignment. As a result, the conduction and valence bands in TiO_2 bend upwards (as shown in Figure 4.4 (B)).

Figure 4.4 (C) shows a schematic of the charge transfer between TiO_2 and 3 nm Au nanoparticles upon illumination by UV radiation based on this work. The Au particles are capable of accepting photoexcited electrons from the TiO_2 particle. During the continuous UV irradiation, the photoexcited electrons favorably transfer to Au particles where they may be trapped (Figure 4.4 (D)). As a result, due to the short circuit occurring through Au, the recombination process for photogenerated electrons and holes at defect sites in TiO_2 is strongly suppressed by the Au nanoparticles as indicated by very low PL intensity for the Au/TiO_2 sample. By this process, the holes in the TiO_2 particle reach the interface where they recombine **non-radiatively** with the trapped electrons in the Au nanoparticles, emitting heat. There are two important processes: (1) photoexcited electrons in TiO_2 are trapped by Au nanoparticles; and (2) photogenerated holes in TiO_2 recombine non-radiatively with trapped electrons in Au, reducing almost to zero the normal radiative PL process accompanying electron-hole recombination at a TiO_2 defect site as shown in Figure 4.4C.

4.4.2 Possibility of energy transfer effects between Au and TiO_2

Quenching of photoluminescence by Au nanoparticles could occur by resonance energy transfer from excited TiO_2 to Au.[8-9] This would be facilitated by a Au plasmon which corresponds in energy to the energy of the photon observed in PL for pure TiO_2 – the PL decrease being caused by energy transfer to the Au plasmon.

We show in Figure 4.1(B) that the Au/TiO_2 sample shows no characteristic plasmonic absorbance near 540 nm. Therefore, the quenching of PL is unlikely to be caused by resonance energy transfer between photoexcited TiO_2 and plasmonic excitation in Au nanoparticles; instead electron transfer occurs from TiO_2 to Au followed by recombination at the Au/TiO_2 interface (as shown in Figure 4.4 (C) and (D)).

Many papers report electron capture by metals in contact with irradiated TiO_2. For this effect to operate continuously without significant charging during photoirradiation, the metal-trapped electron must exhibit continuous non-radiative recombination during irradiation, and this is observed for nanoparticle Au/TiO_2.

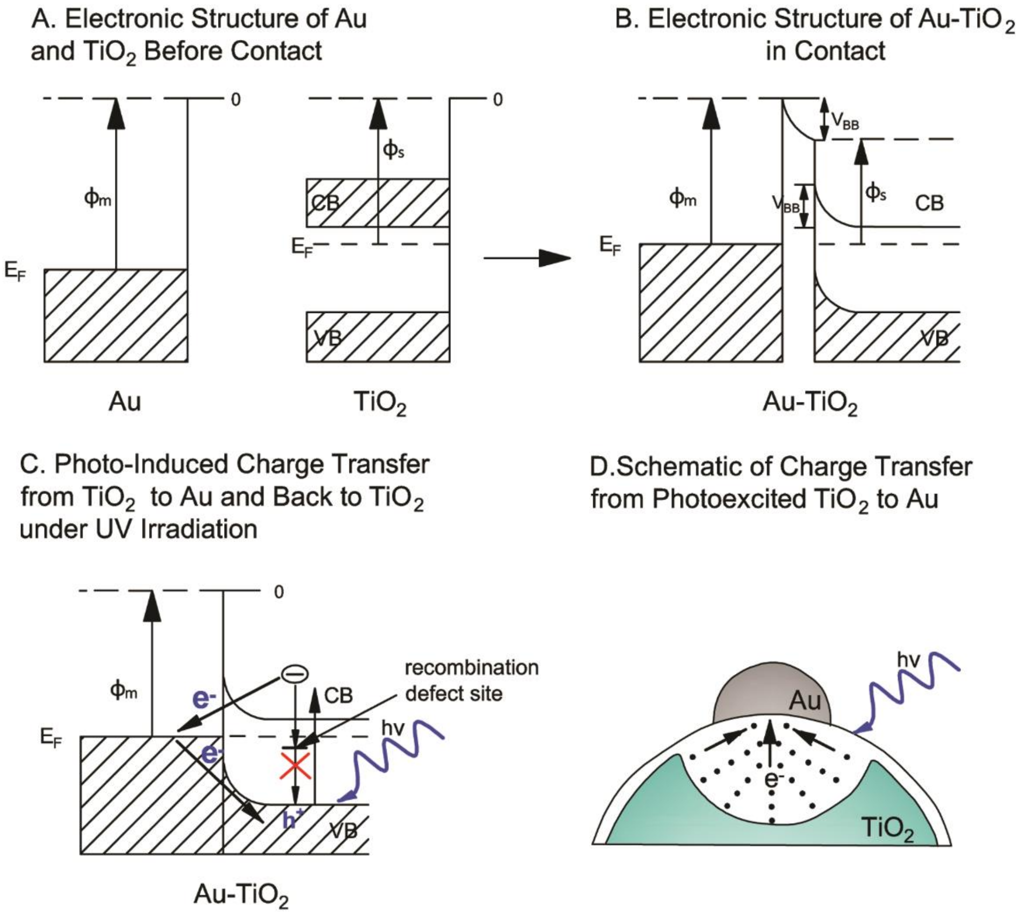

Figure 4.4. A. Electronic structure of Au and TiO_2 before contact; B. Electronic structure of Au and TiO_2 after contact; C. Electronic structure of Au -TiO_2 upon photoexcitation of TiO_2. Gold nanoparticles are capable of accepting photoexcited negative surface charge from TiO_2 resulting in suppression of the PL signal. A possible short-circuit channel for the Au nanoparticles to discharge is through recombination of temporarily-trapped electrons in the Au particles with holes which have transferred to the surface of the TiO_2. This recombination process results in heat emission; D. Schematic of photoexcited charge production in TiO_2, and withdrawal from TiO_2 to Au nanoparticles. The white region schematically shows excited electron drainage from TiO_2 into the Au particle, a phenomenon which occurs over a range of 4 nm or more.

4.4.3 Range of influence of Au on radiative electron-hole recombination

We find that a small number of ~ 3 nm Au particles suppress the PL phenomenon in TiO_2 almost completely as shown in Figure 4.2 and Figure 4.3. Using the average hemispherical Au particle size, and a nominal 50 nm TiO_2 particle size, it was shown that the Au particles cover a fraction of only ~ 0.15 of the TiO_2 surface causing almost complete quenching of the PL from the entire TiO_2 particle. This corresponds to a photoluminescence quenching radius of at least 4 nm from each Au particle which is effective for switching off the photoluminescence. Figure 4.4 (C) shows a schematic of the process leading to a short circuit for photoexcited electrons within the ~ 4 nm radius quenching region bordering the Au particle. Considering the long electron diffusion lengths in porous TiO_2 [34-37] which are in the order of μm before recombination with a hole, it is feasible for electrons in TiO_2 to reach Au nanoparticles upon photoexcitation, and to then undergo efficient recombination at the Au/TiO_2 interface.

4.5 Conclusions

The suppression of the photoluminescence phenomenon in TiO_2 regions surrounding 3 nm Au particles supported on TiO_2 has been observed. Specifically:

(1) Photoluminescence quenching for at least a 4 nm radius beyond the Au particle boundary is observed, indicating the spatial extent of regions contributing photo-generated carriers which undergo non-radiative electron-hole recombination as transport occurs to the Au/TiO_2 contact.

(2) Photoluminescence quenching occurs as a result of a short circuit through Au, delivering photoexcited electrons to photoexcited holes in TiO_2 via conduction

through Au. Normal photoluminescence by way of electron-hole recombination processes in TiO_2 is quenched by the short circuit.

(3) Au nanoparticles on TiO_2 are also effective for quenching the surface photovoltage effect, preventing positive charging of the TiO_2 surface upon exposure to UV excitation. This observation indicates that the Au supplies a non-radiative recombination pathway for separated charge carriers.[38]

(4) For 3 nm Au particles which do not exhibit characteristic plasmonic absorption, the possibility that PL quenching is due to resonance energy transfer from TiO_2 to Au plasmons is unlikely.

References

1. Pillai, S.; Green, M. A., Plasmonics for Photovoltaic Applications. *Solar Energy Materials and Solar Cells* **2010**, *94*, 1481-1486.
2. Yoon, W. J.; Jung, K. Y.; Liu, J. W.; Duraisamy, T.; Revur, R.; Teixeira, F. L.; Sengupta, S.; Berger, P. R., Plasmon-Enhanced Optical Absorption and Photocurrent in Organic Bulk Heterojunction Photovoltaic Devices Using Self-Assembled Layer of Silver Nanoparticles. *Solar Energy Materials and Solar Cells* **2010**, *94*, 128-132.
3. Ingram, D. B.; Linic, S., Water Splitting on Composite Plasmonic-Metal/Semiconductor Photoelectrodes: Evidence for Selective Plasmon-Induced Formation of Charge Carriers near the Semiconductor Surface. *Journal of the American Chemical Society* **2011**, *133*, 5202-5205.
4. Atwater, H. A.; Polman, A., Plasmonics for Improved Photovoltaic Devices. *Nature Materials* **2010**, *9*, 205-213.
5. Kamat, P. V., Photophysical, Photochemical and Photocatalytic Aspects of Metal Nanoparticles. *Journal of Physical Chemistry B* **2002**, *106*, 7729-7744.
6. Choi, H.; Chen, W. T.; Kamat, P. V., Know Thy Nano Neighbor. Plasmonic Versus Electron Charging Effects of Metal Nanoparticles in Dye-Sensitized Solar Cells. *ACS Nano* **2012**, *6*, 4418-4427.
7. Subramanian, V.; Wolf, E. E.; Kamat, P. V., Catalysis with TiO_2/Gold Nanocomposites. Effect of Metal Particle Size on the Fermi Level Equilibration. *Journal of the American Chemical Society* **2004**, *126*, 4943-4950.
8. Zhang, X.; Marocico, C. A.; Lunz, M.; Gerard, V. A.; Gun'ko, Y. K.; Lesnyak, V.; Gaponik, N.; Susha, A. S.; Rogach, A. L.; Bradley, A. L., Wavelength, Concentration, and Distance Dependence of Nonradiative Energy Transfer to a Plane of Gold Nanoparticles. *ACS Nano* **2012**, *6*, 9283-9290.
9. Viste, P.; Plain, J.; Jaffiol, R.; Vial, A.; Adam, P. M.; Royer, P., Enhancement and Quenching Regimes in Metal-Semiconductor Hybrid Optical Nanosources. *ACS Nano* **2010**, *4*, 759-764.
10. Minato, T.; Susaki, T.; Shiraki, S.; Kato, H. S.; Kawai, M.; Aika, K. I., Investigation of the Electronic Interaction between TiO_2(110) Surfaces and Au Clusters by PES and STM. *Surface Science* **2004**, *566*, 1012-1017.
11. Wang, Y.; Hwang, G. S., Adsorption of Au Atoms on Stoichiometric and Reduced TiO_2(110) Rutile Surfaces: A First Principles Study. *Surface Science* **2003**, *542*, 72-80.
12. Goodman, D. W., "Catalytically Active Au on Titania": Yet Another Example of a Strong Metal Support Interaction (SMSI)? *Catalysis Letters* **2005**, *99*, 1-4.
13. Kamat, P. V., Graphene-Based Nanoarchitectures. Anchoring Semiconductor and Metal Nanoparticles on a Two-Dimensional Carbon Support. *Journal of Physical Chemistry Letters* **2010**, *1*, 520-527.
14. Ng, S. P.; Lu, X. Q.; Ding, N.; Wu, C. M. L.; Lee, C. S., Plasmonic Enhanced Dye-Sensitized Solar Cells with Self-Assembly Gold-TiO_2@Core-Shell Nanoislands. *Solar Energy* **2014**, *99*, 115-125.

15. Jo, H.; Sohn, A.; Shin, K. S.; Kumar, B.; Kim, J. H.; Kim, D. W.; Kim, S. W., Novel Architecture of Plasmon Excitation Based on Self-Assembled Nanoparticle Arrays for Photovoltaics. *ACS Applied Materials & Interfaces* **2014**, *6*, 1030-1035.
16. Li, Y.; Wang, H.; Feng, Q. Y.; Zhou, G.; Wang, Z. S., Gold Nanoparticles Inlaid TiO_2 Photoanodes: A Superior Candidate for High-Efficiency Dye-Sensitized Solar Cells. *Energy & Environmental Science* **2013**, *6*, 2156-2165.
17. Bora, T.; Kyaw, H. H.; Sarkar, S.; Pal, S. K.; Dutta, J., Highly Efficient ZnO/Au Schottky Barrier Dye-Sensitized Solar Cells: Role of Gold Nanoparticles on the Charge-Transfer Process. *Beilstein Journal of Nanotechnology* **2011**, *2*, 681-690.
18. Kim, S. M.; Lee, S. J.; Kim, S. H.; Kwon, S.; Yee, K. J.; Song, H.; Somorjai, G. A.; Park, J. Y., Hot Carrier-Driven Catalytic Reactions on Pt-CdSe-Pt Nanodumbbells and Pt/GaN under Light Irradiation. *Nano Letters* **2013**, *13*, 1352-1358.
19. Linsebigler, A. L.; Lu, G. Q.; Yates, J. T., Photocatalysis on TiO_2 Surfaces - Principles, Mechanisms, and Selected Results. *Chemical Reviews* **1995**, *95*, 735-758.
20. Disdier, J.; Herrmann, J. M.; Pichat, P., Platinum Titanium-Dioxide Catalysts - A Photoconductivity Study of Electron-Transfer from the Ultraviolet-Illuminated Support to the Metal and of the Influence of Hydrogen. *Journal of the Chemical Society-Faraday Transactions I* **1983**, *79*, 651-660.
21. Anpo, M.; Takeuchi, M., The Design and Development of Highly Reactive Titanium Oxide Photocatalysts Operating under Visible Light Irradiation. *Journal of Catalysis* **2003**, *216*, 505-516.
22. Takai, A.; Kamat, P. V., Capture, Store, and Discharge. Shuttling Photogenerated Electrons across TiO_2-Silver Interface. *ACS Nano* **2011**, *5*, 7369-7376.
23. Lee, J.; Shim, H. S.; Lee, M.; Song, J. K.; Lee, D., Size-Controlled Electron Transfer and Photocatalytic Activity of ZnO-Au Nanoparticle Composites. *Journal of Physical Chemistry Letters* **2011**, *2*, 2840-2845.
24. Bumajdad, A.; Madkour, M., Understanding the Superior Photocatalytic Activity of Noble Metals Modified Titania under UV and Visible Light Irradiation. *Physical Chemistry Chemical Physics* **2014**, *16*, 7146-7158.
25. Peralta, M. D. R.; Pal, U.; Zeferino, R. S., Photoluminescence (PL) Quenching and Enhanced Photocatalytic Activity of Au-Decorated ZnO Nanorods Fabricated through Microwave-Assisted Chemical Synthesis. *ACS Applied Materials & Interfaces* **2012**, *4*, 4807-4816.
26. Kiyonaga, T.; Fujii, M.; Akita, T.; Kobayashi, H.; Tada, H., Size-Dependence of Fermi Energy of Gold Nanoparticles Loaded on Titanium(IV) Dioxide at Photostationary State. *Physical Chemistry Chemical Physics* **2008**, *10*, 6553-6561.
27. Jain, P. K.; Huang, X.; El-Sayed, I. H.; El-Sayad, M. A., Review of Some Interesting Surface Plasmon Resonance-Enhanced Properties of Noble Metal Nanoparticles and Their Applications to Biosystems. *Plasmonics* **2007**, *2*, 107-118.
28. Green, I. X.; Tang, W. J.; Neurock, M.; Yates, J. T., Spectroscopic Observation of Dual Catalytic Sites During Oxidation of CO on a Au/TiO_2 Catalyst. *Science* **2011**, *333*, 736-739.
29. Zanella, R.; Giorgio, S.; Henry, C. R.; Louis, C., Alternative Methods for the Preparation of Gold Nanoparticles Supported on TiO_2. *Journal of Physical Chemistry B* **2002**, *106*, 7634-7642.

30. Green, I. X.; Tang, W. J.; McEntee, M.; Neurock, M.; Yates, J. T., Inhibition at Perimeter Sites of Au/TiO_2 Oxidation Catalyst by Reactant Oxygen. *Journal of the American Chemical Society* **2012**, *134*, 12717-12723.
31. Green, I. X.; Tang, W. J.; Neurock, M.; Yates, J. T., Insights into Catalytic Oxidation at the Au/TiO_2 Dual Perimeter Sites. *Accounts of Chemical Research* **2014**, *47*, 805-815.
32. Wang, Y. G.; Yoon, Y.; Glezakou, V. A.; Li, J.; Rousseau, R., The Role of Reducible Oxide-Metal Cluster Charge Transfer in Catalytic Processes: New Insights on the Catalytic Mechanism of CO Oxidation on Au/TiO_2 from Ab initio Molecular Dynamics. *Journal of the American Chemical Society* **2013**, *135*, 10673-10683.
33. Stevanovic, A.; Buttner, M.; Zhang, Z.; Yates, J. T., Photoluminescence of TiO_2: Effect of UV Light and Adsorbed Molecules on Surface Band Structure. *Journal of the American Chemical Society* **2012**, *134*, 324-332.
34. Peter, L. M.; Wijayantha, K. G. U., Intensity Dependence of the Electron Diffusion Length in Dye-Sensitised Nanocrystalline TiO_2 Photovoltaic Cells. *Electrochemistry Communications* **1999**, *1*, 576-580.
35. Leng, W. H.; Barnes, P. R. F.; Juozapavicius, M.; O'Regan, B. C.; Durrant, J. R., Electron Diffusion Length in Mesoporous Nanocrystalline TiO_2 Photoelectrodes During Water Oxidation. *Journal of Physical Chemistry Letters* **2010**, *1*, 967-972.
36. Aduda, B. O.; Ravirajan, P.; Choy, K. L.; Nelson, J., Effect of Morphology on Electron Drift Mobility in Porous TiO_2. *International Journal of Photoenergy* **2004**, *6*, 141-147.
37. Kytin, V.; Dittrich, T.; Bisquert, J.; Lebedev, E. A.; Koch, F., Limitation of the Mobility of Charge Carriers in a Nanoscaled Heterogeneous System by Dynamical Coulomb Screening. *Physical Review B* **2003**, *68*.
38. Koryta, J.; Dvořák, J.; Kavan, L., *Principles of Electrochemistry - Second Edition*; John Wiley & Sons Ltd.: England, 1993.

5 Different Effects of Oxygen Adsorption on the Band Bending of Anatase

(modified from *J. Phys. Chem. C*, **2017**, 121(2): 1263-1271)

Abstract

Photoluminescence (PL) spectroscopy was used to infer that oxygen adsorption changes the band bending of the anatase phase of TiO_2 within P25 nanopowder in different ways. On the one hand, oxygen can adsorb through irreversible reaction with defects which reduces the intrinsic upward band bending at the TiO_2 surface and results in increased PL emission. On the other hand, oxygen exposure also leads to molecular chemisorption that yields an outermost negative charge at the surface which increases the upward band bending of TiO_2 and decreases the PL emission. Since band bending plays an active role in directing charge carrier migration to the surface, the finding that oxygen adsorption can have two different, and quite opposite, effects on the band bending of TiO_2 provides a new perspective on how oxygen may influence photocatalytic reaction efficiencies.

5.1 Introduction

TiO_2 has attracted enormous research attention due largely to its prospective application in utilizing solar energy for environmental pollutant purification, hydrogen evolution, and solar cells.[1-6] However, the fast radiative and non-radiative recombination rates of photoexcited charge carriers limits the efficiency of TiO_2-based photochemistry.[3] One effective method to suppress electron/hole recombination in the bulk is by tuning the TiO_2 band bending to help separate charge carriers and direct desired carriers toward the semiconductor surface.[7-10] Band bending is the energy gradient in the electron potential near the surface of a semiconductor caused by the imbalanced charge distribution established under thermal equilibrium for systems such as metal/semiconductor interfaces or adsorbent/semiconductor interfaces. Band bending influences surface photoreaction rates by driving charge carriers toward, or away, from the surface. Zhang *et al.* found that a 25-fold increase in the rate of hole-mediated desorption of molecular oxygen could be achieved by dosing Cl_2, an electron acceptor molecule, on to the TiO_2 surface to make the band bending of TiO_2 more upward and thereby increase the hole availability at the TiO_2 surface.[9] Oxygen plays an important role in the majority of TiO_2 photochemical processes, often serving as an electron scavenger and oxidizer precursor in photo-oxidation reactions.[11-13] However, little attention has been paid to oxygen induced band bending changes for TiO_2 which may significantly influence the availability of photoexcited charge carriers at the TiO_2 surface that can drive nonthermal adsorbate chemistry.

As a contactless and nondestructive method, PL has been shown to be an effective method to determine band bending changes because the dimensions of the PL emission zone are reduced by the PL “dead layer” near the surface whose depth scales with the band bending. Band bending in the near surface region serves to actively separate photoexcited electron-hole pairs such that the electron-hole recombination rate is deeply suppressed as compared to bulk TiO_2. Hence, there is little PL emission from this depletion layer of TiO_2 near the surface, where upward band bending exists.[7, 14-16] Although other factors, such as specific surface reaction with adsorbents and photoexcited charge capture by adsorbed molecules acting as photoexcited charge scavengers, may also affect PL, band bending should still be the main reason for PL intensity change as the trend that donor molecules increase PL and acceptor molecules decrease PL is observed for a wide range of molecules, indicating a physical rather than specific chemical basis for the PL modulation.[16-18] Zhang *et al.* have demonstrated that the effect of band bending significantly outweighs the effect of adsorbents as photoexcited charge scavengers in oxygen desorption from TiO_2 surfaces, which is a process affected by electron-hole pair separation.[9] Because ultraviolet excitation of TiO_2 near 320 nm falls off with a penetration depth of ~ 20 nm[16, 19-20] whereas the depth of the depletion layer is several nm and related to the band banding,[7, 14, 16, 21-22] PL emission from nanoparticles, in which much of the material is close to the surface, can be significantly modulated by changing the depth of the depletion layer, or band bending. More upward band bending extends the depth of the depletion layer and results in lower PL emission intensity, and vice versa, as shown in Figure 5.1.

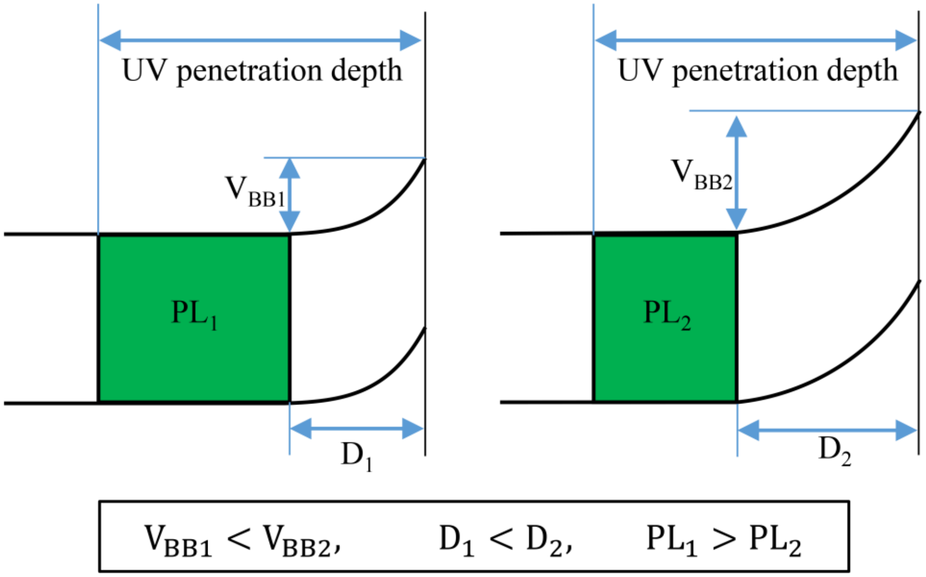

Figure 5.1. Schematics of the relationship between PL, charge depletion layer depth (D), and band bending voltage (V_{BB}). [7, 15-16]

Interaction between oxygen and TiO_2 has been studied primarily on centimeter-scale rutile $TiO_2(110)$ samples using surface science techniques. The chemistry of O_2 with TiO_2(rutile) is complicated and involves several different pathways.[23-35] Using temperature programmed desorption (TPD), Henderson *et al.*[25] found that the saturation of O_2 adsorption on TiO_2 at 120 K is ~ 3 times the number of oxygen vacancies, with two-thirds desorbing from TiO_2 during TPD and one-third remaining behind. The oxygen vacancy coverage on $TiO_2(110)$ surfaces prepared after annealing in vacuum at 850 K was estimated as ~8% of the monolayer or a coverage of 4×10^{13} cm^{-2}. Henderson *et al.* proposed that there are two oxygen adsorption channels on TiO_2 – dissociative chemisorption and molecular chemisorption. When the number of oxygen molecules adsorbed is less than number of oxygen vacancies on TiO_2 surface, an oxygen molecule typically dissociates and heals an oxygen vacancy, leaving an oxygen adatom on a neighboring Ti site. When the number of oxygen molecules adsorbed exceeds the number of oxygen vacancies on the $TiO_2(110)$ surface, molecular oxygen adsorbs at Ti sites on the surface in the form of O_2^-, gaining electrons from the TiO_2 lattice. Only the molecularly adsorbed oxygen can be recovered through TPD because oxygen adsorbed through the dissociative channel remains in filled oxygen vacancy sites.[25] Besides TPD, molecularly adsorbed oxygen can also be removed by photodesorption wherein O_2^- is neutralized by photoexcited holes.[9, 23-24, 36] Both the dissociative[26, 28] and the molecular[29-30, 35] chemisorption channels have been independently confirmed by direct observations using scanning tunneling spectroscopy (STM), although the exact extent of charge transfer in the molecular adsorption channel is still unclear and O_2^{2-} rather than O_2^- has also been suggested by some researchers.[23, 33, 37] In addition to the TiO_2 oxygen vacancy mediated oxygen dissociation, it was also found that molecularly adsorbed oxygen on Ti sites can dissociate into two neighboring oxygen adatoms on Ti sites without the participation of oxygen vacancies.[27, 30] Some recent studies proposed that excess Ti interstitials yield ionized Ti^{3+} subsurface defect sites that may play an important role in the adsorption of oxygen.[27, 31] Since significant electron transfer is involved in both the molecular and dissociative adsorption of O_2 on TiO_2, band bending changes in TiO_2 are likely to be significant because of the substantial electron transfer involved.

The chemistry of oxygen on TiO_2 has been extensively studied for the rutile phase, however, anatase is considered more photoactive and is more widely used as a photocatalyst than is rutile. In this report, we use PL to monitor oxygen chemistry on P25 powder which is an experimental reference standard form of TiO_2 because of the reliable consistency of its properties. The high purity of P25 and its 20-80 nm diameter particle sizes make it well suited for high vacuum PL experiments. By monitoring the PL emission, we find that the adsorption of oxygen influences the band bending of anatase TiO_2 in two different manners. A small amount of oxygen exposure results in oxygen reaction with defects that decreases the upward band bending of TiO_2 which leads to more PL emission. Further oxygen exposure allows molecularly chemisorbed oxygen species to form which accumulates negative charge on the TiO_2 surface that increases the upward band bending of TiO_2 which leads to less PL emission.

5.2 Experimental methods

The instrument setup was described in chapter 2. The TiO_2 examined in this study was typically the widely used P25 powder (Evonik Industries, formerly Degussa) which contains ~ 75 % of the anatase and ~ 25 % of the rutile phase of TiO_2, as particles with 85 and 25 nm mean diameters, respectively.[38] Pure anatase (30 nm diameter, >99.98% purity, US Research Nanomaterials Inc.) was also studied as a comparison. Before measuring the PL, the TiO_2 sample was first heated to 680.0 K in ~ 0.7 Torr O_2 for 40 min to clean the sample. Then the cell was pumped out for 10 min at 680.0 K and then cooled down to ~ 84 K with the cell pressure reading ~ 5×10^{-9} Torr. After the above treatment, the sample was heated to a temperature of 110.0 K in this study to take PL measurements. PL was examined after, or during three different types of O_2 adsorption experiments. (1) Post-oxygen exposure: a selected pressure of O_2 was introduced to the chamber and enclosed for 10 min in the dark, and then the cell was continuously pumped out for 5 min before a PL measurement was made under high vacuum conditions. (2) Oxygen flow at a selected pressure: several valves were partially opened to establish a flow of O_2 gas in the cell which maintained a selected pressure over the course of an experiment. (3) Oxygen dose: a selected pressure of oxygen was introduced and trapped into the cell and the PL was measured continuously.

5.3 Results and discussion

5.3.1 Different effects of oxygen adsorption on PL and band bending of TiO_2

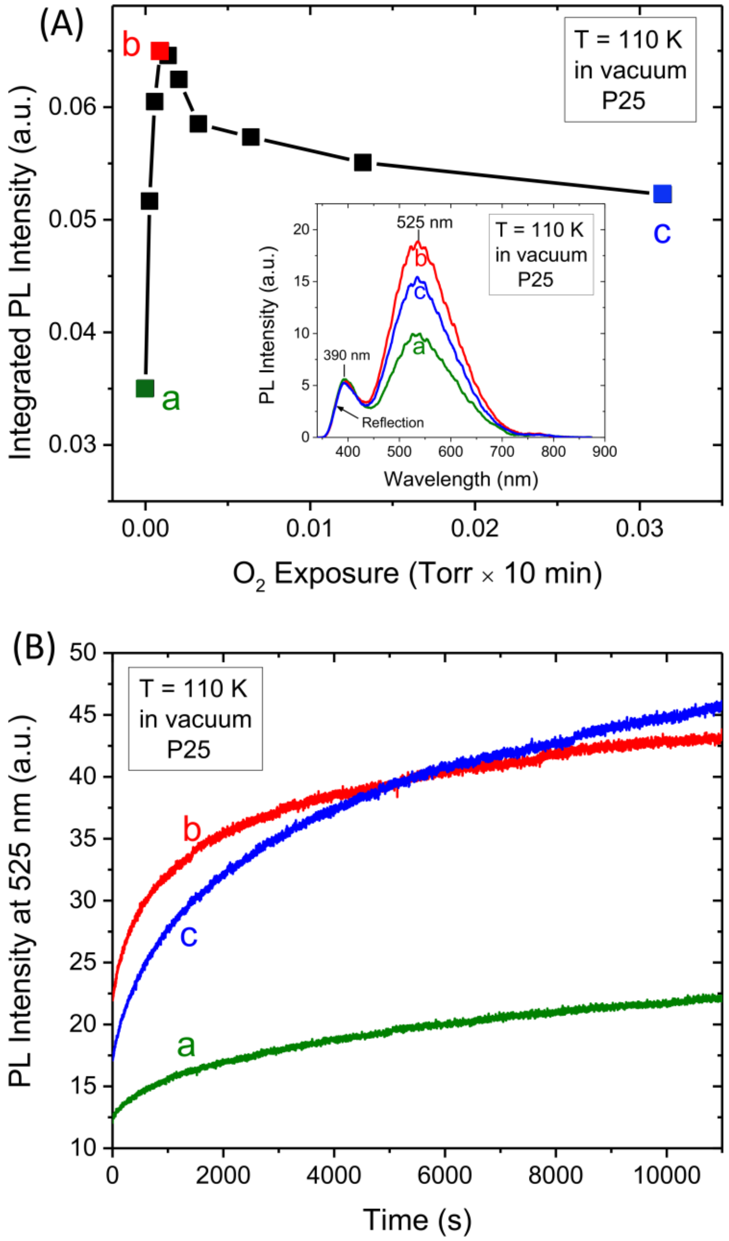

Figure 5.2. Effect of O_2 exposure on the PL of TiO_2 photoexcited at 320 nm (post-oxygen exposure measurement). (A) Integrated PL intensity (emission peak area) after O_2 exposure in the dark measured at 110 K in vacuum. The inset shows PL spectra of samples after O_2 exposure of (a) 0 Torr × 10 min, (b) 9.1×10^{-4} Torr × 10 min and (c) 3.1×10^{-2} Torr × 10 min. (B) PL intensity at 525 nm under continuous UV irradiation of

states (a), (b) and (c) prepared in part (A). The photon irradiation flux at 320 nm was 1.5 × 10^{14} cm^{-2} s^{-1} at the sample surface.

The inset of Figure 5.2 (A) shows the typical PL emissions from P25, under 320 nm irradiation after different oxygen exposures: (a) 0 Torr × 10 min, (b) 9.1 × 10^{-4} Torr × 10 min, and (c) 3.1 × 10^{-2} Torr × 10 min. Only intensity changes of the ~ 525 nm PL emission peak of P25 are observed across different measurements. Figure 5.2 (A) shows the integrated PL emission intensity of TiO_2 following different amounts of O_2 exposure in the dark. The PL trend of an increase followed by decrease with increasing O_2 exposure suggests that the O_2 exposure has two different effects on the band bending of TiO_2. When the exposure is small, the PL emission increases with O_2 exposure, suggesting that small O_2 exposures cause the band bending of TiO_2 to be less upward. The PL intensity reaches a maximum for a critical O_2 exposure of ~ 9.1 × 10^{-4} Torr for 10 min [state (b) in Figure 5.2 A; a 174,720 Langmuir dose]. When TiO_2 is exposed to further O_2, the PL intensity monotonically decreases, indicating that the band bending becomes more upward with increasing O_2 exposure beyond the critical amount.

Surface science studies on oxygen adsorption on the rutile TiO_2(110) surface show that both irreversible dissociative and reversible molecular oxygen adsorption coexist. Initially when the oxygen exposure is small, the adsorption is mainly through the dissociative channel, which heals the oxygen vacancies[25, 32] or reacts with other defects, such as Ti^{3+}. [27, 31] When the oxygen exposure exceeds the critical amount, there are less defects (such as oxygen vacancies) available and therefore the adsorption is mainly molecular chemisorption which forms O_2^- (or O_2^{2-}) [8, 18, 23] on TiO_2 surfaces.[25, 32] Although the interaction between oxygen and anatase has not been extensively studied using surface science techniques, due to the limited stability of macroscopic anatase surfaces, and there is no solid conclusion as to which site (or defect) is responsible for oxygen adsorption, certain results suggest that both reversible molecular oxygen chemisorption and irreversible oxygen adsorption due to reaction with defects are likely to occur on anatase TiO_2. The molecular chemisorption of oxygen as O_2^- on anatase surface has been demonstrated using electron paramagnetic resonance (EPR)[39-41] and density functional theory (DFT) calculations.[42-43] Diebold *et al.*[44] found by STM observation and supporting DFT calculations that molecularly chemisorbed oxygen can react with the oxygen vacancies at the anatase surface (or subsurface) and subsequently heal oxygen vacancies.

We propose that the TiO_2 band bending change observed through PL are caused by the two different oxygen absorption channels on the anatase phase of P25: (1) an oxygen-defect reactive adsorption channel, and (2) a molecular chemisorption channel. When the O_2 exposure is low, the oxygen adsorption preferentially occurs through reaction with surface defects, outweighing the molecular chemisorption channel. This lowers the upward band bending of TiO_2 and increases the PL emission (region a-b in Figure 5.2 (A)). With increasing O_2 exposure, the population of available defects decreases and reactions with defects may be saturated at state b in Figure 5.2 (A). Consequently, the molecular chemisorption channel which accumulates negative charge by forming O_2^- or O_2^{2-} at the TiO_2 surface becomes the predominant agent of PL emission change once the O_2 exposure exceeds the critical amount. The accumulation of negative charges at the surface increases the upward band bending of TiO_2 [7, 16, 45] and therefore causes decreasing PL emission with increasing O_2 exposure (region b-c in Figure 5.2 (A)).

Figure 5.2 (B) shows the PL development under continuous UV irradiation of states a, b, and c prepared in Figure 5.2 (A) by oxygen exposures in the dark. All three PL curves increase under continuous UV irradiation, a portion of which can be explained by photoinduced band flattening (e.g., all of case “a” with no O_2 exposure). Under the energy gradient across the depletion layer of TiO_2, photoexcited holes preferentially migrate to the TiO_2 surface and neutralize the negative charges at the surface, causing the band bending to be less upward and the PL intensity to increase.[16] We propose that the initial band bending changes observed are caused by the oxygen-defect reactive adsorption and the molecular oxygen chemisorption. Under continuous UV irradiation, photodesorption of molecularly chemisorbed oxygen occurs as a result of its neutralization by photoexcited holes,[9, 33] leading to a diminishing chemisorbed O_2 coverage. However, continuous UV irradiation is not expected to influence the oxygen adsorption through reactions with defects because the oxygen atoms involved have become part of the TiO_2 lattice, either by healing the defects or forming new defects. The results of Figure 5.2 (B) are consistent with the proposed band bending model. The PL developing rate of $a < b < c$, caused by the photodesorption of molecularly adsorbed oxygen, is consistent with the O_2 exposure of $a < b < c$ during the preparation of these states, which indicates a molecularly chemisorbed oxygen coverage of $a < b < c$. The final PL intensity after UV irradiation is an indication of the band bending of the three states after the removal of molecularly adsorbed oxygen. The final intensity of curves b and c are close, suggesting that the band structures of b and c after the removal of chemisorbed oxygen are similar, which is consistent with the premise that the reaction between defects and oxygen was essentially saturated after the O_2 exposure of state b. Also, the fact that the final PL intensity of states b and c is much larger than that of state a, the state without any O_2 exposure, reconfirms the upward band bending lowering effect caused by reaction between near surface defects and adsorbed oxygen and suggests that the oxygen-defect reaction is irreversible under UV irradiation.

Figure 5.3 shows dynamical change of PL intensity in flowing O_2 gas with different pressures. From regions (a) to (e), it is shown that the PL intensity drops immediately after an increase of O_2 pressure, indicating that additional chemisorbed oxygen forms immediately after an O_2 pressure increase. In region (c), (d) and (e), the gradual increase of PL intensity is ascribed to the upward band banding lowering effect caused by oxygen-defect reactive adsorption. The immediate PL drop followed by gradual increase implies that molecularly adsorbed oxygen forms first and then gradually reacts with defects (e.g., requiring diffusion), consistent with the literature.[30, 43] This suggests that the oxygen-defect reactive channel discussed in Figure 5.2 occurs through an intermediate step of molecular chemisorption, which would have occurred during the 10 min oxygen exposure in the dark. The abnormal absence of the oxygen-defect reaction effect [gradual PL increase] in (b) may be caused by the extremely low oxygen pressure. The decrease of curve slope [gradual PL increase rate] in region (e) compared to region (d) is caused by the gradual decrease of available defects for reaction with adsorbed oxygen. In region (f) where the sample was pumped out again, the chemisorbed oxygen is gradually removed by photodesorption and therefore the PL intensity increases. The net increase of PL intensity in region (f) compared to (a) is because of the irreversible oxygen-defect reaction effect, which was invoked earlier to describe the Figure 5.2 (B) behavior. These results reinforce that the band bending of TiO_2 is affected by the oxygen-defect reaction and molecularly chemisorbed oxygen in different ways.

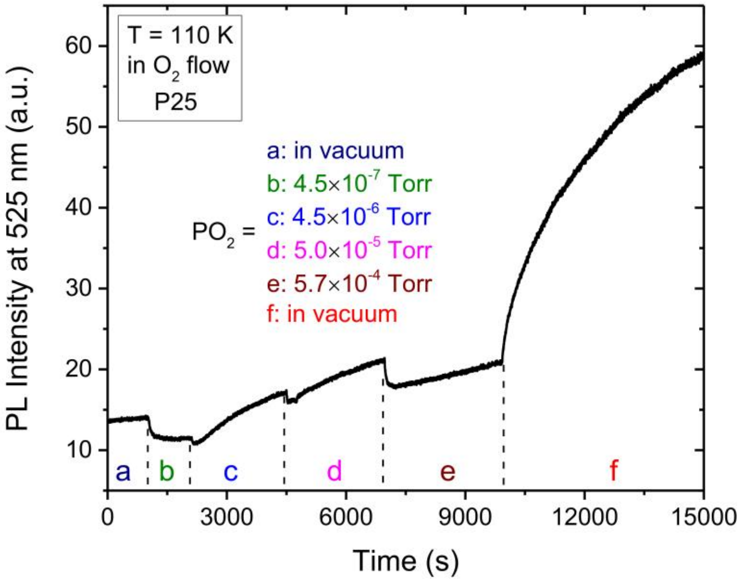

Figure 5.3. PL intensity at 525 nm in steady O_2 flow with selected pressures: (a) in vacuum, (b) 4.5×10^{-7} Torr, (c) 4.5×10^{-6} Torr, (d) 5.0×10^{-5} Torr, (e) 5.7×10^{-4} Torr and (f) in vacuum. Photon flux at 320 nm is 1.5×10^{14} cm^{-2} s^{-1} at the sample surface.

Figure 5.4 shows PL measurement with oxygen doses, in which certain pressures of oxygen were introduced into the chamber, then enclosed and isolated from the pump. The pressure curve in Figure 5.4 (A) shows that after each dose of oxygen, the chamber pressure immediately increases to the nominal value. Because of the adsorption onto the TiO_2 sample and the inner wall of liquid N_2 cooled reentrant dewar, the pressure in the chamber gradually decreases to the vacuum level. As shown in Figure 5.4 (A), the PL intensity first decreases and then increases after each dose of oxygen under UV irradiation. The decrease of PL intensity, which correlates to the more upward band bending, is caused by immediate formation of molecularly chemisorbed oxygen which is negatively charged by extracting electrons from the TiO_2.[16, 33, 45] However, the increase of PL intensity which correlates to less upward band bending originates from two mechanisms (discussed in

Appendix D): (1) oxygen reaction with defects,[26, 28] and (2) photodesorption of oxygen caused by reaction between photoexcited holes with molecularly chemisorbed oxygen.[9, 33] The overall oxygen treatment of TiO_2 shows a ~ 5-fold increase in PL intensity (end point of red curve) compared to the one without oxygen treatment (gray dash curve), indicating that the changing band bending of TiO_2 has a significant effect on the photoexcited electron-hole recombination rate that is correlated with the PL intensity. Appendix E provides a mathematical model calculating the ratio of photoexcitation in depletion layer where there is no PL emission to illustrate the effect of band bending on PL emission. Further examination of Figure 5.4 (A) shows that the net increase in PL intensity is only obvious for dose (a) and (b), while the net increase of PL intensity from dose (c) to (f) follows the same trend curve depicted in the Figure (dash dot arrowed curve), suggesting that the oxygen-defect reactive path has already saturated during dose (b) and the increase and decrease of PL in region (c) to (f) are mainly caused by the reversible adsorption and desorption of molecular oxygen, which agrees with our proposed model. The decrease followed by increase exceeding the original PL emission intensity observed in Figure 5.4 (D) carried out on pure anatase sample, which is the same as observed on P25, reconfirms that the proposed TiO_2-oxygen interaction model is plausible for anatase.

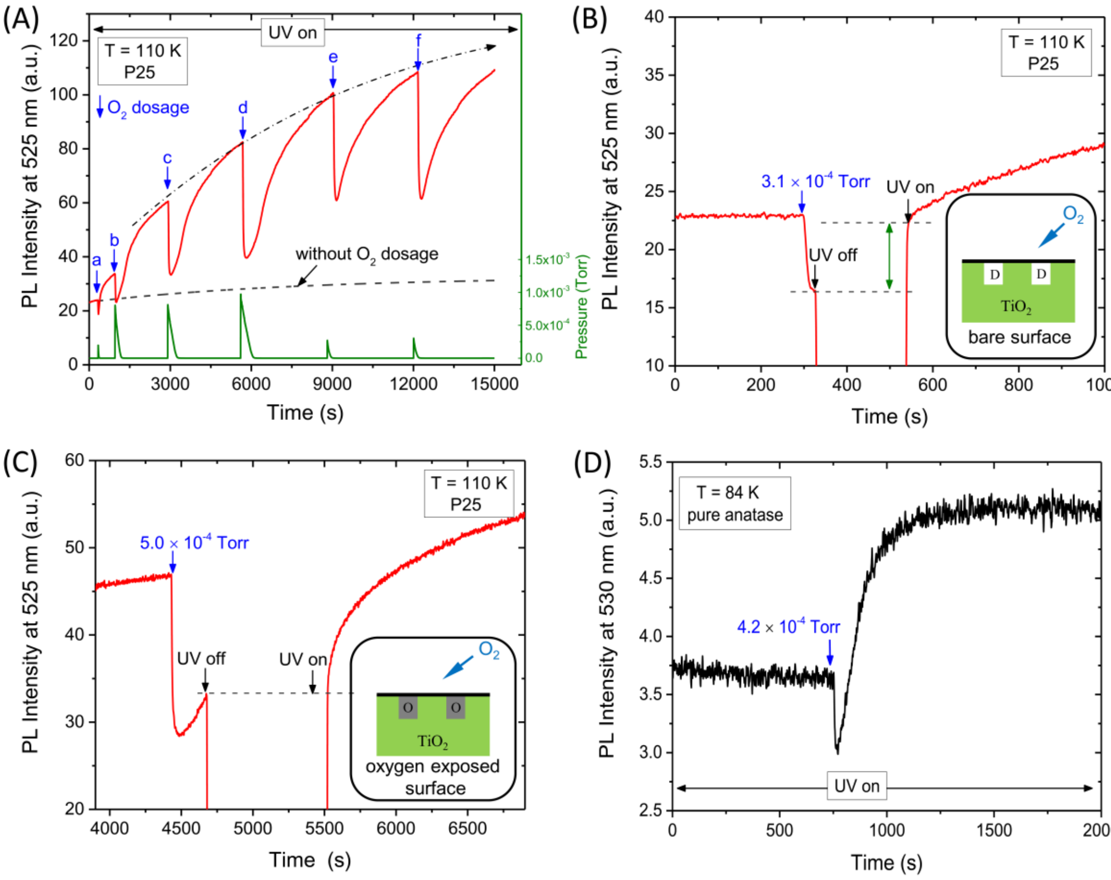

Figure 5.4. Effect of oxygen dose on PL of TiO_2. (A) Time-dependent PL intensity at 525 nm with UV irradiation kept on (red curve on the top). O_2 is introduced into the cell by 6 consecutive doses: (a) 3.1×10^{-4}, (b) 9.4×10^{-4}, (c) 9.4×10^{-4}, (d) 10.6×10^{-4}, (e) 3.1×10^{-4} and (f) 3.1×10^{-4} Torr. After each dose, O_2 is enclosed in the cell. The green curve on the bottom shows the measured oxygen pressure in the chamber. (B) UV irradiation dependence of PL intensity development when O_2 is introduced to a bare TiO_2 which has not been exposed to any O_2. (C) UV irradiation dependence of PL intensity development when O_2 is introduced to a TiO_2 surface which was initially exposed to 4.1×10^{-4} Torr O_2. (D) PL intensity change for a pure anatase sample subjected to a step oxygen dose of 4.2×10^{-4} Torr from high vacuum condition.

Figure 5.4 (B) and 5 (C) show the UV irradiation dependence of oxygen-defect reaction and desorption of molecularly adsorbed oxygen in the increase of PL intensity. In Figure 5.4 (B), O_2 was dosed to clean TiO_2 surface near which defects are available. Although UV irradiation is turned off, an increase of PL in the dark is still observed, suggesting that UV irradiation is not indispensable for the oxygen-defect reaction, which can also be concluded from the PL increase caused by oxygen exposure for 10 min in the dark as illustrated in Figure 5.2 (A). In Figure 5.4 (C), O_2 was dosed to a TiO_2 surface which had already been dosed with a large amount of O_2 to consume available near surface defects. The fact that there is no PL intensity increase in the dark demonstrates that the desorption of chemisorbed oxygen only occurs under UV irradiation.

5.3.2 Summarized oxygen adsorption and band bending change model

Figure 5.5 summarizes the two effects of oxygen adsorption on changing band bending of anatase TiO_2 observed from above PL measurements. There are defects near the surface of clean TiO_2 and the band bending is upward (Figure 5.5a).[16] After oxygen exposure, molecular oxygen chemisorbs immediately on TiO_2 surface by extracting electrons from TiO_2. The negatively charged chemisorbed oxygen accumulates negative charge on TiO_2 surface and therefore increases the upward band bending of TiO_2 (Figure 5.5b). When defects (such as oxygen vacancy or Ti^{3+}) are available, molecularly adsorbed oxygen further interacts with defects, either by healing the defects or forming new defects, resulting in decrease of the upward TiO_2 band bending (Figure 5.5c). When the O_2 exposure is small, the oxygen-defect reaction effect outweighs the molecular chemisorption effect, causing less upward band bending of TiO_2 and increased PL compared to clean TiO_2. While O_2 exposure exceeds a critical amount, the molecular chemisorption of oxygen is predominant and upward band bending increases with increasing O_2 exposure. When UV irradiation is applied, molecularly adsorbed oxygen reversibly desorbs from TiO_2 surface via its reaction with photoexcited holes but the oxygen-defect reaction is irreversible and retained. This causes even less upward band bending and even higher PL intensity (Figure 5.5d). These PL observations and the band bending model are consistent with the interactions between oxygen and the anatase TiO_2 surface elucidated by direct STM observations and DFT calculations by Diebold *et al.*[44]

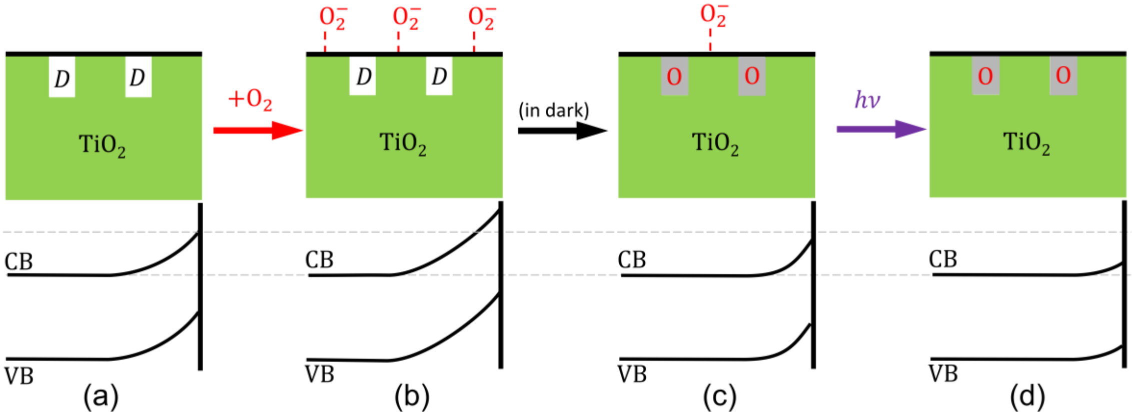

Figure 5.5. Schematics showing the band banding change of TiO_2 caused by interaction with oxygen. The *D* means defect site near TiO_2 surface.

5.3.4 Possible origin of band bending change

Several reports have indicated that as-prepared TiO_2 yields an upward band bending.[16, 18] The initial upward band bending of TiO_2 may mainly come from the Fermi level alignment. TiO_2 is usually oxygen deficient which may result in defects such as Ti^{3+}

interstitials ($\mathrm{Ti_i^{3+}}$) [27, 31] or oxygen vacancies ($\mathrm{V_O^{2+}}$). The formation of $\mathrm{Ti_i^{3+}}$ and $\mathrm{V_O^{2+}}$ can be written as the following equations:

$$\mathrm{Ti} \rightarrow \mathrm{Ti_i^{3+}} + 3\mathrm{e^-} \tag{5.1}$$

$$\mathrm{O_O} \rightarrow \mathrm{V_O^{2+}} + 2\mathrm{e^-} + \frac{1}{2}\mathrm{O_2(g)} \tag{5.2}$$

Both reactions donate free electrons to TiO_2 lattice and thus make TiO_2 n-type and shift the Fermi energy upward, which can be described according to equation (5.3)[46]:

$$E_F = (E_C + E_V)/2 + k_B T \ln(N_D/n_i) \tag{5.3}$$

in which E_C and E_V are the energy of conduction and valence band, N_D is the donor (i.e. defects) density, and n_i is the electron/hole density for the intrinsic semiconductor, which is a constant at certain temperature. Because the bulk of TiO_2 experiences lower oxygen pressure during preparation, we postulate that the bulk contains more defects than the surface of TiO_2, hence resulting in a higher Fermi level of the bulk compared to the surface before equilibrium (Figure 5.6 (A)). Upon equilibrium, electrons flow from the bulk of TiO_2, where the Fermi level is higher, to the surface, where the Fermi level is lower, until Fermi levels align. The rearrangement of electrons results in extra electrons accumulated at the surface and leads to upward band bending near the surface of TiO_2, as depicted in Figure 5.6 (B). In addition, the unpaired electrons in surface dangling bonds interacting with each other also contributes to upward band bending by forming an electronic state with a narrow energy band.[7]

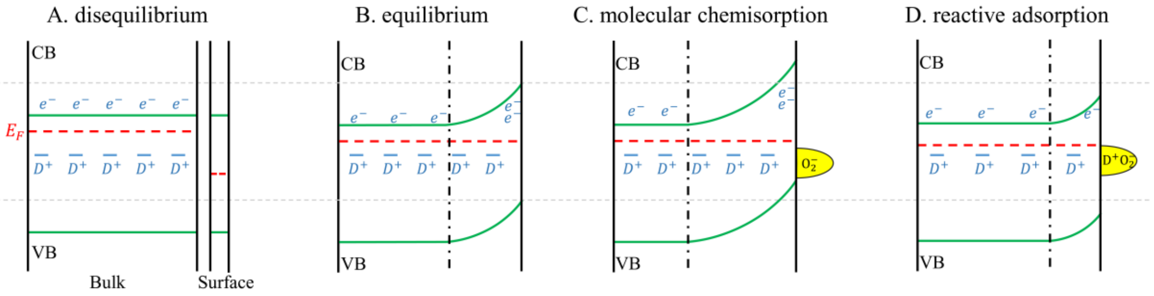

Figure 5.6. Schematics showing the possible origin of TiO_2 band bending change caused by oxygen adsorption. E_F – Fermi level, D^+ – donor defects. (A) Fermi energy difference caused by imbalanced impurities; (B) upward band bending formed upon Fermi level pinning; (C) increased upward band bending due to molecularly oxygen adsorption, O_2^- – negatively charged molecularly adsorbed oxygen; (D) decreased band bending caused by oxygen-defect reactive adsorption, $D^+O_2^-$ – product due to reaction between oxygen and the defect site.

When oxygen adsorbs through the molecular chemisorption channel, electrons in the TiO_2 lattice are extracted to the surface and forms negatively charged oxygen species. This accumulates more electrons at the surface thus making the band bending more upward (Figure 5.6 (C)). The chemisorbed oxygen may further react with defects diffused from the bulk to the surface through the oxygen-defect reaction channel. Besenbacher *et al.* [27] have found that near surface Ti interstitials can migrate to rutile $TiO_2(110)$ surface and react with oxygen to form TiO_x (x~2) islands on TiO_2 surface. Because the defect sites reacting with O_2^- such as Ti_i^{3+} or V_O^{2+} are positively charged (using the lattice as reference), the oxygen-defect reaction channel decreases the upward band bending by reducing the accumulated negative charge on TiO_2 surface (Figure 5.6 (D)). Compared to the original lattice, the complete oxygen-defect reaction via an intermediate step of molecularly adsorbed oxygen decreases the density of donor defects beneath the surface and therefore decreases the Fermi level according to equation (3), thus resulting in less upward band bending compared to the state without oxygen adsorption, as shown by comparing Figure 5.6 (D) to Figure 5.6 (B), which explains the overall PL increase caused by the oxygen-defect reaction channel.

5.4 Conclusion

By employing anatase-selective PL spectroscopy of P25 TiO_2 and the dead-layer model, we observed different band bending changes in anatase TiO_2 due to oxygen adsorption, which have not been directly observed for anatase in the past but are similar to expectations based on O_2/rutile chemistries. The main findings include the following:

(1) Oxygen adsorption changes the band bending of anatase TiO_2 in two different ways by two adsorption channels: oxygen-defect reactive adsorption channel and molecular oxygen adsorption channel.

(2) Through the molecular oxygen adsorption channel, negatively charged oxygen molecules chemisorbs on TiO_2 surfaces by extracting electrons from TiO_2 lattice, resulting in more upward band bending of TiO_2. Molecularly adsorbed oxygen and its effect on band bending of TiO_2 can be reversibly removed by UV irradiation.

(3) When defects are available, oxygen-defect reactive adsorption channel occurs preferentially through an intermediate step of molecular oxygen adsorption. The

reaction between oxygen and defect sites decreases the upward band bending of TiO_2 irreversibly.

(4) A 5-fold PL intensity increase was observed, suggesting interaction between oxygen and TiO_2 has significant effect on changing charge recombination via band bending changes.

The proposed oxygen TiO_2 band bending changes originate from anatase, which has been rarely studied by surface science techniques but is more important in photocatalysis. The anatase-selective PL from P25 provides a new tool to investigate anatase surface chemistry. This report on band bending of TiO_2 provides a new perspective on how TiO_2 photocatalytic reactions may be modulated by oxygen.

References

1. Hoffmann, M. R.; Martin, S. T.; Choi, W. Y.; Bahnemann, D. W., Environmental Applications of Semiconductor Photocatalysis. *Chemical Reviews* **1995**, *95*, 69-96.
2. Linsebigler, A. L.; Lu, G. Q.; Yates, J. T., Photocatalysis on TiO_2 Surfaces - Principles, Mechanisms, and Selected Results. *Chemical Reviews* **1995**, *95*, 735-758.
3. Ni, M.; Leung, M. K. H.; Leung, D. Y. C.; Sumathy, K., A Review and Recent Developments in Photocatalytic Water-Splitting Using TiO_2 for Hydrogen Production. *Renewable & Sustainable Energy Reviews* **2007**, *11*, 401-425.
4. Kamat, P. V., Quantum Dot Solar Cells. Semiconductor Nanocrystals as Light Harvesters. *Journal of Physical Chemistry C* **2008**, *112*, 18737-18753.
5. Panayotov, D. A.; Morris, J. R., Thermal Decomposition of a Chemical Warfare Agent Simulant (DMMP) on TiO_2: Adsorbate Reactions with Lattice Oxygen as Studied by Infrared Spectroscopy. *Journal of Physical Chemistry C* **2009**, *113*, 15684-15691.
6. Dohnalek, Z.; Lyubinetsky, I.; Rousseau, R., Thermally-Driven Processes on Rutile TiO_2(110)-(1 X 1): A Direct View at the Atomic Scale. *Progress in Surface Science* **2010**, *85*, 161-205.
7. Zhang, Z.; Yates, J. T., Band Bending in Semiconductors: Chemical and Physical Consequences at Surfaces and Interfaces. *Chemical Reviews* **2012**, *112*, 5520-5551.
8. Zhang, Z.; Yates, J. T., Electron-Mediated CO Oxidation on the TiO_2(110) Surface During Electronic Excitation. *Journal of the American Chemical Society* **2010**, *132*, 12804-12807.
9. Zhang, Z.; Yates, J. T., Effect of Adsorbed Donor and Acceptor Molecules on Electron Stimulated Desorption: O_2/TiO_2(110). *Journal of Physical Chemistry Letters* **2010**, *1*, 2185-2188.
10. Zeng, Y.; Cheng, G. F.; Wen, M.; Wu, W., Effect of External Bias Voltage and Coating Thickness on the Photocatalytic Activity of Thermal Sprayed TiO_2 Coating. *Progress in Organic Coatings* **2008**, *61*, 321-325.
11. Konstantinou, I. K.; Albanis, T. A., TiO_2-Assisted Photocatalytic Degradation of Azo Dyes in Aqueous Solution: Kinetic and Mechanistic Investigations - A Review. *Applied Catalysis B-Environmental* **2004**, *49*, 1-14.
12. Min, L. Y.; Wu, X. Z.; Tetsuya, S.; Inoue, H., Time-Resolved Chemiluminescence Study of the TiO_2 Photocatalytic Reaction and Its Induced Active Oxygen Species. *Luminescence* **2007**, *22*, 105-112.
13. Pichat, P., Some Views About Indoor Air Photocatalytic Treatment Using TiO_2: Conceptualization of Humidity Effects, Active Oxygen Species, Problem of C-1-C-3 Carbonyl Pollutants. *Applied Catalysis B-Environmental* **2010**, *99*, 428-434.
14. Hollingsworth, R. E.; Sites, J. R., Photo-Luminescence Dead Layer in P-Type InP. *Journal of Applied Physics* **1982**, *53*, 5357-5358.
15. Meyer, G. J.; Lisensky, G. C.; Ellis, A. B., Evidence for Adduct Formation at the Semiconductor Gas Interface - Photoluminescent Properties of Cadmium Selenide in the Presence of Amines. *Journal of the American Chemical Society* **1988**, *110*, 4914-4918.

16. Stevanovic, A.; Buttner, M.; Zhang, Z.; Yates, J. T., Photoluminescence of TiO_2: Effect of UV Light and Adsorbed Molecules on Surface Band Structure. *Journal of the American Chemical Society* **2012**, *134,* 324-332.
17. Stevanovic, A.; Yates, J. T., Probe of NH_3 and CO Adsorption on the Very Outermost Surface of a Porous TiO_2 Adsorbent Using Photoluminescence Spectroscopy. *Langmuir* **2012**, *28*, 5652-5659.
18. Anpo, M.; Tomonari, M.; Fox, M. A., *in situ* Photoluminescence of TiO_2 as a Probe of Photocatalytic Reactions. *Journal of Physical Chemistry* **1989**, *93*, 7300-7302.
19. Mo, S. D.; Ching, W. Y., Electronic and Optical-Properties of 3 Phases of Titanium-Dioxide - Rutile, Anatase, and Brookite. *Physical Review B* **1995**, *51*, 13023-13032.
20. Ghosh, A. K.; Maruska, H. P., Photoelectrolysis of Water in Sunlight with Sensitized Semiconductor Electrodes. *Journal of the Electrochemical Society* **1977**, *124*, 1516-1522.
21. Ioannides, T.; Verykios, X. E., Charge Transfer in Metal Catalysts Supported on Doped TiO_2: A Theoretical Approach Based on Metal-Semiconductor Contact Theory. *Journal of Catalysis* **1996**, *161*, 560-569.
22. Luth, H., *Solid Surfaces, Interfaces and Thin Films*; Springer: New York, 2010.
23. Lu, G. Q.; Linsebigler, A.; Yates, J. T., The Photochemical Identification of 2 Chemisorption States for Molecular-Oxygen on TiO_2(110). *Journal of Chemical Physics* **1995**, *102*, 3005-3008.
24. Lu, G. Q.; Linsebigler, A.; Yates, J. T., The Adsorption and Photodesorption of Oxygen on the TiO_2(110) Surface. *Journal of Chemical Physics* **1995**, *102*, 4657-4662.
25. Henderson, M. A.; Epling, W. S.; Perkins, C. L.; Peden, C. H. F.; Diebold, U., Interaction of Molecular Oxygen with the Vacuum-Annealed TiO_2(110) Surface: Molecular and Dissociative Channels. *Journal of Physical Chemistry B* **1999**, *103*, 5328-5337.
26. Wendt, S.; Schaub, R.; Matthiesen, J.; Vestergaard, E. K.; Wahlstrom, E.; Rasmussen, M. D.; Thostrup, P.; Molina, L. M.; Laegsgaard, E.; Stensgaard, I., et al., Oxygen Vacancies on TiO_2(110) and Their Interaction with H_2O and O_2: A Combined High-Resolution STM and DFT Study. *Surface Science* **2005**, *598*, 226-245.
27. Wendt, S.; Sprunger, P. T.; Lira, E.; Madsen, G. K. H.; Li, Z. S.; Hansen, J. O.; Matthiesen, J.; Blekinge-Rasmussen, A.; Laegsgaard, E.; Hammer, B., et al., The Role of Interstitial Sites in the Ti3d Defect State in the Band Gap of Titania. *Science* **2008**, *320*, 1755-1759.
28. Lira, E.; Hansen, J. O.; Huo, P.; Bechstein, R.; Galliker, P.; Laegsgaard, E.; Hammer, B.; Wendt, S.; Besenbacher, F., Dissociative and Molecular Oxygen Chemisorption Channels on Reduced Rutile TiO_2(110): An STM and TPD Study. *Surface Science* **2010**, *604*, 1945-1960.
29. Scheiber, P.; Riss, A.; Schmid, M.; Varga, P.; Diebold, U., Observation and Destruction of an Elusive Adsorbate with STM: O_2/TiO_2(110). *Physical Review Letters* **2010**, *105*.
30. Wang, Z. T.; Du, Y. G.; Dohnalek, Z.; Lyubinetsky, I., Direct Observation of Site-Specific Molecular Chemisorption of O_2 on TiO_2(110). *Journal of Physical Chemistry Letters* **2010**, *1*, 3524-3529.

31. Lira, E.; Wendt, S.; Huo, P. P.; Hansen, J. O.; Streber, R.; Porsgaard, S.; Wei, Y. Y.; Bechstein, R.; Laegsgaard, E.; Besenbacher, F., The Importance of Bulk Ti^{3+} Defects in the Oxygen Chemistry on Titania Surfaces. *Journal of the American Chemical Society* **2011**, *133*, 6529-6532.
32. Wang, Z. T.; Deskins, N. A.; Lyubinetsky, I., Direct Imaging of Site-Specific Photocatalytical Reactions of O_2 on TiO_2(110). *Journal of Physical Chemistry Letters* **2012**, *3*, 102-106.
33. Henderson, M. A.; Shen, M. M.; Wang, Z. T.; Lyubinetsky, I., Characterization of the Active Surface Species Responsible for UV-Induced Desorption of O_2 from the Rutile TiO_2(110) Surface. *Journal of Physical Chemistry C* **2013**, *117*, 5774-5784.
34. Petrik, N. G.; Kimmel, G. A., Oxygen Photochemistry on TiO_2(110): Recyclable, Photoactive Oxygen Produced by Annealing Adsorbed O_2. *Journal of Physical Chemistry Letters* **2011**, *2*, 2790-2796.
35. Tan, S. J.; Ji, Y. F.; Zhao, Y.; Zhao, A. D.; Wang, B.; Yang, J. L.; Hou, J. G., Molecular Oxygen Adsorption Behaviors on the Rutile TiO_2(110)-1 X 1 Surface: An *in situ* Study with Low-Temperature Scanning Tunneling Microscopy. *Journal of the American Chemical Society* **2011**, *133*, 2002-2009.
36. Yates, J. T., Photochemistry on TiO_2: Mechanisms Behind the Surface Chemistry. *Surface Science* **2009**, *603*, 1605-1612.
37. Petrik, N. G.; Kimmel, G. A., Electron- and Hole-Mediated Reactions in UV-Irradiated O_2 Adsorbed on Reduced Rutile TiO_2(110). *Journal of Physical Chemistry C* **2011**, *115*, 152-164.
38. Ohno, T.; Sarukawa, K.; Tokieda, K.; Matsumura, M., Morphology of a TiO_2 Photocatalyst (Degussa, P-25) Consisting of Anatase and Rutile Crystalline Phases. *Journal of Catalysis* **2001**, *203*, 82-86.
39. Konstantinova, E.; Weidmann, J.; Dittrich, T., Influence of Adsorbed Water and Oxygen on the Photoluminescence and EPR of Por-TiO_2 (Anatase). *Journal of Porous Materials* **2000**, *7*, 389-392.
40. Coronado, J. M.; Maira, A. J.; Conesa, J. C.; Yeung, K. L.; Augugliaro, V.; Soria, J., EPR Study of the Surface Characteristics of Nanostructured TiO_2 under UV Irradiation. *Langmuir* **2001**, *17*, 5368-5374.
41. Berger, T.; Sterrer, M.; Diwald, O.; Knozinger, E., Charge Trapping and Photoadsorption of O_2 on Dehydroxylated TiO_2 Nanocrystals - An Electron Paramagnetic Resonance Study. *Chemphyschem* **2005**, *6*, 2104-2112.
42. Aschauer, U.; Chen, J.; Selloni, A., Peroxide and Superoxide States of Adsorbed O_2 on Anatase TiO_2 (101) with Subsurface Defects. *Physical Chemistry Chemical Physics* **2010**, *12*, 12956-12960.
43. Li, Y. F.; Aschauer, U.; Chen, J.; Selloni, A., Adsorption and Reactions of O_2 on Anatase TiO_2. *Accounts of Chemical Research* **2014**, *47*, 3361-3368.
44. Setvin, M.; Aschauer, U.; Scheiber, P.; Li, Y. F.; Hou, W. Y.; Schmid, M.; Selloni, A.; Diebold, U., Reaction of O_2 with Subsurface Oxygen Vacancies on TiO_2 Anatase (101). *Science* **2013**, *341*, 988-991.
45. Porsgaard, S.; Jiang, P.; Borondics, F.; Wendt, S.; Liu, Z.; Bluhm, H.; Besenbacher, F.; Salmeron, M., Charge State of Gold Nanoparticles Supported on Titania under Oxygen Pressure. *Angewandte Chemie-International Edition* **2011**, *50*, 2266-2269.

46. Roulston, D. J., *An Introduction to the Physics of Semiconductor Devices*; Oxford University Press: New York, 1999, p xviii, 290 p.

6 Photoreduction of Hydrogen Cations on TiO_2 and Its Impact on Surface Band Bending and the Charge Carrier Recombination Rate: A Photoluminescence Study under High Vacuum Conditions

(modified from *J. Phys. Chem. C*, **2018**, 122(15): 8288-8294)

Abstract

The interaction between hydrogen species and TiO_2 surfaces is important because of its relevance to hydrogen production in the photocatalytic splitting of water on TiO_2. In this study, the effect of the photocatalytic reduction of hydrogen cations, a half photoelectrochemical reaction run under high vacuum conditions, on the surface band bending of TiO_2 was investigated by photoluminescence (PL) spectroscopy. Exposure of TiO_2 to molecular hydrogen had no effect on the PL emission from TiO_2 but the PL intensity increased under UV irradiation when TiO_2 was exposed to hydrogen cations produced by ionization of molecular hydrogen by a cold cathode pressure gauge. The PL intensity increase, signaling a decrease in the upward band bending and increased electron-hole radiative recombination rate, is caused by charge transfer during photoreduction of hydrogen cations. Residual photoexcited holes left in TiO_2 due to the transfer of photoexcited electrons to hydrogen cations tend to accumulate at the TiO_2 surface, balancing the originally trapped electrons at the TiO_2 surface and thereby lowering the original upward band bending. These unusual observations point out that charge transfer during a photoelectrochemical reaction at a semiconductor interface alters the surface band

bending and photoexcited electron-hole recombination rate in ways that are likely to impact the efficiency of photocatalytic devices.

6.1 Introduction

Enhancing photoexcited electron-hole pair separation and suppressing their recombination in TiO_2 have attracted vast research interest due to their central roles in improving the efficiency of photocatalytic hydrogen production, pollutant decomposition, and photovoltaic cells based on TiO_2.[1-3] Though it has been rarely studied, tuning the surface band bending of TiO_2 to more efficiently promote electron-hole pair separation and actively sweep desired charge carriers to the surfaces is a promising method to improve photocatalytic activity. Upward band bending is usually observed at TiO_2 surfaces because negative charges accumulate at its surfaces upon the equilibration of the bulk and surface Fermi energies.[4-5] The upward band bending towards the surface directs photoexcited electrons and holes formed near the surface to migrate in opposite directions, and thus improves charge separation.[6-8] Sheppard *et al.*[9] showed by surface photovoltage measurements that surface band bending introduced by doping niobium at different concentrations influences charge separation rates in TiO_2 during illumination. Zhang *et al*.[7] reported that a 100-fold difference in the hole-mediated photodesorption rate of O_2 from the $TiO_2(110)$ surface can be achieved by modulating the band bending of TiO_2 through donor or acceptor molecule adsorption. In addition, the effects of doping various cations into TiO_2 on photocatalytic hydrogen production rates, attributed to the band bending change by Karakitsou *et al*.,[10] indicate that band bending change is a physical process that can be applied to a wide range of situations rather than a site/molecule specific chemical process which is only valid for certain sites or molecules. Thus, studying band bending may provide fundamental insights to better understand and improve a broad range of photocatalytic processes and devices involving TiO_2.

Photoluminescence (PL) spectroscopy which observes the radiative recombination of photoexcited charge carries (electron-hole pair) serves as a contactless and nondestructive method to characterize the band bending change of TiO_2 based on a dead-layer model in which there is little PL emission from the band bending region (depletion layer) underneath the surface where the local potential drives the photoexcited electrons and holes in opposite directions.[4-6, 11-13] Hence, the measured PL emission originates mainly from the TiO_2 bulk. Because the 320 nm UV irradiation only penetrates ~ 25 nm into the TiO_2 sample,[14] which is comparable to the length of the depletion layer, PL intensity change due to the band bending change in TiO_2 can be easily observed under high vacuum conditions.[5-6] An increase in upward band bending that increases the depth of the depletion layer and reduces the dimensions of the flat-band bulk region where radiative electron-hole pair recombination can take place, causes PL emission intensity to decrease. Therefore, a decrease in PL intensity indicates an increase in the upward band bending of TiO_2 and vice versa.[5]

The interaction between hydrogen and TiO_2 has been extensively studied due to its relevance to the final step in hydrogen production through photocatalytic water splitting. Although it was reported that H_2 only interacts with TiO_2 weakly through van der Waals interactions at room temperature,[15-17] heating TiO_2 in H_2 at elevated temperature introduces a new visible light response to TiO_2 and improves its photoactivity. These high temperature H_2/TiO_2 changes were attributed to hydrogen atom incorporation and subsequent OH and TiH formation in the TiO_2 lattice.[18-20] Studies have also shown that at room temperature, atomic hydrogen can diffuse into the TiO_2 lattice and form OH and TiH species, during which the Ti^{3+} concentration is increased due to the donation of electrons from hydrogen atoms, making TiO_2 a more n-type doped semiconductor.[15, 21-23] A key reaction, of unsurpassed interest, between hydrogen and TiO_2 is the reduction of protons by photoexcited electrons to form hydrogen molecules.[24] Nevertheless, little attention has been paid to the band bending of TiO_2 that modulates the electron-hole pair separation efficiency and which may change during photochemical reaction because charge transfer is involved.[5]

In this study, we use PL spectroscopy to report that the upward band bending of TiO_2 is decreased due to charge transfer incurred during the photoreduction of hydrogen cations at a TiO_2 nanopowder sample held at 90 K in a high vacuum chamber. A high vacuum is employed to eliminate possible band bending changes caused by adsorption of unknown species that might otherwise occur in air or aqueous solutions. The low sample temperature rules out the possibility that any atomic hydrogen present might be able to thermally diffuse into the lattice and thereby change the band bending. Similar PL behavior observed during photoreduction of gas phase helium cations suggests that the band bending change is a general physical outcome that will apply to other photocatalytic processes at semiconductor interfaces where charge transfer is involved.

6.2 Experimental

Experiments were conducted with the equipment illustrated in Figure 6.1, which was described in chapter 2 besides that an elbow with a tungsten filament was attached to study the effect of atomic hydrogen. The TiO_2 used in this study is P25 (Evonik Industries, formerly Degussa), a nanopowder that is widely used in research as a reference standard. The TiO_2 samples were heated in ~ 0.50 Torr O_2 at 600 K for 30 min and then pumped out for 10 min before each set of experiments to remove adsorbates from the TiO_2 surfaces and to make their properties consistent. To study the effects of gases, a selected amount of gas molecules was dosed into the chamber and isolated from the turbopump by closing the gate valve. To study the effect of atomic hydrogen, a tungsten filament connected to the chamber through an elbow was heated to 2300 K, which was measured by an optical pyrometer (Pyrometer Instrument Co.), to dissociate molecular hydrogen into hydrogen atoms.[25]

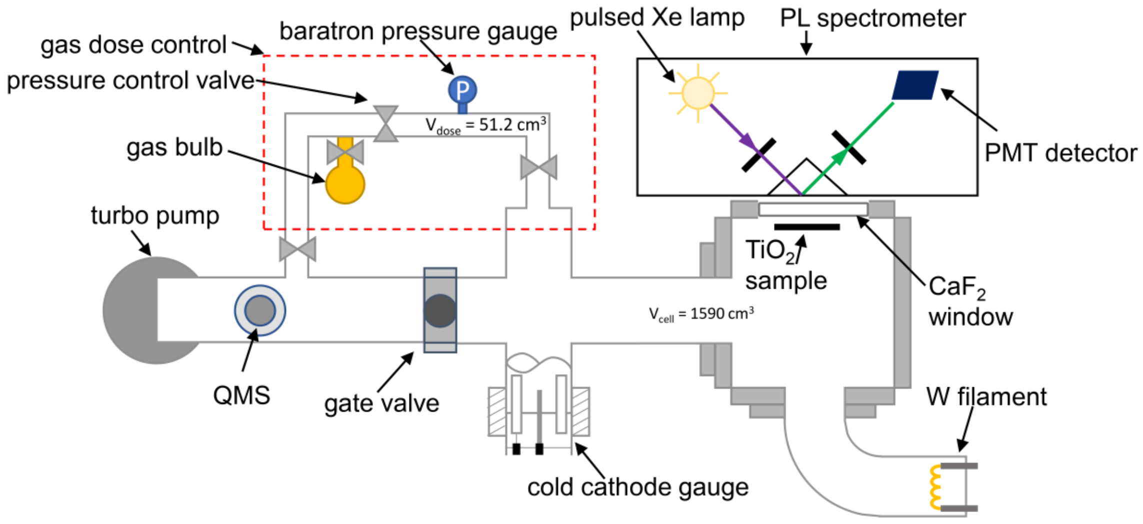

Figure 6.1. Configuration of the high vacuum system employed in this study.

6.3 Results and discussion

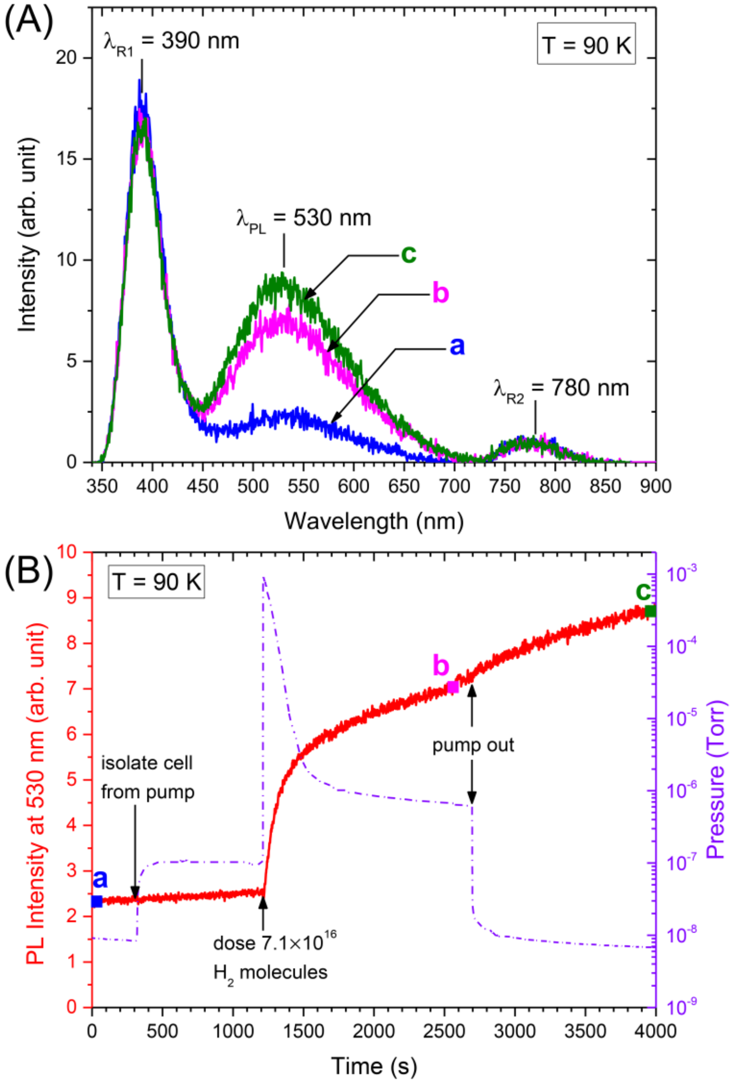

Figure 6.2. Effects of hydrogen dose on the PL of TiO_2. (A) PL spectra of TiO_2 collected at different states. (B) PL peak intensity change caused by H_2 dose (red) and chamber pressure measured by cold cathode gauge (purple).

6.3.1 *Effect of H_2 dosing on PL of TiO_2*

The PL spectra of P25 TiO_2 depicted in Figure 6.2 (A) are collected at the three different states marked in Figure 6.2 (B). Figure 6.2 (B) shows the effect of dosing H_2 on the PL peak intensity of TiO_2. Before dosing H_2, the chamber pressure increased from 10^{-8} to 10^{-7} Torr due to the isolation of the chamber from the vacuum pumps. This pressure increase shows no impact on the PL trend. However, it is clearly shown that the dose of 7.1×10^{16} H_2 molecules causes PL intensity to increase rapidly. The fast pressure drop after the H_2 dose is mainly due to the adsorption of H_2 onto the inner chamber walls experiencing liquid N_2 cooling, while the gradual drop of pressure is due to the equilibration of gas consumption due to ionization by the cold cathode gauge and gas adsorption/desorption on the chamber walls. A comparison between the chamber pressure and the PL increase rate suggests that the PL increase rate is correlated with the chamber H_2 pressure.

TiO_2 is an n-type semiconductor and naturally develops upward band bending underneath its surfaces[4-5], which can be treated as due to trapped negative charges on its surfaces for simplicity. The upward band bending of TiO_2 can be reduced when electron donor molecules are adsorbed on its surfaces because the donor molecules which donate electrons into the TiO_2 lattice possess positive charges on TiO_2 surfaces and therefore balance the originally trapped negative charges which causes the upward band bending. Similarly, the adsorption of electron acceptor molecules increases the upward band bending of TiO_2.[4, 6-7] It might be argued that the increase of PL upon H_2 dose should be attributed to H_2 acting as electron donor at the TiO_2 surfaces. However, various studies have shown that molecular hydrogen interacts only weakly with both anatase and rutile TiO_2.[16-17, 26-27] Lin *et al.*[16] reported only van der Waals interactions between H_2 molecules and anatase TiO_2 such that the extent of charge transfer between H_2 and TiO_2 is negligible. Consequently, the observed increase of PL intensity caused by H_2 dosing on TiO_2 may be more complicated.

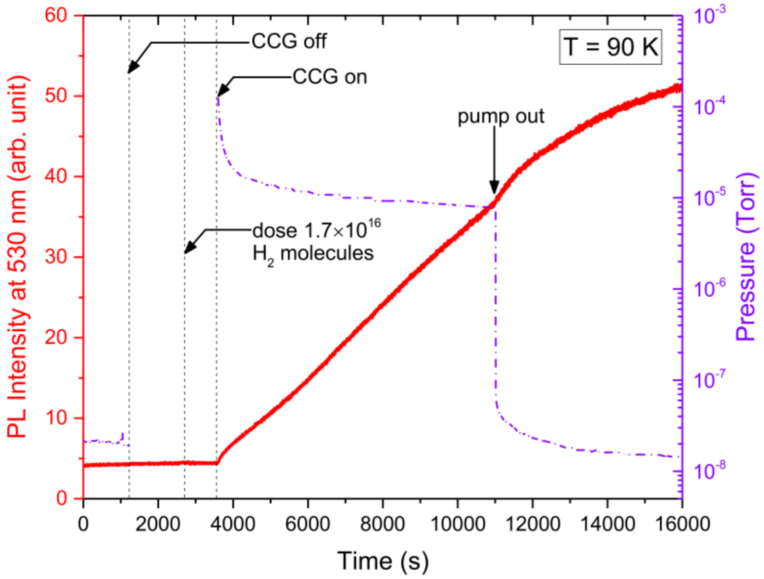

Figure 6.3. The role of the CCG in PL intensity increase caused by hydrogen dosing.

6.3.2 Role of cold cathode gauge (CCG) as ionizer

Figure 6.3 shows evidence that the increase of PL emission is not solely due to the introduction of hydrogen molecules. Instead, the CCG, which measures the chamber pressure, also plays an important role. As depicted, switching off the CCG at 1100 s shows no impact on PL of TiO_2 in vacuum. However, when the CCG is turned off, the effect that H_2 dosing increases PL emission from TiO_2 shown in Figure 6.2 is absent, as revealed by the dose of 1.7×10^{16} H_2 molecules at ~ 2800 s in Figure 6.3. The effect begins immediately after the CCG is switched on. These results indicate that the PL increase due to H_2 dosing is caused by species formed during the interaction between the CCG and H_2 molecules, instead of molecular hydrogen, which is consistent with reports that molecular H_2 interacts only weakly with TiO_2.[16-17, 26-27] It is worth noting that our finding at 90 K does not conflict with reports of black TiO_2 or hydrogen doped TiO_2 for which a processing temperature above 600 K is usually required.[18-19, 28] Figure 6.3 also shows that the PL intensity does not flatten out immediately after pump out but continues to increase with gradually decreasing slope. This behavior is mainly because the TiO_2 nanoparticle sample is porous and therefore gaseous species can be trapped by the pores.[29] The overall PL increase from ~ 5 to ~ 50 (arb. unit) in Figure 6.3 indicates that a 10-fold difference in the photoexcited electron-hole radiative recombination rate is caused by interaction between TiO_2 and the active hydrogen species produced by the CCG.

The CCG operates at a voltage of ~ 5 kV, wherein electrons extracted from the cathode are accelerated towards the anode. When gas molecules are present, the accelerated electrons can strike and ionize the gas molecules. The ions formed are collected by the cathode and the ion current provides a measure of the pressure. Based on the working mechanism of the CCG, it is reasonable to assume that the active species causing the PL increase are hydrogen cations formed during the ionization of H_2 molecules.[26] The fact that the CCG used to measure the chamber pressure also serves as an ionization source of H_2 molecules points to the attention that should be paid to the possibility that a measurement process may influence an experiment.

One possible but unlikely interference to the above postulation is that oxygen which may adsorb on the walls of the CCG during cleaning the sample can desorb by electron-stimulation from the CCG and cause changes to the PL of TiO_2. To rule out this possibility, the data shown in Figure 6.3 were collected after sample pretreatment in 0.500 Torr of H_2 for 20 minutes at measurement temperature (i.e. 90 K) after cleaning the sample in oxygen to exchange the oxygen adsorbed on the inner walls of the chamber. Due to the adsorption of hydrogen to the inner walls of the chamber, the starting chamber pressure in Figure 6.3 (> 10^{-8} Torr) is higher than that of Figure 6.2 (< 10^{-8} Torr). This also causes a slower pressure drop rate and a significantly higher chamber pressure before pump out (~ 10^{-5} Torr) than Figure 6.2 (< 10^{-6} Torr). This pretreatment by H_2 significantly decreases the possibility that the PL increase is caused by electron-stimulated oxygen desorption from the CCG. In addition, the result shown in Appendix G that oxygen desorption decreases PL intensity of TiO_2 completely rules out the possible effect by oxygen since oxygen works in the reverse way.

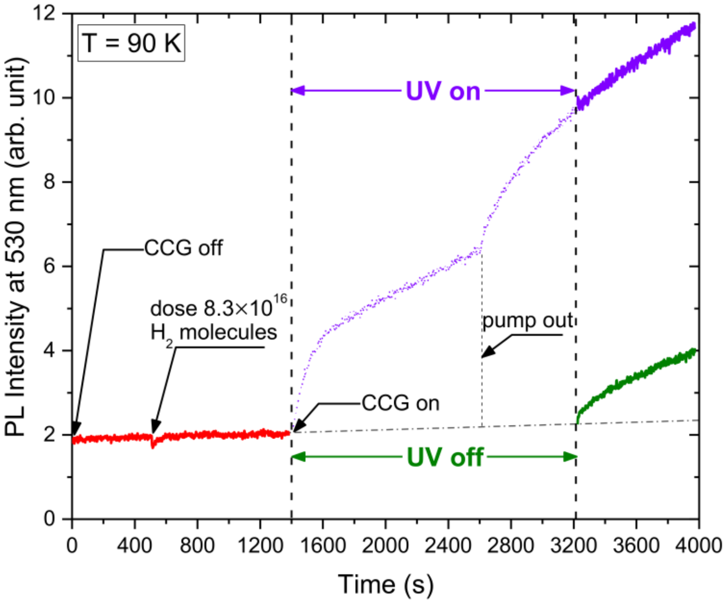

Figure 6.4. UV dependence of PL increase caused by interaction between CCG and H_2 molecules.

6.3.3 UV induced photoreaction

Figure 6.4 illustrates the influence of UV irradiation on the PL increase caused by active species produced during the interaction between the CCG and H_2 molecules, which are most likely to be hydrogen cations as discussed above. The green curve in Figure 6.4 shows that there is no PL increase without UV irradiation, even though the CCG is turned on and the active species contributing to the PL increase are produced. Instead, the purple curve collected under UV irradiation shows normal PL increase as observed before. The indispensability of UV irradiation for PL to increase elucidated in Figure 6.4 indicates that the PL increase is caused by reaction between photoexcited charges and the active hydrogen species generated by the CCG, which is most likely to be hydrogen cations.

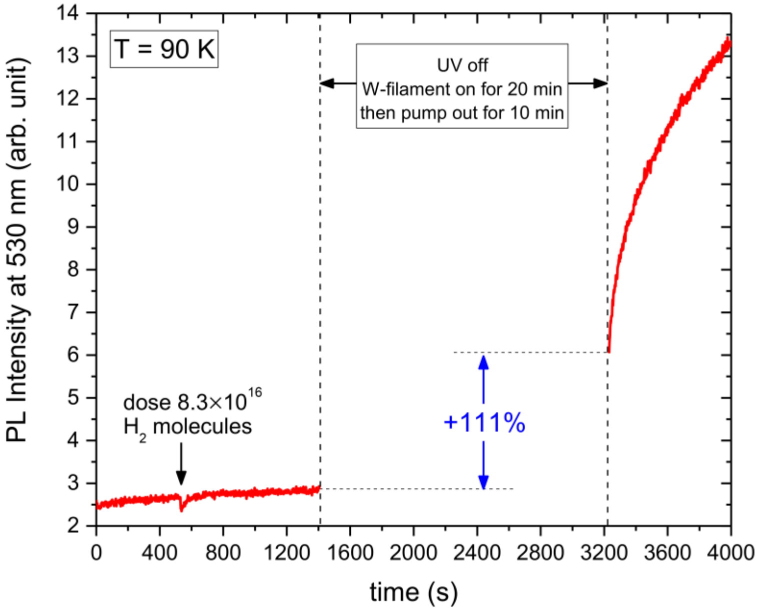

Figure 6.5. Effect of atomic hydrogen on PL development with the CCG off

6.3.4 Ruling out possibility of atomic hydrogen

Although the active species causing PL to increase is most likely to be H_2^+ based on the working mechanism of the CCG, which agrees well with the pressure dependent measurements shown in Appendix F, it is also possible that atomic hydrogen (H·) may be produced by collision or ionization of H_2 molecules by high energy electrons, or by collision of H_2^+ with H_2 molecules.[30-31] The latter two processes allow for the production of several kinds of H_n^+ (n=1, 2 or 3) cations. It can be deduced that atomic hydrogen adsorption onto TiO_2 should increase PL intensity based on reports from the literature. Although it was reported that atomic hydrogen can diffuse into TiO_2 lattices,[21-22] due to its small diffusion coefficient at low temperature,[15, 21-22] it is reasonable to assume that hydrogen atoms adsorbed onto TiO_2 at 90 K stay mainly on the surface. It was found that atomic hydrogen donates delocalized electrons into the TiO_2 lattice and thus atomic hydrogen acts as an electron donor.[23] Consequently, atomic hydrogen adsorbed on TiO_2 surfaces should be positively charged after donating electronic charge into the TiO_2 lattice, which will decrease the upward band bending of TiO_2 and increase PL. Hence, it is necessary to differentiate whether the PL increase due to molecular hydrogen gas exposure with CCG on is caused by hydrogen cations or atomic hydrogen.

Figure 6.5 illustrates the effect of atomic hydrogen, which was introduced to the TiO_2 sample by dissociating H_2 through a hot tungsten filament at 2300 K,[25] on the PL of TiO_2. The finding that atomic hydrogen exposure increases PL is consistent with the expectations expressed above. But, unlike the effect observed in Figure 6.4, atomic hydrogen not only causes PL to increase under UV irradiation, but also causes PL to increase without UV irradiation. The difference in the PL behavior between dosing atomic hydrogen and the active species produced by molecular hydrogen with the CCG on indicates that the active species produced by the CCG is unlikely to be atomic hydrogen. Hence, we propose that the active species that cause the PL to increase during molecular hydrogen dosing are hydrogen cations (H_n^+, with n most likely 2 [32]) which are produced by the ionization of hydrogen molecules by the CCG.

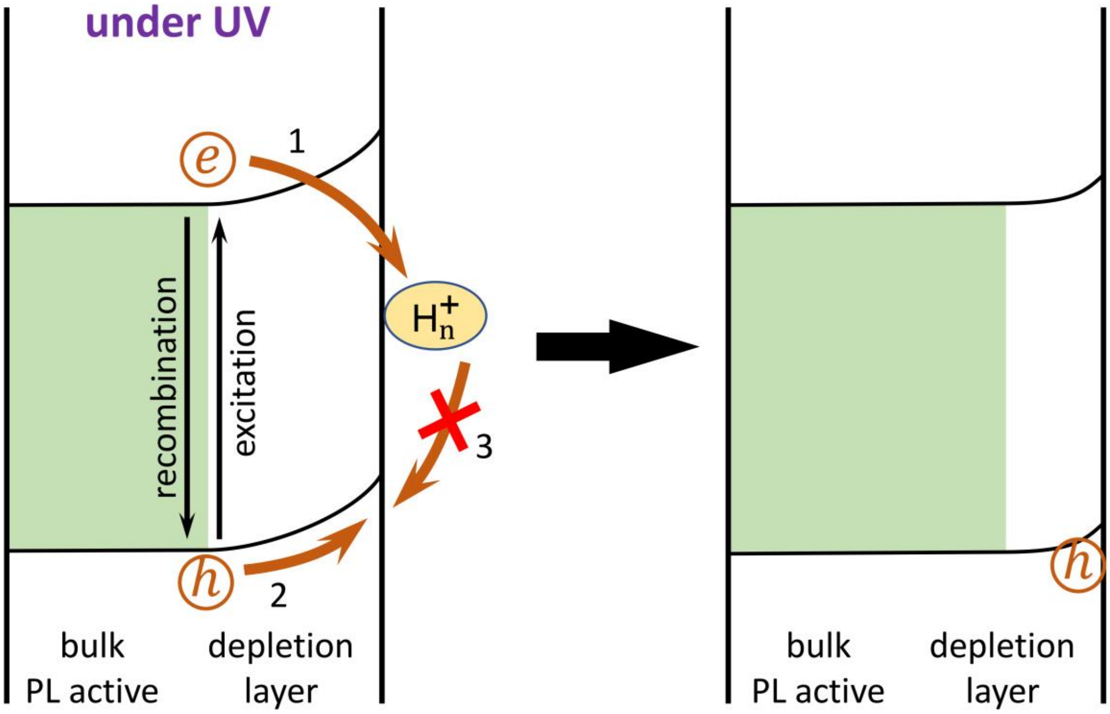

Figure 6.6. Schematic of processes occurring on the TiO_2 surface. The energy level diagrams are for electrons where the direction of increasing energy is reversed for holes.

6.3.5 *Band bending and charge recombination rate change model*

A proposed schematic explaining the PL increase caused by hydrogen cations under UV irradiation is illustrated as Figure 6.6. Hydrogen cations are produced during the measurement of chamber pressure through the CCG which ionizes hydrogen molecules. Under UV irradiation photoexcited electron-hole pairs are generated in TiO_2. Because the photoexcited electrons are strong reducing agents, hydrogen cations that arrive at TiO_2 surfaces are reduced by the photoexcited electrons (process 1). The photoexcited holes left in the valence band tend to migrate toward the surface of TiO_2 (process 2) under the electric field in the band bending region (depletion layer). The accumulation of holes at the surface of TiO_2 balances the originally trapped negative charges under TiO_2 surfaces and thus causes the band bending to be less upward. The reduction of upward band bending decreases the volume of the band bending (depletion) region and accordingly the radiative recombination rate of photoexcited charge carriers increases as monitored by the PL intensity. The overall photoreaction results in positive charge transfer from hydrogen cations to TiO_2 nanoparticles, making TiO_2 particles positively charged. Because the 320-nm UV penetration depth into TiO_2 is only ~ 25 nm,[14] the observed PL only comes from the first layer of TiO_2 particles, which are insulated from the tungsten grid by thousands of layers of TiO_2 particles. Hence, it is reasonable that the observed top layer TiO_2 can gain some excess positive charges without quasi-instantaneous discharge. In addition, the fact that hydrogen cations cause no change to the PL of TiO_2 in dark without the assistance of photoexcited electrons suggests that the positive charge held by the hydrogen cations cannot be directly injected into the valence band of TiO_2 (process 3, which cannot occur spontaneously) because the photoexcited holes are strong oxidants and occupy an energy level higher than that of hydrogen cations, which can be inferred from other studies in which H_2 acts as a hole scavenger.[15]

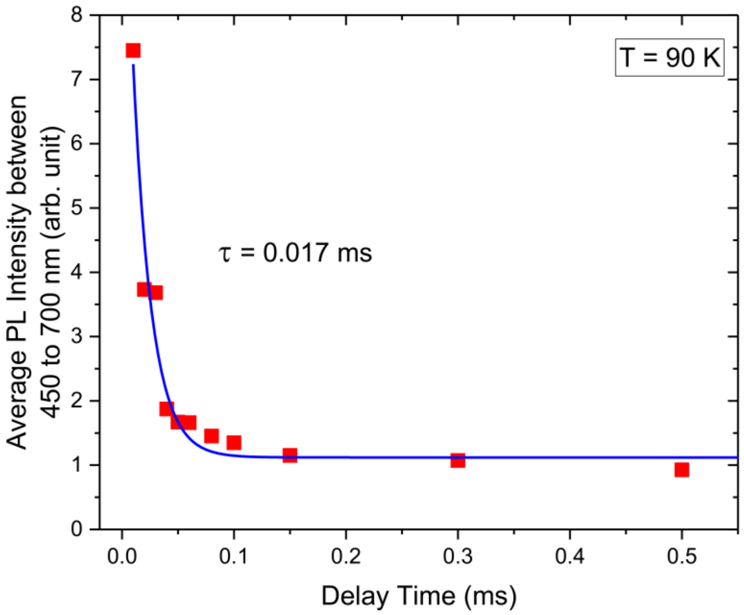

Figure 6.7. PL intensity of TiO_2 decay after turning off UV irradiation.

6.3.6 *Quantitative analysis*

Although reaction between photoexcited electrons and hydrogen cations will increase PL because of the associated band bending change as discussed above, it is worth considering if consumption of photoexcited electrons by reaction could substantially quench the PL intensity. As detailed below, the latter effect is negligible. The number of photons incident on each TiO_2 particle at the surface during the period from 3500 s to 11000 s in Figure 6.3, wherein the PL changes from ~ 4 to ~ 35 intensity units, is about 6.3×10^7 with the assumption that the particle size of the PL-active, anatase particles in P25 is ~ 85 nm.[33] Essentially all of the incident UV photons are absorbed to produce e/h pair excitations given the 20 nm UV absorption length of TiO_2. According to the dead-layer PL model we developed earlier,[5] it only requires at most ~ 150 leftover holes per TiO_2 particle to reduce 88% of the upward band bending compared to its flat band (maximum PL) condition given a TiO_2 volume defect density of 10^{18} cm^{-3}. Therefore, in this study, the ratio of photoexcited electrons reacting with hydrogen cations to leave leftover holes and the incident photons absorbed is at most ~ 0.00024%, which is negligible. Non-radiative and radiative (ca. 0.25%)[34] e/h pair recombination dominate the photoexcitation relaxation. Therefore, the side-effect of PL quenching caused by reaction between photoexcited electron and hydrogen cations via consumption of photoexcited electrons available for recombination, is negligible in this study.

If the number of photoexcited electron-hole pairs is much larger than the number of inhomogeneously positioned charges establishing the band bending potential gradient, a possible concern is whether the band bending could be electrostatically scrambled by charge redistribution of the photoexcited electrons and holes over the TiO_2 particle. However, the short life time of photoexcited electron-hole pairs observed as ~ 17 μs in Figure 6.7 indicates that there are only ~ 0.15 photoexcited electron-hole pairs per TiO_2 particle on average at any time during continuous UV irradiation as in Figure 6.3. Sufficient upward band bending to quench the PL to 12% of its maximal (flat band) value would be established with 150 immobilized electrons at the surface and the counter positive charges distributed across defects in the depletion zone at a defect density of 10^{18} cm^{-3}. Consequently, modulation of the TiO_2 band bending by the steady-state photoexcited charge density in our experiments should be negligible.

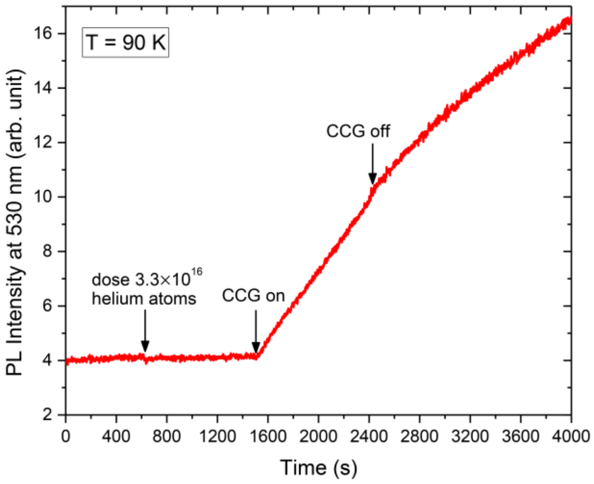

Figure 6.8. Effect of helium on PL intensity of TiO_2. Influence of CCG on PL development.

Because the decrease in upward band bending, signaled by a PL increase, is caused by positive charge transfer from the hydrogen cations into TiO_2 through photoinduced reduction, it is plausible that photoinduced reduction of other cations should also induce a similar band bending change. Figure 6.8 shows similar PL intensity changes caused by exposure to helium gas with the CCG off or on. As depicted in Figure 6.8, neutral helium atoms have no impact on PL of TiO_2 with the CCG off. But the PL increases when the CCG is turned on and ions are formed. The finding that helium cation exposure also causes PL of TiO_2 to increase lends further support to the idea that the active species in the hydrogen dosing PL experiments are hydrogen cations, rather than hydrogen atoms, and that a band bending decrease is a general physical consequence of cation photoreduction.

These unusual PL observations, enabled by low temperature, high vacuum, and a TiO_2 nanopowder sample not subject to prompt charge neutralization in its environment, show that charge transfer during a photoelectrochemical reaction at a semiconductor interface alters the photoexcited electron-hole pair recombination rate and surface band bending in ways that are likely to impact the efficiency of photocatalytic devices.

6.4 Conclusion

By employing PL spectroscopy to monitor the photoexcited electron-hole radiative recombination and the dead-layer model to analyze the band bending of TiO_2, it was found that the reduction of hydrogen cations by photoexcited electrons, which is a half photoelectrochemical reaction achieved under high vacuum conditions, alters the surface band bending and charge recombination rate of TiO_2. The main findings include:

(1) Molecular hydrogen exposure had no effect on the band bending of TiO_2 at 90 K.

(2) Molecular hydrogen could be ionized into hydrogen cations by the cold cathode gauge measuring the chamber pressure and these cations could reach the TiO_2 sample.

(3) The reduction of hydrogen cations by photoexcited electrons decreases the upward band bending of TiO_2, signaled by increased PL intensity (electron-hole radiative recombination rate), because of the accumulation of positively charged holes at TiO_2 surface.

(4) The band bending and charge carrier recombination rate changes observed for TiO_2 due to photoreduction of both hydrogen and helium cations are physical consequences of cation photoreduction at a semiconductor interface.

References

1. Ni, M.; Leung, M. K. H.; Leung, D. Y. C.; Sumathy, K., A Review and Recent Developments in Photocatalytic Water-Splitting Using TiO_2 for Hydrogen Production. *Renewable & Sustainable Energy Reviews* **2007**, *11*, 401-425.
2. Hoffmann, M. R.; Martin, S. T.; Choi, W. Y.; Bahnemann, D. W., Environmental Applications of Semiconductor Photocatalysis. *Chemical Reviews* **1995**, *95*, 69-96.
3. Yan, Y.; Shi, W. D.; Yuan, Z.; He, S. G.; Li, D. M.; Meng, Q. B.; Ji, H. W.; Chen, C. C.; Ma, W. H.; Zhae, J. C., The Formation of Ti-H Species at Interface Is Lethal to the Efficiency of TiO_2-Based Dye-Sensitized Devices. *Journal of the American Chemical Society* **2017**, *139*, 2083-2089.
4. Zhang, Z.; Yates, J. T., Band Bending in Semiconductors: Chemical and Physical Consequences at Surfaces and Interfaces. *Chemical Reviews* **2012**, *112*, 5520-5551.
5. Ma, S. L.; Reish, M. E.; Zhang, Z.; Harrison, I.; Yates, J. T., Anatase-Selective Photoluminescence Spectroscopy of P25 TiO_2 Nanoparticles: Different Effects of Oxygen Adsorption on the Band Bending of Anatase. *Journal of Physical Chemistry C* **2017**, *121*, 1263-1271.
6. Stevanovic, A.; Buttner, M.; Zhang, Z.; Yates, J. T., Photoluminescence of TiO_2: Effect of UV Light and Adsorbed Molecules on Surface Band Structure. *Journal of the American Chemical Society* **2012**, *134*, 324-332.
7. Zhang, Z.; Yates, J. T., Effect of Adsorbed Donor and Acceptor Molecules on Electron Stimulated Desorption: $O_2/TiO_2(110)$. *Journal of Physical Chemistry Letters* **2010**, *1*, 2185-2188.
8. Zhang, Z.; Yates, J. T., Electron-Mediated CO Oxidation on the $TiO_2(110)$ Surface During Electronic Excitation. *Journal of the American Chemical Society* **2010**, *132*, 12804-12807.
9. Sheppard, L. R.; Dittrich, T.; Nowotny, M. K., The Impact of Niobium Surface Segregation on Charge Separation in Niobium-Doped Titanium Dioxide. *Journal of Physical Chemistry C* **2012**, *116*, 20923-20929.
10. Karakitsou, K. E.; Verykios, X. E., Effects of Altervalent Cation Doping of TiO_2 on Its Performance as a Photocatalyst for Water Cleavage. *Journal of Physical Chemistry* **1993**, *97*, 1184-1189.
11. Hollingsworth, R. E.; Sites, J. R., Photo-Luminescence Dead Layer in P-Type InP. *Journal of Applied Physics* **1982**, *53*, 5357-5358.
12. Meyer, G. J.; Lisensky, G. C.; Ellis, A. B., Evidence for Adduct Formation at the Semiconductor Gas Interface - Photoluminescent Properties of Cadmium Selenide in the Presence of Amines. *Journal of the American Chemical Society* **1988**, *110*, 4914-4918.
13. Anpo, M.; Tomonari, M.; Fox, M. A., Insitu Photoluminescence of TiO_2 as a Probe of Photocatalytic Reactions. *Journal of Physical Chemistry* **1989**, *93*, 7300-7302.
14. Ghosh, A. K.; Maruska, H. P., Photoelectrolysis of Water in Sunlight with Sensitized Semiconductor Electrodes. *Journal of the Electrochemical Society* **1977**, *124*, 1516-1522.
15. Berger, T.; Diwald, O.; Knozinger, E.; Napoli, F.; Chiesa, M.; Giamello, E., Hydrogen Activation at TiO_2 Anatase Nanocrystals. *Chemical Physics* **2007**, *339*, 138-145.

16. Lin, F.; Zhou, G.; Li, Z. Y.; Li, J.; Wu, J.; Duan, W. H., Molecular and Atomic Adsorption of Hydrogen on TiO_2 Nanotubes: An Ab initio Study. *Chemical Physics Letters* **2009**, *475*, 82-85.
17. Kunat, M.; Burghaus, U.; Woll, C., The Adsorption of Hydrogen on the Rutile TiO_2(110) Surface. *Physical Chemistry Chemical Physics* **2004**, *6*, 4203-4207.
18. Chen, X. B.; Liu, L.; Yu, P. Y.; Mao, S. S., Increasing Solar Absorption for Photocatalysis with Black Hydrogenated Titanium Dioxide Nanocrystals. *Science* **2011**, *331*, 746-750.
19. Wang, B.; Shen, S. H.; Mao, S. S., Black TiO_2 for Solar Hydrogen Conversion. *Journal of Materiomics* **2017**, *3*, 96-111.
20. Lavrov, E. V., Hydrogen Donor in Anatase TiO_2. *Physical Review B* **2016**, *93*.
21. Tao, J. G.; Cuan, Q.; Gong, X. Q.; Batzill, M., Diffusion and Reaction of Hydrogen on Rutile TiO_2(011)-2x1: The Role of Surface Structure. *Journal of Physical Chemistry C* **2012**, *116*, 20438-20446.
22. Aschauer, U.; Selloni, A., Hydrogen Interaction with the Anatase TiO_2(101) Surface. *Physical Chemistry Chemical Physics* **2012**, *14*, 16595-16602.
23. Panayotov, D. A.; Yates, J. T., N-Type Doping of TiO_2 with Atomic Hydrogen-Observation of the Production of Conduction Band Electrons by Infrared Spectroscopy. *Chemical Physics Letters* **2007**, *436*, 204-208.
24. Chen, X. B.; Shen, S. H.; Guo, L. J.; Mao, S. S., Semiconductor-Based Photocatalytic Hydrogen Generation. *Chemical Reviews* **2010**, *110*, 6503-6570.
25. Zheng, W. G.; Gallagher, A., Hydrogen Dissociation on High-Temperature Tungsten. *Surface Science* **2006**, *600*, 2207-2213.
26. Yang, Y.; Sushchikh, M.; Mills, G.; Metiu, H.; McFarland, E., Reactivity of TiO_2 with Hydrogen and Deuterium. *Applied Surface Science* **2004**, *229*, 346-351.
27. Fukada, K.; Matsumoto, M.; Takeyasu, K.; Ogura, S.; Fukutani, K., Effects of Hydrogen on the Electronic State and Electric Conductivity of the Rutile TiO_2(110) Surface. *Journal of the Physical Society of Japan* **2015**, *84*.
28. An, H. R.; Park, S. Y.; Kim, H.; Lee, C. Y.; Choi, S.; Lee, S. C.; Seo, S.; Park, E. C.; Oh, Y. K.; Song, C. G., et al., Advanced Nanoporous TiO_2 Photocatalysts by Hydrogen Plasma for Efficient Solar-Light Photocatalytic Application. *Scientific Reports* **2016**, *6*.
29. Stevanovic, A.; Yates, J. T., Probe of NH_3 and CO Adsorption on the Very Outermost Surface of a Porous TiO_2 Adsorbent Using Photoluminescence Spectroscopy. *Langmuir* **2012**, *28*, 5652-5659.
30. Padovani, M.; Galli, D.; Glassgold, A. E., Cosmic-Ray Ionization of Molecular Clouds. *Astronomy & Astrophysics* **2009**, *501*, 619-631.
31. Wobschall, D.; Fluegge, R. A.; Graham, J. R., Collision Cross Sections of Hydrogen and Other Ions as Determined by Ion Cyclotron Resonance. *The Journal of Chemical Physics* **1967**, *47*, 4.
32. Bauer, N.; Beach, J. Y., Differences in Mass Spectra of H_2 and D_2. *The Journal of Chemical Physics* **1947**, *15*, 150-151.
33. Ohno, T.; Sarukawa, K.; Tokieda, K.; Matsumura, M., Morphology of a TiO_2 Photocatalyst (Degussa, P-25) Consisting of Anatase and Rutile Crystalline Phases. *Journal of Catalysis* **2001**, *203*, 82-86.

34. Abazovic, N. D.; Comor, M. I.; Dramicanin, M. D.; Jovanovic, D. J.; Ahrenkiel, S. P.; Nedeljkovic, J. M., Photoluminescence of Anatase and Rutile TiO_2 Particles. *Journal of Physical Chemistry B* **2006**, *110*, 25366-25370.

Appendices

Appendix A. Quantitative analysis of photoexcited charge trapping by metal on semiconductor surface

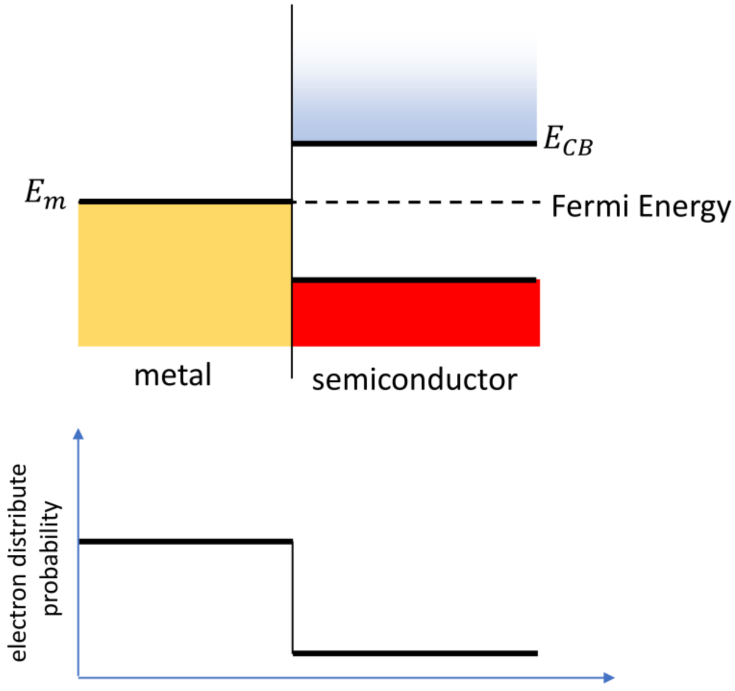

Figure A.1. Band structure of metal/semiconductor

One common idea for the enhancement of photoactivity by noble metal deposition is that photoexcited electrons can be injected into metals due to the energy difference between the CB of semiconductor and the Fermi energy of metal, as shown in Figure A.1. However, because the Fermi energy (chemical potential for electrons) for both the metal and the semiconductor are the same in equilibrium without photoexcitation, there should exist no net charge flow. Therefore, understanding the driving force of electron transport during photoexcitation is important.

Upon equilibrium without photoexcitation, the probability for electrons to reside in the metal according to Boltzmann distribution is

$$P_m = \frac{N_m e^{-E_m/k_BT}}{N_m e^{-E_m/k_BT} + N_s e^{-E_{CB}/k_BT}} = \frac{K}{K + e^{-\Delta E/k_BT}} \tag{A.1}$$

in which $K = N_m/N_s$ is the ratio of available sites in metal and in semiconductor and $\Delta E = E_{CB} - E_m$ is the energy difference between the CB of semiconductor and the Fermi energy of metal. And the probability for electrons to be found in the semiconductor CB is

$$P_s = 1 - P_m = \frac{e^{-\Delta E/k_BT}}{K + e^{-\Delta E/k_BT}} \tag{A.2}$$

Because ΔE is usually ~ 0.9 eV [1]and N_m is usually larger than N_s, $P_m \gg P_s$.

Assuming that under photoexcitation at steady state, the above statement may still hold. Thus, the additional photoexcited electrons should follow the same distribution as $P_m \gg P_s$. Hence, photoexcited electrons are mainly trapped by metals deposited on semiconductor surfaces.

The above model is too simple and may not be applicable to real situations due to various reasons. First, the effects of holes are neglected. Second, potential energy change due to charge separation is not considered. Third, Fermi-Dirac distribution should be used to replace the Boltzmann distribution if Pauli exclusion is a consideration. It has been reported that due to the generation of extra electrons and holes under photoexcitation, the Fermi energy of electrons and holes are no longer the same and they separate from each other. The Fermi energy of electrons and holes during photoexcitation are named quasi-Fermi energy and are not uniform, thus causing directed net flow of charges.[2]

References

1. Sangpour, P.; Hashemi, F.; Moshfegh, A. Z., Photoenhanced Degradation of Methylene Blue on Cosputtered M:TiO_2 (M = Au, Ag, Cu) Nanocomposite Systems: A Comparative Study. *Journal of Physical Chemistry C* **2010**, *114*, 13955-13961.
2. Kronik, L.; Shapira, Y., Surface Photovoltage Phenomena: Theory, Experiment, and Applications. *Surface Science Reports* **1999**, *37*, 1-206.

Appendix B. Band bending at the SWNT/TiO$_2$ interface

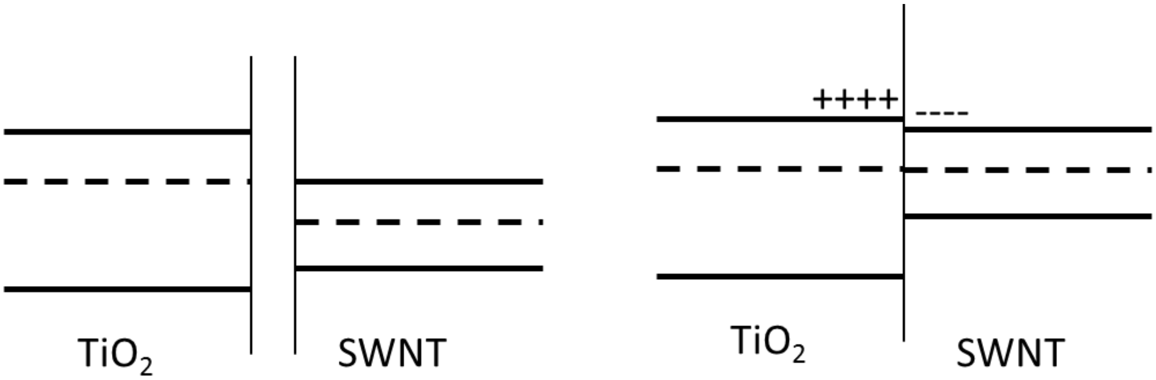

Figure B.1. Band alignment of TiO$_2$ and SWNT. The Fermi energy of TiO$_2$ is higher than that of SWNT. Upon contact, electrons flow from TiO$_2$ to SWNT, causing charge separation across the interface. TiO$_2$ is positively charged, while SWNT is negatively charged at equilibrium.

The band structures of TiO$_2$ and SWNT are shown in Figure B.1. Because the Fermi energy of TiO$_2$ is higher than that of SWNT, upon contact, electrons flow from TiO$_2$ to SWNT, causing charge separation at the interface. TiO$_2$ will be positively charged while SWNT will be negatively charged at equilibrium. The band bending is caused by the electrostatic field induced by imbalanced charges across the interface.

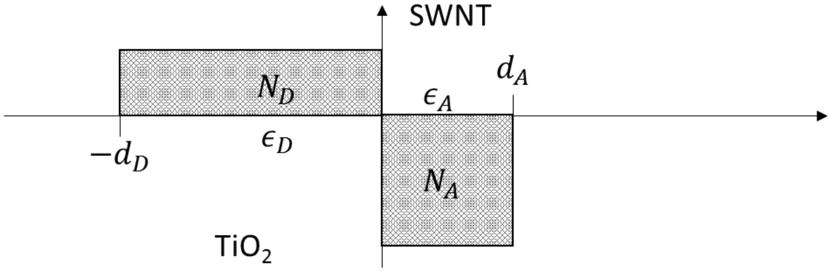

Figure B.2. Charge distribution along the interface between TiO$_2$ and SWNT

The charge distribution along the distance from the interface can be modeled as Figure B.2. the charge in TiO$_2$ are positive with charge density N_D in a region of d_D, while the charge in SWNT are negative with charge density N_A in a region of d_A. Because of charge conservation,

$$N_A d_A = N_D d_D \tag{B.1}$$

From Poison's Equation, we can also get

$$\nabla^2\phi = \frac{\partial^2\phi}{\partial x^2} = -\frac{4\pi\rho(x)}{\varepsilon} = \begin{cases} 0, & x < -d_D \\ -\frac{4\pi e N_D}{\varepsilon}, & -d_D \le x < 0 \\ \frac{4\pi e N_A}{\varepsilon}, & 0 \le x \le d_A \\ 0, & x > -d_A \end{cases} \tag{B.2}$$

in which ε is the permittivity and N is the defect density. Because there will be no electric field outside the charged interface, therefore, we should have $\phi(-\infty) = \phi(+\infty) =$ constant, $\phi'(-\infty) = \phi'(+\infty) = 0$. By solving equation (B.2), we can get

$$\phi(x) = \begin{cases} \phi(-\infty), & x < -d_D \\ \phi(-\infty) - \frac{2\pi e N_D}{\varepsilon_D}(x + d_D)^2, & -d_D \le x < 0 \\ \phi(+\infty) + \frac{2\pi e N_A}{\varepsilon_A}(x - d_A)^2, & 0 \le x \le d_A \\ \phi(+\infty), & x > d_A \end{cases} \tag{B.3}$$

From equation (B.3), the potential at $x = 0$ should be the same, thus

$$\phi(-\infty) - \frac{2\pi e N_D}{\varepsilon_D} d_D^2 = \phi(+\infty) + \frac{2\pi e N_A}{\varepsilon_A} d_A^2 \tag{B.4}$$

$$\phi(-\infty) - \phi(+\infty) = 2\pi e\left(\frac{N_D d_D^2}{\varepsilon_D} + \frac{N_A d_A^2}{\varepsilon_A}\right) \tag{B.5}$$

The left side of equation (B.5) should be the difference of work function between TiO_2 and SWNT, $\Delta\phi$. The following relationship can be derived by solving equation (B.1) and (B.5).

$$d_D = \sqrt{\frac{\Delta\phi}{2\pi e N_D \left(\frac{1}{\varepsilon_D} + \frac{N_D}{N_A \varepsilon_A}\right)}} \tag{B.6}$$

The band bending from TiO_2 and SWNT can be further be calculated as

$$\Delta\phi_{\mathrm{TiO_2}} = \frac{\Delta\phi}{1 + \frac{N_D \varepsilon_D}{N_A \varepsilon_A}} \tag{B.7}$$

$$\Delta\phi_{\mathrm{SWNT}} = \frac{\Delta\phi}{1 + \frac{N_A \varepsilon_A}{N_D \varepsilon_D}} \tag{B.8}$$

The potential due to separated charge is plotted as Figure B.3(a). Because electrons are negatively charged, the potential energy for electrons is reversed from the potential, shown as Figure B.3(b). The band energy of electrons across the SWNT/TiO_2 interface, shown in Figure B.4, is a superposition of flat band energy in Figure B.1 and the potential energy caused by separated charges in Figure B.3(b). The resulting band bending in TiO_2 is upward while in SWNT is downward. Equation (B.7) and (B.8) shows that the value of band bending is related to the $N\varepsilon$ value. Because SWNT has a higher $N\varepsilon$ value, there is more band bending in TiO_2. For the extreme case where $N_A \varepsilon_A \gg N_D \varepsilon_D$, such as the Au/$TiO_2$ junction, there is no band bending in the metal side and all the band bending occurs in the semiconductor.

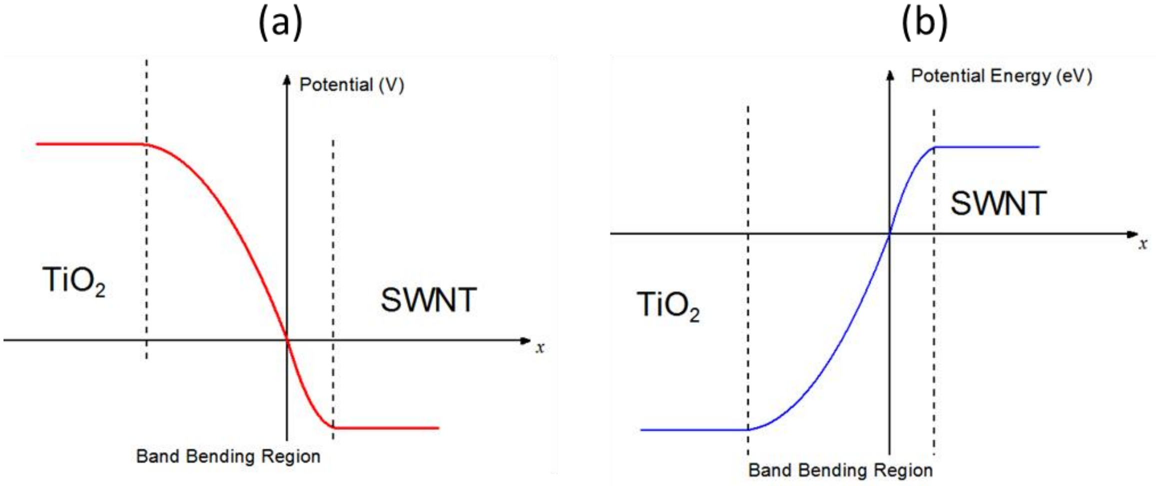

Figure B.3. (a) Potential and (b) potential energy for electrons induced by charge separation across TiO_2 and SWNT interfaces

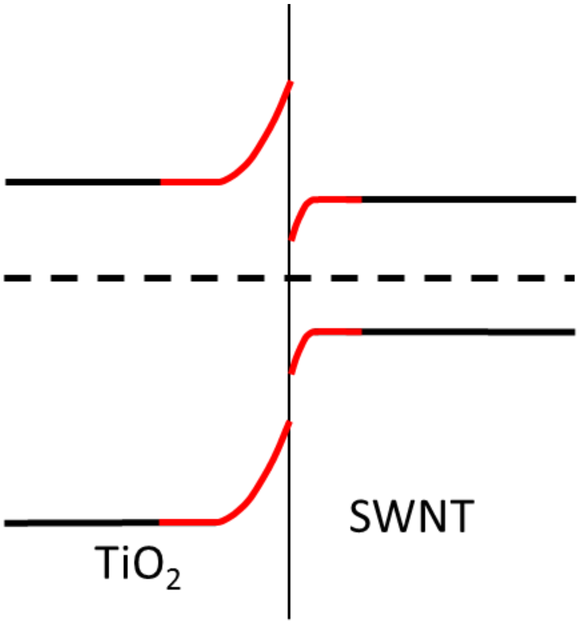

Figure B.4. Band Structure at the TiO_2/SWNT junction

Appendix C. Effect of diffusion and drift in charge transport

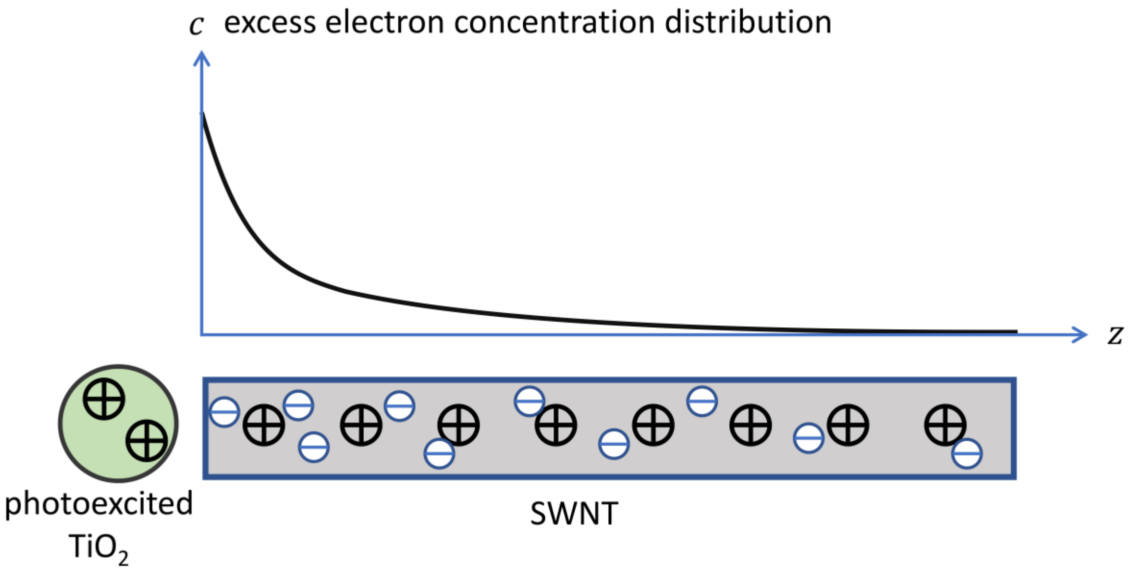

Figure C.1. Schematic model of electron transport through SWNT

As shown in Figure C.1, photoexcited electrons from TiO$_2$ are injected into SWNT. The transport of electrons in SWNT is modelled by treating SWNT as a conductive cylinder. The transport of electrons is driven by two forces. On the one hand, electrons tend to move toward the positive *z* direction under diffusion caused by charge injection from TiO$_2$. On the other hand, electrons are electrostatically attracted toward the negative *z* direction due to the holes left in TiO$_2$. Therefore, the final distribution of excess electrons in SWNT is determined by the competition of the above two driving forces. The electron diffusion flux due to concentration gradient is described by Fick's law as equation (C.1) and the drift flux due to electric field is shown as equation (C.2).

$$F_{diff} = -D\frac{\partial(c+N)}{\partial z} = -D\frac{\partial c}{\partial z} \tag{C.1}$$

$$F_{drift} = -(N+c)\mu \boldsymbol{E} = (N+c)\mu \frac{\partial \phi}{\partial z} \approx N\mu \frac{\partial \phi}{\partial z} \tag{C.2}$$

where z is the distance along SWNT, c is the excess electron density distribution along z, F_{diff} is the flux caused by diffusion, D is the diffusion coefficient, F_{drift} is the flux due to electric field induced drift, N is the intrinsic charge carrier density (assuming $c \ll N$), μ is the charge carrier mobility, E is the electric field, and V is the electric potential. At steady state, the total flux of electrons should be zero at any z , i.e. $F_{diff} + F_{drift} = 0$. Therefore,

$$N\mu \frac{\partial \phi}{\partial z} - D\frac{\partial c}{\partial z} = 0 \tag{C.3}$$

The potential ϕ in equation (C.3) can be described by Poisson's equation,

$$\frac{\partial^2 \phi}{\partial z^2} = -\frac{\rho}{\varepsilon_r \varepsilon_0} \tag{C.4}$$

where ε_r is the relative permittivity, ε_0 is the vacuum permittivity and ρ is the excess charge carrier density distribution along z which is related to the excess electron density by

$$\rho = -ec \tag{C.5}$$

By solving equations (C.3)-(C.5), the distribution of excess electron density along the SWNT is

$$c = A\exp\left(-\sqrt{\frac{N\mu e}{\varepsilon_r \varepsilon_0 D}}\, z\right) \tag{C.6}$$

in which, A is a constant that is proportional to the total number of electrons injected into the SWNT. Along with the Einstein relation

$$D = \frac{\mu k_B T}{e} \tag{C.7}$$

Equation (C.6) can be simplified into

$$c = A\mathrm{exp}(\mathrm{z}/\lambda) \tag{C.8}$$

$$\lambda = \sqrt{\frac{\varepsilon_0 \varepsilon_r k_B T}{N e^2}} \tag{C.9}$$

in which λ is the Debye screening length.

Appendix D. Irreversibility of oxygen-defect reaction effect

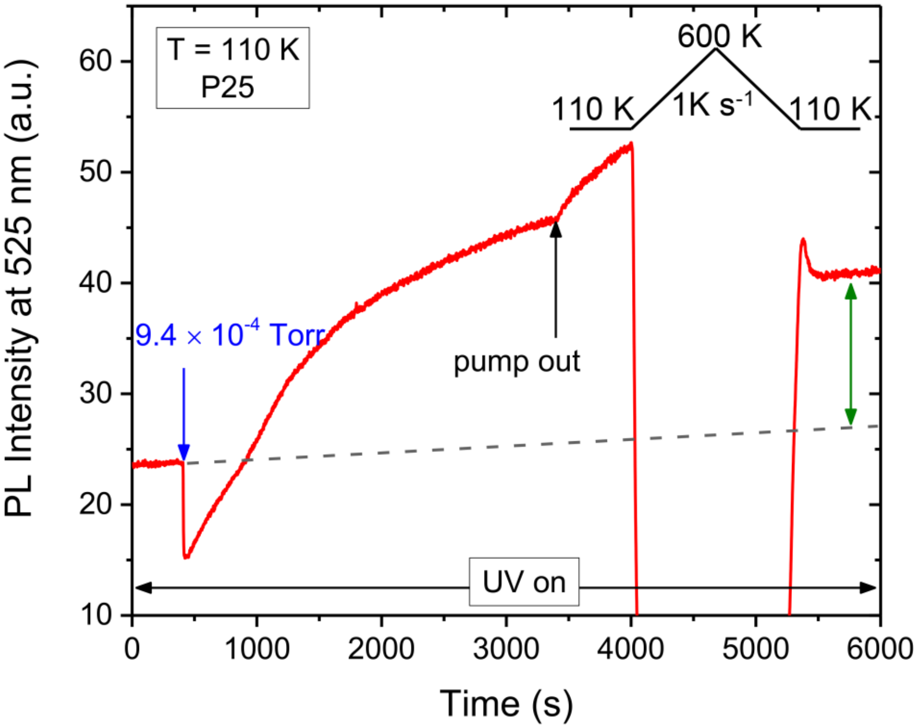

Figure D.1. Influence of pumping out and heating on the O_2 effect on PL of TiO_2.

In Figure D.1, a large amount of oxygen (9.4×10^{-4} Torr) was dosed to TiO_2, the PL behavior is the same as described previously. However, when the continuous pump out starts, the PL intensity growth rate increases. This is caused by the enhanced rate of photodesorption of chemisorbed oxygen under UV irradiation due to a high vacuum condition surrounding the sample when the pump out starts. Then the sample was heated up to 600 K and cooled back to 110 K under continuous pump out conditions. During the heating process, all the molecularly chemisorbed oxygen has been removed from the TiO_2 surface[1-2] and this can be concluded from the slope of PL curve after the heat treatment, which is close to that of the initial state of TiO_2 before oxygen dose. The net increase of PL intensity after heat treatment compared to that of the initial state of TiO_2 before oxygen dose provides solid proof to confirm that the oxygen-defect reaction effect is irreversible, which has been stated in Figure 5.3.

References

1. Henderson, M. A.; Epling, W. S.; Perkins, C. L.; Peden, C. H. F.; Diebold, U., Interaction of Molecular Oxygen with the Vacuum-Annealed TiO_2(110) Surface: Molecular and Dissociative Channels. *Journal of Physical Chemistry B* **1999**, *103*, 5328-5337.
2. Lira, E.; Hansen, J. O.; Huo, P.; Bechstein, R.; Galliker, P.; Laegsgaard, E.; Hammer, B.; Wendt, S.; Besenbacher, F., Dissociative and Molecular Oxygen Chemisorption Channels on Reduced Rutile TiO_2(110): An STM and TPD Study. *Surface Science* **2010**, *604*, 1945-1960.

Appendix E. Ratio of photoexcitation in band bending region

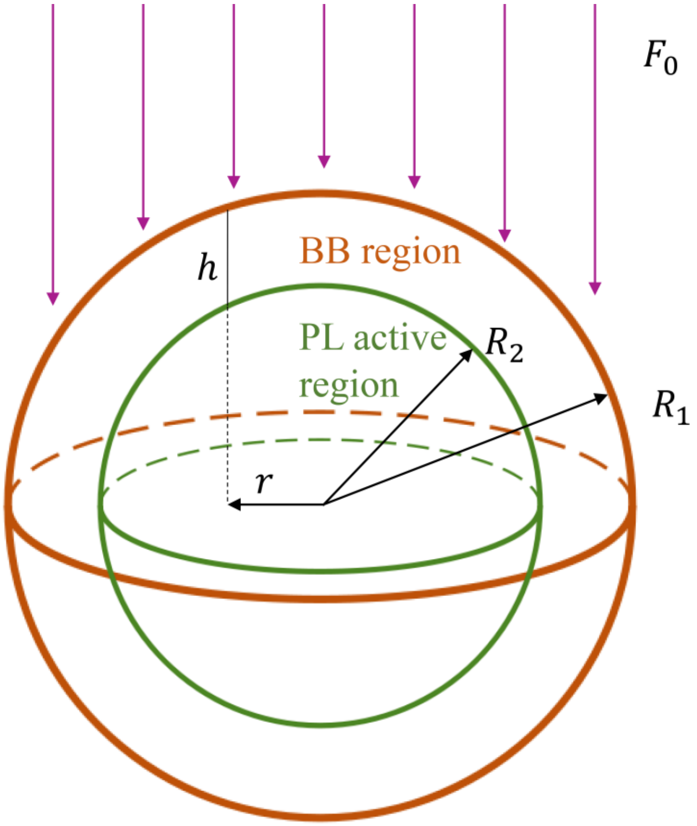

Figure E.1. Model for calculating photoexcitation ratio in the band bending region. The sphere with radius R_1 is the TiO_2 particle; the sphere with radius R_2 is the PL active region where there is no band bending; the band bending region is between sphere R_1 and R_2, with a depth of $R_1 - R_2$. F_0 is the photon flux irradiated to the particle.

Figure E.1 shows a model to calculate the photoexcitation ratio in the band bending region. The band bending region can be described by Poisson's equation[1-2]

$$\nabla^2 \phi = -\frac{\rho}{\varepsilon_r \varepsilon_0} \tag{E.1}$$

in which, ϕ is the potential, ρ is the charge density, ε_r is the relative permittivity, and ε_0 is the vacuum permittivity.

The above equation can be solved in spherical coordinates as

$$\Delta\phi = \frac{eN_D}{6\varepsilon_r\varepsilon_0}(R_1^2 - R_2^2) \tag{E.2}$$

in which ΔV is the band bending potential and N_D is defect density.

The total number of photons (per unit time) irradiated to the TiO_2 particle is

$$N_T = \pi R_1^2 F_0 \tag{E.3}$$

The photon flux at depth z should be

$$F(z) = F_0 \exp\left(-\frac{z}{d}\right) \tag{E.4}$$

in which d is the light penetration depth.

The number of photons that can pass through the TiO_2 particle can be calculated as

$$N_F = \int_0^{R_1} 2\pi r dr F_0 \exp\left(-\frac{2\sqrt{R_1^2 - r^2}}{d}\right) \tag{E.5}$$

The number of photons reaching the PL active region after the adsorption from band bending region is

$$N_T' = \int_0^{R_2} 2\pi r dr F_0 \exp\left(-\frac{\sqrt{R_1^2 - r^2} - \sqrt{R_2^2 - r^2}}{d}\right) \tag{E.6}$$

The number of photons leaving the PL active region is

$$N_F' = \int_0^{R_2} 2\pi r dr F_0 \exp\left(-\frac{\sqrt{R_1^2 - r^2} + \sqrt{R_2^2 - r^2}}{d}\right) \tag{E.7}$$

The ratio of photoexcitation in the band bending region compared to the whole particle is calculated as

$$\eta = 1 - \frac{N_T' - N_F'}{N_T - N_F} \tag{E.8}$$

The ratio of photoexcitation in the band bending region compared to the whole particle can be numerically calculated using MATLAB by combining equations (E.2), (E.3) and (E.5) – (E.8). The typical values for this study are taken as $R_1 = 42.5$ nm (diameter of 85 nm), $d = 20$ nm, and $\varepsilon_r = 100$. Some values with different charge density and band bending voltages are given in Table E.1. The values in Table E.1 suggest that the ratio of photoexcitation in the band bending region can be largely tuned by changing the band bending voltage, especially at conditions with low charge densities.

Table E.1. Ratio of photoexcitation in the band bending region (η) of TiO_2 and the band bending region depth ($bb = R_1 - R_2$) under different defect density (N_D) and band bending voltage ($\Delta\phi$).

$N_D = 10^{19}$ cm^{-3}			$N_D = 10^{18}$ cm^{-3}			$N_D = 3 \times 10^{17}$ cm^{-3}		
$\Delta\phi$ (V)	bb (nm)	η (%)	$\Delta\phi$ (V)	bb (nm)	η (%)	$\Delta\phi$ (V)	bb (nm)	η (%)
0.02	0.8	10	0.002	0.8	10	0.001	1.3	16
0.06	2.4	27	0.006	2.4	27	0.003	4.1	41
0.10	4.1	41	0.010	4.1	41	0.005	7.1	59
0.16	6.8	57	0.016	6.8	57	0.007	10.4	73
0.22	9.7	70	0.022	9.7	70	0.009	14.0	83
0.28	12.9	80	0.028	12.9	80	0.011	18.2	91
0.34	16.5	88	0.034	16.5	88	0.013	23.3	96
0.40	20.6	94	0.040	20.6	94	0.015	30.4	99

References

1. Ioannides, T.; Verykios, X. E., Charge Transfer in Metal Catalysts Supported on Doped TiO_2: A Theoretical Approach Based on Metal-Semiconductor Contact Theory. *Journal of Catalysis* **1996**, *161*, 560-569.
2. Zhang, Z.; Yates, J. T., Band Bending in Semiconductors: Chemical and Physical Consequences at Surfaces and Interfaces. *Chemical Reviews* **2012**, *112*, 5520-5551.

Appendix F. Dependence of PL increase rate on hydrogen pressure

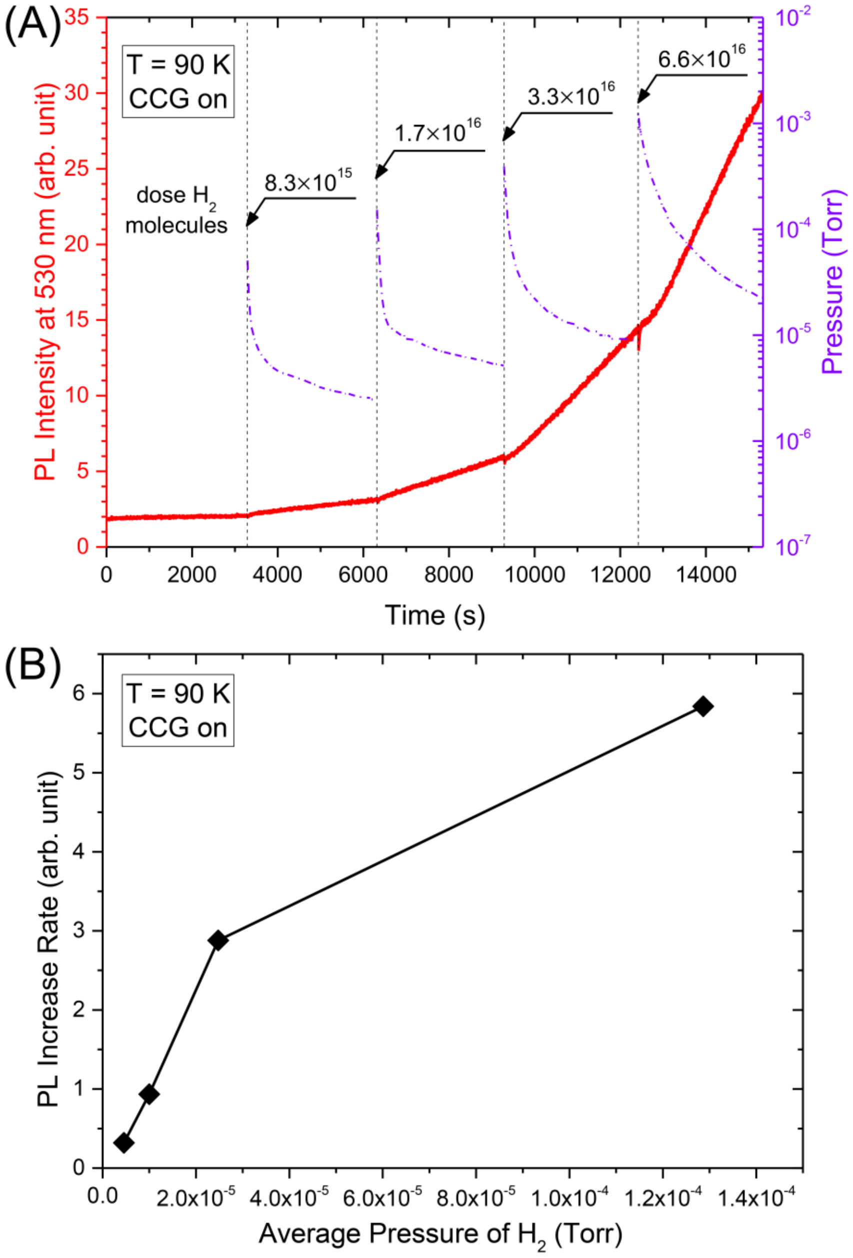

Figure F.1. Influence of hydrogen pressure on rate of increase of PL increase from TiO_2 with cold cathode gauge (CCG) on. (A) 530-nm PL intensity increase after doses of different amounts of hydrogen molecules. (B) relationship between PL intensity increase rate and the average chamber pressure.

Figure F.1(A) shows that the PL intensity of TiO_2 is nearly invariant in vacuum before the introduction of hydrogen. The PL intensity starts to increase with the dose of hydrogen and the PL increase rate increases with the pressure of hydrogen inside the vacuum chamber. Figure F.1(B) shows the relationship between the PL increase rate and the average pressure of hydrogen surrounding the sample. As depicted in the figure, at low hydrogen pressures less than 3×10^{-5} Torr, the PL increase rate is nearly proportional to the hydrogen pressure, but the increase of the PL increase rate slows down at high hydrogen pressure. As discussed in this report, the increase of PL originates from the charge transfer that occurred during photoreduction of hydrogen cations, in which the hydrogen cations are produced during the measurement of the chamber pressure by the cold cathode gauge (CCG). The CCG's internal current can be expressed as $i=kP^n$, where i is the current, k is a constant, P is the pressure, and n is a constant usually in the range of 1.00 to 1.15. In a small range of pressure, the sensor current can be treated as proportional to the pressure since n is close to 1. Assuming that the probability of a hydrogen cation escaping the CCG is a constant, the linear increase of PL increase rate at low pressure in Figure F.1(B) should be attributed to linear relationship between the number of cations available at the TiO_2 surface and the hydrogen pressure. At high hydrogen pressure, although the number of cations produced by the CCG is increased, the actual number of hydrogen cation near the TiO_2 surfaces may not increase proportionally due to collisions with ambient hydrogen molecules. The mean free path of a gas molecule is given by $\lambda = k_B T/\sigma P$, where σ is the cross section, which is ~ 68 $Å^2$ between H_2^+ and H_2.[1] The mean free path at several different pressures computed at a temperature of 90 K is shown in Table F.1. The table shows that the mean free path of H_2^+ is of the same order of magnitude as the 30 cm spatial distance between the CCG and the TiO_2 sample when the pressure is between 2 ~ 5 × 10^{-5} Torr. This result suggests that the gradual flattening of PL increase rate at high pressure is due to inhibited cation transport from the CCG to the TiO_2 surfaces as the cation mean free path is reduced.

Table F.1. Mean free path of H_2^+ in H_2 at 90 K calculated with cross section of 68 $Å^2$

Pressure (Torr)	Mean Free Path (cm)	Pressure (Torr)	Mean Free Path (cm)
1×10^{-6}	969	5×10^{-5}	19.4
2×10^{-6}	484	1×10^{-4}	9.69
5×10^{-6}	194	2×10^{-4}	4.84
1×10^{-5}	96.9	5×10^{-4}	1.94
2×10^{-5}	48.4	1×10^{-3}	0.97

References

1. Wobschall, D.; Fluegge, R. A.; Graham, J. R., Collision Cross Sections of Hydrogen and Other Ions as Determined by Ion Cyclotron Resonance. *The Journal of Chemical Physics* **1967**, *47*, 4.

Appendix G. Effect of oxygen on the PL intensity of TiO_2

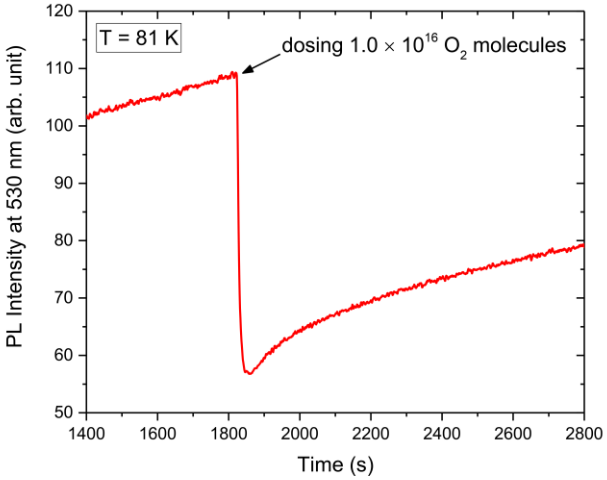

Figure G.1. Effect of oxygen molecules on the PL intensity of TiO_2.

Figure G.1 shows the effect of oxygen molecules on the PL intensity of TiO_2. Before dosing the oxygen molecules, the TiO_2 sample has been exposed to 2.0×10^{16} H_2 molecules with CCG on and the PL was brought to ~ 110 before dosing oxygen. As the figure depicts, the dose of oxygen causes an immediate drop of PL intensity to ~ 55, which is in the reverse way of hydrogen acts. Hence, Figure G.1 rules out the possibility that electron-stimulated oxygen desorption may interfere the result observed in this paper. The immediate drop of PL when dosing oxygen is caused by the adsorption of oxygen as an electron acceptor on TiO_2 surface and the gradual recovery of PL after oxygen dose is mainly due to photoinduced oxygen desorption from TiO_2 surface, which has been described before.[1] The relatively higher PL intensity compared to Figure F.1 is because Figure G.1 was measured at a lower temperature and it is well-known that higher temperature quenches PL due to enhanced non-radiatively recombination.[2]

References

1. Ma, S. L.; Reish, M. E.; Zhang, Z.; Harrison, I.; Yates, J. T., Anatase-Selective Photoluminescence Spectroscopy of P25 TiO_2 Nanoparticles: Different Effects of Oxygen Adsorption on the Band Bending of Anatase. *Journal of Physical Chemistry C* **2017**, *121*, 1263-1271.
2. Leroux, M.; Grandjean, N.; Beaumont, B.; Nataf, G.; Semond, F.; Massies, J.; Gibart, P., Temperature Quenching of Photoluminescence Intensities in Undoped and Doped Gan. *Journal of Applied Physics* **1999**, *86*, 3721-3728.

Appendix H. List of publications

1. Shiliang Ma, Zhen Zhang, Ian Harrison. Photoreduction of Hydrogen Cations on TiO_2 and its Impact on Surface Band Bending and the Charge Carrier Recombination Rate: A Photoluminescence Study Under High Vacuum Conditions. Accepted by *Journal of Physical Chemistry C*. **2018**, 122(15): 8288-8294
2. Shiliang Ma, Matt Reish, Zhen Zhang, Ian Harrison, John T. Yates, Jr. Anatase-Selective Photoluminescence Spectroscopy of P25 TiO_2 Nanoparticles: Different Effects of Oxygen Adsorption on the Band Bending of Anatase. *Journal of Physical Chemistry C*, **2017**, 121(2): 1263-1271.
3. Matt Reish, Zhen Zhang, Shiliang Ma, Ian Harrison, Henry Everitt. How Annealing and Charge Scavengers Affect Visible Emission from ZnO Nanocrystals. *Journal of Physical Chemistry C*, **2016**, 120(9): 5108-5113.
4. Ana Stevanovic, Shiliang Ma, John T. Yates, Jr. Photoexcited Electron Hopping between TiO_2 Particles: Effect of Single-Walled Carbon Nanotubes. *Journal of Physical Chemistry C*, **2014**, 118(41): 23614-23620.
5. Ana Stevanovic, Shiliang Ma, John T. Yates, Jr. Effect of Gold Nanoparticles on Photoexcited Charge Carriers in Powdered TiO_2 – Long Range Quenching of Photoluminescence. *Journal of Physical Chemistry C*, **2014**, 118(36): 21275-21280.